

**A BIFILAR HELICAL ANTENNA WITH
AN OUTER LAYER OF FERRITE**

by

Alan Geetran Cha

This document is subject to special export controls and each transmittal to foreign governments or foreign nationals may be made only with prior approval of AFAL (AVWE), Wright-Patterson AFB, Ohio 45433.

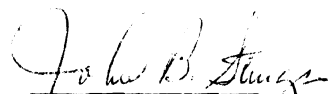
FOREWORD

This report, 1770-4-T, was prepared by the Radiation Laboratory of The University of Michigan, Department of Electrical Engineering, 201 East Catherine Street, Ann Arbor, Michigan 48108, under the direction of Professor Ralph E. Hiatt and Professor John A. M. Lyon on Air Force Contract F33615-68-C-1381, Task 627801 of Project 6278, "Study and Investigation of UHF-VHF Antennas." The work was administered under the direction of the Air Force Avionics Laboratory, Wright-Patterson Air Force Base, Ohio 45433. The Task Engineer was Mr. Olin E. Horton and the Project Engineer, Mr. Edwin M. Turner, AVWE. This report was submitted by the author in June 1970.

ACKNOWLEDGMENT

The author wishes to express his deep appreciation to Professor John A. M. Lyon and members of this Doctoral Committee for their advice and encouragement. The author also wishes to thank Mrs. Austra Liepa for writing part of the computer program and Mrs. Claire White and Mrs. Mary Wright for typing the manuscript.

This technical report has been reviewed and is approved.



JOHN B. STURGES

Lt Colonel USAF

Chief, Electronic Warfare Division

ABSTRACT

In this text, a bifilar helical antenna with an outer layer of ferrite is studied. Both the characteristic equation and the far field patterns are investigated.

The characteristic equation is found to have different branches of roots as in the case of the unloaded helix. The correct branch of roots is identified both on a theoretical basis and on an experimental basis. The calculated patterns based on this particular branch of roots are found to be in good agreement with the measured patterns. The antenna is found to be backfire over a wide band if properly designed. Tested models show sizable reduction in diameter results from the loading when compared with unloaded helical antennas.

The analysis in this work also establishes important conditions on the backfire and endfire operations of the class of antennas that have a wave-like source distribution function along the axis.

TABLE OF CONTENTS

I	INTRODUCTION	1
II	THE SHEATH HELIX	4
	2.1 Models for Solving the Propagation Constant of Helices	4
	2.2 An Infinite Helix with an Outer Layer of Loading Material; The Sheath Model	5
	2.3 The Unloaded Sheath Helices	14
	2.4 The Very Slow Wave Approximation	15
	2.5 Two Bases for the Selection of the Right Branch of Roots	17
	2.6 Numerical Solutions to the Characteristic Equations	17
III	THE RADIATION PATTERNS OF THE TUBE ANTENNA EXCITED BY A BIFILAR HELIX	23
	3.1 The Equivalence Principle	23
	3.2 Radiation from the Side Surface of a Cylinder	25
	3.3 Radiation from the Ends of a Cylinder	35
	3.4 The Backfire Bifilar Helix	42
	3.5 Numerical Results of the Pattern Calculation	47
IV	EXPERIMENTS	53
	4.1 The Model Antennas	53
	4.2 The Near Field Measurements	54
	4.3 The Radiation Pattern	61
V	CONCLUSIONS AND RECOMMENDATIONS	66
	5.1 General	66
	5.2 Conclusions Pertaining to the Helical Antenna with an Outer Layer of Ferrite	67
	5.3 Suggestions for Future Efforts	68
	REFERENCES	69

LIST OF ILLUSTRATIONS

<u>Number</u>	<u>Caption</u>	<u>Page</u>
2-1	An Infinite Helix with an Outer Layer of Ferrite.	6
2-2	Some Solutions to the Characteristic Equation (2.69) with Parameters as in (2.73).	20
2-3	Some Roots to the Characteristic Equation , $k=2\pi(m^{-1})$.	22
3-1	A Helical Antenna Loaded with a Layer of Ferrite.	26
3-2	$C_x(kb \sin\theta)$ and $C_y(kb \sin\theta)$, $\phi=0$.	31
3-3	$ A(\theta) $ for Different Values of $\beta_r; \beta_i=0, kL=12\pi$.	34
3-4	$ B(\theta) $ for $\beta_r=k, \beta_i=0$.	43
3-5	$ B(\theta) $ for $\beta_r=k, \beta_i=-0.1k$.	44
3-6	$ B(\theta) $ for $\beta_r=k, \beta_i=-0.2k$	45
3-7	Calculated Patterns .	49
3-8	Influences of β_r on the Patterns .	50
3-9	Influence of β_i on the Patterns .	51
4-1	Near Field Measurements of E_r .	55
4-2	The Set-up for Measurement of β_r .	57
4-3	Measurements of the Guided Wavelength Along the Antenna .	58
4-4	The Measured Patterns of the Bifilar Helical Antenna with an Outer Layer of Ferrite (L=15 in.) .	62
4-5	The Measured Patterns of the Bifilar Helical Antenna with an Outer Layer of Ferrite (L= 25 in.) .	63
4-6	The Measured Patterns of the Unloaded Bifilar Helical Antenna (L= 25 in.) .	64
C-1	Graphical Solution of the Equation $x=\tan x$.	78
C-2	$f(x) = \sin x/x$ and its Zeros and Extremums .	81
C-3	Relative Positions of Maximums and Zeros of $ A(\theta) $.	86
C-4	Relative Levels of $ A(\theta) $.	87
C-5	Factor $A(\theta)$ for Fast Waves .	89
C-6	$ A(\theta) $ for Fast Waves, $\beta/k = 0.6$.	92
C-7	$ A(\theta) $ for Slow Waves, $\beta/k = 1.3$.	95
C-8	$ A(\theta) $ for Slow Waves, $kL=12\pi$.	98
C-9	Effects of β/k on $ A(\theta) $, $kL=12\pi$.	99
C-10	The Function $F(x, y)$ in Eq. (C.6) .	101
C-11	Effect of β_i on $ A(\theta) $, $\beta_r/k = 0.8$.	103
C-12	Effects of β_i on $ A(\theta) $, $\beta_r/k = 1.0$.	104
C-13	Effects of β_i on $ A(\theta) $, $kL = 12 \pi$.	105

LIST OF APPENDICES

A	SOME USEFUL RELATIONS INVOLVING THE BESSEL FUNCTIONS WITH COMPLEX ARGUMENT	70
B	EVALUATION OF THE UNDETERMINED COEFFICIENTS IN CONNECTION WITH THE FIELDS ON THE ANTENNA	73
C	A FACTOR $A(\theta)$ FOR THE FAR FIELDS OF SOME LONG ANTENNAS	75
	C. 1 Introduction	75
	C. 2 The Factor $A(\theta)$	75
	C. 3 Properties of the Real Function $f(x)$	77
	C. 4 The Mapping $x(\theta)$ and its Inverse for a Real β	80
	C. 5 The Factor $A(\theta)$ for a Real Propagation β	83
	C. 6 Classification of Waves	85
	C. 7 Fast Waves with a Real Propagation Constant β	88
	C. 8 Slow Waves with a Real Propagation Constant β	91
	C. 9 The Factor $A(\theta)$ with a Complex Propagation Constant $\beta = \beta_r + j\beta_i$	97

I

INTRODUCTION

The work on the helix antenna dates back as early as 1897, when Pocklington¹¹ formulated an integral equation for the structure and obtained two approximate solutions. After the use of the structure as a slow wave device in traveling wave tubes and as an antenna, the literature on the helix becomes very large. An extensive bibliography on the work before 1955 can be found in Sensiper^{1, 2}.

In dealing with the boundary value problem associated with an infinite helix, two models are generally used. These are the sheath model and the tape model. In the sheath model, the helix winding is assumed to be infinitesimally thin. Each of the wave functions in cylindrical coordinates is found to satisfy the boundary conditions. Each can therefore be referred to as a mode of the infinite helix. In the tape mode, the finite width of the helix winding is taken into consideration. No single mode can satisfy the corresponding boundary value problem. An infinite series of all the wave functions is required to satisfy the boundary conditions.

Prior to 1962, the solutions to the characteristic equation were restricted to real roots. Complex roots were thought to be non-existent². Mittra³ was first in suggesting the existence of the complex roots and their importance in the radiation phenomenon of the helical antenna. Subsequently, Klock⁴ made an extensive study on these complex roots based on the tape model. He found, among other things, that there were many different branches of roots to the equation.

Rassweiler⁵, with an eye on size reduction, worked on the problem of the loaded helical antenna, or more specifically, on infinite helix with a solid core of ferrite or dielectric material.

Another class of work on the helix as a radiator deals with the far field patterns of a finite helix. Kraus and Williamson¹² calculated the far fields of the helical antenna from the current wave on the winding. An empirically determined phase constant was used for the current. Patton¹³ also obtained the far field pattern, using a transform method.

Also relevant to the present work is the extensive collection of research results on tube antennas and rod antennas. Different approaches were used to calculate the radiation patterns of these antennas. A careful survey of the various approaches is given by Chen⁹. The endfire radiation mechanism of these antennas is attributed to the HE_{11} mode excited on the structure.

The present work deals with a helical antenna loaded with an outer layer of ferrite. From another point of view, the structure can equally well be described as a tube antenna excited by helical windings inside.

It is interesting to note that present explanations of the radiation process of helical antennas are different from those of tube and rod antennas. The radiation of helical antennas is explained by a wave traveling along the helical winding with a phase velocity of the order of the free space light velocity. The radiation of a tube or a rod antenna is explained, on the other hand, by a wave traveling along the axis of the antenna with a velocity close to the free space light velocity.

With a wave-like source distribution, the radiation pattern is determined largely by a propagation constant of the wave which comes from the solution to the characteristic equation. The characteristic equation for either the tube antenna or the helical antenna is very complicated and involves some transcendental functions. It is found that the characteristic equation to the helix has many roots. This multi-root situation is quite common to equations involving transcendental functions. Inasmuch as all the roots are valid mathematical solutions to the characteristic equation, it remains to be decided which are responsible for the far field radiation phenomenon of the antenna.

This critical question is answered for the particular type of antennas considered in this text.

The radiation pattern is then calculated based on the knowledge of the propagation constant. It is obvious that the method of direct integration of the current on the helical winding is not applicable in the present case. The fields on the outer surface of the ferrite layer are integrated instead, using Schelkunoff's Equivalence Principle⁷. The contributions to the far fields from the end faces and from the side cylindrical surface are looked at separately. It is found that the side cylindrical surface is mainly responsible for the radiation phenomenon of the antenna through a factor $A(\theta)$. The factor $A(\theta)$ is, in turn, largely determined by the complex propagation constant β .

II

THE SHEATH HELIX

2.1 Models for Solving the Propagation Constant of Helices

There are two models that can be used to solve the propagation constant of the helical structure. These are the sheath model and the tape model. The sheath model assumes infinitesimal width for the helical winding. Using this model, cylindrical wave functions corresponding to any integer n can be used to meet the boundary conditions. The resultant characteristic equation consists of modified Bessel function of n -th order and some other elementary functions. The tape model takes into account the finite width of the helical winding. An infinite series of wave functions corresponding to all integers n have to be used to satisfy the boundary conditions. The resultant characteristic equation consists of an infinite sum of modified Bessel functions of integer orders. The tape model, while a more realistic physical model, poses a considerably more difficult task in the numerical calculation than the sheath model. For thin helical windings, the numerical results of both models have been found to be in close agreement.

The characteristic equation of the helix as a transcendental equation has many branches of roots as noted before. These roots are normally obtained numerically by a trial and error (or iteration) process. The selected initial trial values for the process have much to do with the final result. Obviously, different initial trial values might well lead to roots on different branches of the k - β diagram. For example, Klock⁴ has found at least five different branches of roots and numbered these mode 1 to mode 5. Rassweiler⁵ also reported the existence of a high attenuation mode in addition to the so called "slow wave approximation" solutions which he placed much emphasis on. There is no doubt that all these roots are valid mathematical solutions to the characteristic equation. It is also possible that many of them can be excited by proper feeding

techniques. The question remains as to which of these roots would be responsible for the endfire operation of the helical antenna. Amazingly, very little work has been done toward answering this important question. One unfortunate result is that some roots that are taken for granted to be responsible for the radiation phenomenon of loaded helical antennas do not really have anything to do with the mechanism.

The critical problem facing the solution of the characteristic equation is therefore the determination of the right branch of roots. It is felt that the use of the sheath model is adequate for this purpose. This is especially true if one is mainly interested in the far fields, which do not change much with small variations of the source distribution. The use of the more rigorous but also much more complicated tape model for pattern calculation would hardly be worthwhile. The misuse of a wrong mode, on the other hand, would cause drastic changes in both the source distribution and the far fields.

In the next section, a characteristic equation for a helical antenna with an outer layer of ferrite loading will be given based on the sheath model, followed by results of numerical calculation.

2.2 An Infinite Helix with an Outer Layer of Loading Material; The Sheath Model

Figure 2-1 shows an infinite helix with an outer layer of loading material. The wave functions \bar{E} and \bar{H} , which satisfy the wave equation

$$(\nabla^2 + k^2) \begin{pmatrix} \bar{E} \\ \bar{H} \end{pmatrix} = 0 \quad (2.1)$$

will be given in cylindrical coordinates. Only two of the six components of \bar{E} and \bar{H} are independent in each region. We will pick E_z and H_z as these two independent components. Other components can then be expressed as a combination of E_z and H_z . The functions I_n and K_n in the expressions of the fields are Bessel functions as defined in Watson. Omitting the time harmonic factor $e^{j\omega t}$, the wave functions are:

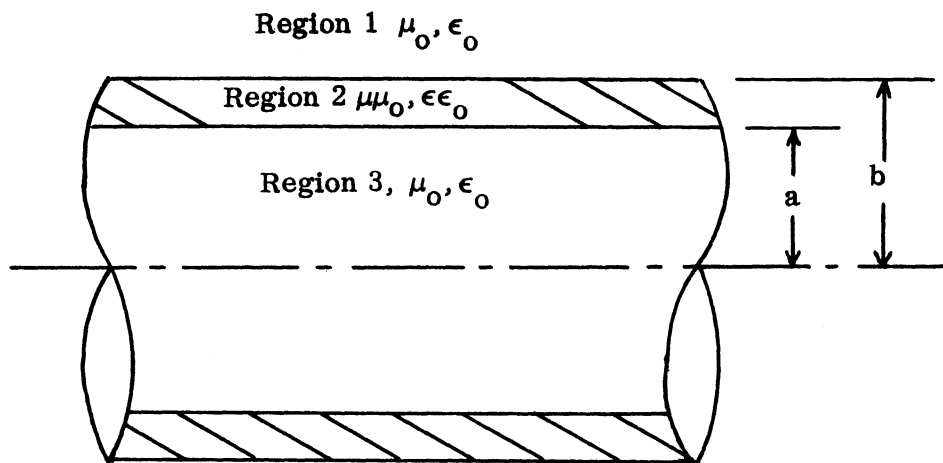


FIG. 2-1: An Infinite Helix with an Outer Layer of Ferrite.
The helix winding is on the cylindrical surface $r=a$.

Region I:

$$E_{zn} = F_n K_n(\Gamma_n r) e^{j(n\phi - \beta_n z)} \quad (2.2)$$

$$H_{zn} = G_n K_n(\Gamma_n r) e^{j(n\phi - \beta_n z)} \quad (2.3)$$

where F_n, G_n are constants,

$$\Gamma_n = \sqrt{\beta_n^2 - k^2} \quad (2.4)$$

n is any integer.

Region II:

$$e_{zn} = f_n \left[I_n(\gamma_n r) + C_{1n} K_n(\gamma_n r) \right] e^{j(n\phi - \beta_n z)} \quad (2.5)$$

$$h_{zn} = g_n \left[I_n(\gamma_n r) + C_{2n} K_n(\gamma_n r) \right] e^{j(n\phi - \beta_n z)} \quad (2.6)$$

$$\gamma_n = \sqrt{\beta_n^2 - k^2 \mu \epsilon} \quad (2.7)$$

Region III:

$$E_{zn}^{(3)} = F_n^{(3)} I_n(\Gamma_n r) e^{j(n\phi - \beta_n z)} \quad (2.8)$$

$$H_{zn}^{(3)} = G_n^{(3)} I_n(\Gamma_n r) e^{j(n\phi - \beta_n z)} \quad (2.9)$$

For wave functions E_z and H_z of the form $Z_n(\gamma r) e^{j(n\phi - \beta_n z)}$, where $Z_n(\gamma r)$ is any linear combination of $I_n(\gamma r)$ and $K_n(\gamma r)$, the other components are given by:

$$E_{\phi n} = (-) \frac{\beta_n}{\gamma^2 r} E_{zn} + \left(\frac{-j\omega\mu}{\gamma} \right) \frac{\partial H_{zn}}{\partial(\gamma r)} \quad (2.10)$$

$$H_{\phi n} = \frac{j\omega\epsilon}{\gamma} \frac{\partial E_z}{\partial(\gamma r)} - \frac{\beta n}{\gamma^2} H_z, \quad (2.11)$$

$$E_{rn} = \frac{j\beta}{\gamma} \frac{\partial E_z}{\partial(\gamma r)} - \frac{\omega\mu n}{\gamma^2} H_z, \quad (2.12)$$

$$H_{rn} = \frac{\omega\epsilon n}{\gamma^2} E_z + \frac{j\beta}{\gamma} \frac{\partial H_z}{\partial(\gamma r)}. \quad (2.13)$$

For the sheath helix, it is found that each set of the vectors \bar{E}_n and \bar{H}_n corresponding to any integer n are sufficient to meet the boundary conditions of the structure under consideration by themselves in the absence of a source. Each set of these vectors are therefore a solution to the source free boundary value problem and may be referred to as a mode. In the presence of a source, a solution can in principle be found as a linear combination of all these modes. In the subsequent derivation of the characteristic equation for the sheath helix, we shall suppress the subscript n in connection with the quantities γ_n , Γ_n , F_n , G_n , etc. and the functions I_n and K_n . Making use of (2.10) through (2.13), the other components are found as, suppressing the factor $e^{j(\omega t + n\phi - \beta z)}$:

Region I:

$$E_r = \frac{j\beta F}{\Gamma} \frac{\partial K(\Gamma r)}{\partial(\Gamma r)} - \frac{\omega\mu_0 n}{\Gamma^2} G K(\Gamma r) \quad (2.14)$$

$$E_{\phi} = (-1) \frac{F n \beta}{\Gamma^2} K(\Gamma r) - \frac{G j \omega \mu_0}{\Gamma} \frac{\partial K(\Gamma r)}{\partial(\Gamma r)} \quad (2.15)$$

$$H_r = \frac{\omega\epsilon_0 n F}{\Gamma^2} K(\Gamma r) + \frac{j\beta G}{\Gamma} \frac{\partial K(\gamma r)}{\partial(\gamma r)} \quad (2.16)$$

$$H_{\phi} = F \frac{j\omega\epsilon_0}{\Gamma} \frac{\partial K(\Gamma r)}{\partial(\Gamma r)} - G \left(\frac{n\beta}{\Gamma^2} \right) K(\Gamma r) \quad (2.17)$$

Region II:

$$e_r = \frac{j\beta f}{\gamma} \left[\frac{\partial I(\gamma r)}{\partial(\gamma r)} + C_1 \frac{\partial K(\gamma r)}{\partial(\gamma r)} \right] - \frac{\omega \mu \mu_0 n g}{\gamma^2 r} \left[I(\gamma r) + C_2 K(\gamma r) \right] \quad (2.18)$$

$$e_\phi = (-) \frac{fn\beta}{\gamma^2 r} \left[I(\gamma r) + C_1 K(\gamma r) \right] - \frac{gj\omega\mu\mu_0}{\gamma} \left[\frac{\partial I(\gamma r)}{\partial(\gamma r)} + C_2 \frac{\partial K(\gamma r)}{\partial(\gamma r)} \right] \quad (2.19)$$

$$h_r = \frac{\omega \epsilon_0 n f}{\gamma^2 r} \left[I(\gamma r) + C_1 K(\gamma r) \right] + \frac{j\beta g}{z} \left[\frac{\partial I(\gamma r)}{\partial(\gamma r)} + C_2 \frac{\partial K(\gamma r)}{\partial(\gamma r)} \right] \quad (2.20)$$

$$h_\phi = f \frac{j\omega\epsilon_0}{\gamma} \left[\frac{\partial I(\gamma r)}{\partial(\gamma r)} + C_1 \frac{\partial K(\gamma r)}{\partial(\gamma r)} \right] - \frac{gn\beta}{\gamma^2 r} \left[I(\gamma r) + C_2 K(\gamma r) \right] \quad (2.21)$$

Region III:

$$E_r^{(3)} = \frac{j\beta F^{(3)}}{\Gamma} \frac{\partial I(\Gamma r)}{\partial(\Gamma r)} - \frac{\omega \mu_0 n}{\Gamma^2 r} G^{(3)} I(\Gamma r) \quad (2.22)$$

$$E_\phi^{(3)} = (-) \frac{F^{(3)} n \beta}{\Gamma^2 r} I(\Gamma r) - \frac{G^{(3)} j\omega\mu_0}{\Gamma} \frac{\partial I(\Gamma r)}{\partial(\Gamma r)} \quad (2.23)$$

$$H_r^{(3)} = \frac{\omega \epsilon_0 n F^{(3)}}{\Gamma^2 r} I(\Gamma r) + \frac{j\beta G^{(3)}}{\Gamma} \frac{\partial I(\Gamma r)}{\partial(\Gamma r)} \quad (2.24)$$

$$H_\phi^{(3)} = \frac{F^{(3)} j\omega\epsilon_0}{\Gamma} \frac{\partial I(\Gamma r)}{\partial(\Gamma r)} - \frac{G^{(3)} n \beta}{\Gamma^2 r} I(\Gamma r) \quad (2.25)$$

There are four independent boundary conditions on each boundary. For $r = b$,

$$E_\phi = e_\phi \quad (2.26)$$

$$E_z = e_z \quad (2.27)$$

$$H_{\phi} = h_{\phi} \quad (2.28)$$

$$H_z = h_z \quad (2.29)$$

can be used. For $r = a$,

$$e_{\phi} = E_{\phi}^{(3)} \quad (2.30)$$

$$e_z = E_z^{(3)} \quad (2.31)$$

$$e_z + e_{\phi} \cot \psi = 0 \quad (2.32)$$

$$h_z + h_{\phi} \cot \psi - H_z^{(3)} - H_{\phi}^{(3)} \cot \psi = 0 \quad (2.33)$$

can be used. The angle ψ in (2.32) and (2.33) is the pitch angle of the helix. Note that (2.32) says the component of \bar{E} tangential to the helical winding is zero. (2.33) says the component of \bar{H} parallel to the winding is continuous.

(2.26) through (2.33) form a set of eight homogeneous equations for the eight undetermined coefficients $F, G, f, g, fC_1, gC_2, F^{(3)}$ and $G^{(3)}$. For non-trivial solution to exist, the determinant of the coefficients must be zero. This condition would yield the characteristic equation for the infinite helix. We will, however, follow a more detailed elimination process which would provide values of the undetermined coefficients f, g , etc., Substitute the wave functions into (2.27), we get

$$FK(\Gamma b) = f \left[I(\gamma b) + C_1 K(\gamma b) \right] . \quad (2.34)$$

Substitute the wave functions into (2.29), we get

$$GK(\Gamma b) = g \left[I(\gamma b) + C_2 K(\gamma b) \right] . \quad (2.35)$$

Substituting (2.34), (2.35), and the wave functions, (2.26) becomes, after collecting terms,

$$p_1(fC_1) + q_1(gC_2) = s_1 f + t_1 g \quad . \quad (2.36)$$

The same process for (2.28) gives

$$p_2(fC_1) + q_2(gC_2) = s_2 f + t_2 g \quad (2.37)$$

where

$$p_1 = \frac{n\beta}{b} \left(\frac{1}{\gamma^2} - \frac{1}{\Gamma^2} \right) K(\gamma b) \quad , \quad (2.38)$$

$$q_1 = j\omega\mu_o \left[\frac{\mu}{\gamma} K'(\gamma b) - \frac{1}{\Gamma} \frac{K'(\Gamma b)}{K(\Gamma b)} K(\gamma b) \right] \quad , \quad (2.39)$$

$$s_1 = \frac{n\beta}{b} \left(\frac{1}{\Gamma^2} - \frac{1}{\gamma^2} \right) I(\gamma b) \quad , \quad (2.40)$$

$$t_1 = j\omega\mu_o \left[\frac{1}{\Gamma} \frac{K'(\Gamma b)}{K(\Gamma b)} I(\gamma b) - \frac{\mu}{\gamma} I'(\gamma b) \right] \quad (2.41)$$

$$p_2 = j\omega\epsilon_o \left[\frac{1}{\Gamma} \frac{K'(\Gamma b)}{K(\Gamma b)} K(\gamma b) - \frac{\epsilon}{\gamma} K'(\gamma b) \right] \quad , \quad (2.42)$$

$$q_2 = p_1 \quad , \quad (2.43)$$

$$s_2 = j\omega\epsilon_o \left[\frac{\epsilon}{\gamma} I'(\gamma b) - \frac{1}{\Gamma} \frac{K'(\Gamma b)}{K(\Gamma b)} I(\gamma b) \right] \quad , \quad (2.44)$$

$$t_2 = s_1 \quad , \quad (2.45)$$

f and g can now be solved in terms of fC_1 and gC_2 .

$$f = D^{pt}(fC_1) + D^{qt}(gC_2) \quad , \quad (2.46)$$

$$g = D^{sp}(fC_1) + D^{sq}(gC_2) \quad , \quad (2.47)$$

where D^{pt} , D^{qt} , D^{sp} , D^{sq} are given by the formula

$$D^{ab} = \frac{\Delta_{ab}}{\Delta_{st}} \quad , \quad (2.48)$$

$$\Delta_{ab} = a_1 b_2 - a_2 b_1 \quad , \quad (2.49)$$

$$\Delta_{st} = s_1 t_2 - s_2 t_1 \quad . \quad (2.50)$$

Substitute (2.30) and (2.31) in (2.33) to eliminate $F^{(3)}$ and $G^{(3)}$,

$$\begin{aligned} & f \frac{j\omega\epsilon_0}{\gamma} \left[I'(\gamma a) + C_1 K'(\gamma a) \right] \cot \psi + g \left[I(\gamma a) + C_2 K(\gamma a) \right] \left(1 - \frac{n\beta}{\gamma^2 a} \cot \psi \right) \\ & - f \frac{\left[I(\gamma a) + C_1 K(\gamma a) \right]}{I(\Gamma a)} \frac{j\omega\epsilon_0}{\Gamma} I'(\Gamma a) \cot \psi \\ & + \left(1 - \frac{n\beta}{\Gamma^2 a} \cot \psi \right) I(\Gamma a) \frac{\Gamma}{j\omega\mu_0 I'(\Gamma a)} \\ & \cdot \left\{ \frac{fn\beta}{a} \left(\frac{1}{\Gamma^2} - \frac{1}{\gamma^2} \right) \left[I(\gamma a) + C_1 K(\gamma a) \right] - \frac{gj\omega\mu_0}{\gamma} \left[I'(\gamma a) + C_2 K'(\gamma a) \right] \right\} \\ & = 0 \quad . \quad (2.51) \end{aligned}$$

Substitute (2.46) and (2.47) in (2.51). After rearranging terms,

$$\begin{aligned} & (A_1 D^{pt} + A_2 D^{sp} + A_3) (fC_1) \\ & + (A_1 D^{qt} + A_2 D^{sq} + A_4) (gC_2) = 0 \quad . \quad (2.52) \end{aligned}$$

Substitute (2.46) and (2.47) in (2.32) and rearrange terms,

$$A_5(fC_1) + A_6(gC_2) = 0 \quad (2.53)$$

The coefficients A_i 's are given by

$$A_1 = \frac{j\omega\epsilon_0}{\gamma} I'(\gamma a) \cot \psi - \frac{I(\gamma a)}{I(\Gamma a)} \frac{j\omega\epsilon_0}{\Gamma} I(\Gamma a) \cot \psi \\ + \left(1 - \frac{n\beta}{\Gamma^2 a} \cot \psi\right) \frac{I}{j\omega\mu_0} \frac{I(\Gamma a)}{I'(\Gamma a)} \frac{n\beta}{a} \left(\frac{1}{\Gamma^2} - \frac{1}{\gamma^2}\right) I(\gamma a) \quad (2.54)$$

$$A_2 = \left(1 - \frac{n\beta}{\gamma^2 a} \cot \psi\right) I(\gamma a) - \left(1 - \frac{n\beta}{\Gamma^2 a} \cot \psi\right) \frac{\mu\Gamma I(Ia)}{\gamma I'(\Gamma a)} I'(\gamma a) \quad (2.55)$$

$$A_3 = \frac{j\omega\epsilon_0}{\gamma} K'(\gamma a) \cot \psi - \frac{j\omega\epsilon_0}{\Gamma} \frac{K(\gamma a)}{I(\Gamma a)} I'(\Gamma a) \cot \psi \\ + \left(1 - \frac{n\beta}{\Gamma^2 a} \cot \psi\right) \frac{\Gamma}{j\omega\mu_0} \frac{I(\Gamma a)}{I'(\Gamma a)} \frac{n\beta}{a} \left(\frac{1}{\Gamma^2} - \frac{1}{\gamma^2}\right) K(\gamma a) \quad (2.56)$$

$$A_4 = \left(1 - \frac{n\beta}{\gamma^2 a} \cot \psi\right) K(\gamma a) - \left(1 - \frac{n\beta}{\Gamma^2 a} \cot \psi\right) \frac{\mu\Gamma I(\Gamma a)}{\gamma I'(\Gamma a)} K(\gamma a) \quad (2.57)$$

$$A_5 = \left(1 - \frac{\beta n}{\gamma^2 a} \cot \psi\right) \left[D^{pt} I(\gamma a) + K(\gamma a) \right] \\ - \frac{j\omega\mu_0}{\gamma} I'(\gamma a) \cot \psi D^{sp} \quad (2.58)$$

$$A_6 = D^{qt} \left(1 - \frac{\beta n}{\gamma^2 a} \cot \psi\right) - \frac{j\omega\mu_0}{\gamma} \cot \psi \left[I'(\gamma a) D^{sq} + K'(\gamma a) \right] \quad (2.59)$$

(2.52) and (2.53) are two homogeneous equations for fC_1 and gC_2 . The condition for nontrivial solutions to exist is the determinant of the coefficients to be zero. Or,

$$\begin{aligned} & (A_1 D^{pt} + A_2 D^{sp} + A_3) \cdot A_6 \\ & - (A_1 D^{qt} + A_2 D^{sq} + A_4) \cdot A_5 = 0 \end{aligned} \quad (2.60)$$

(2.60) is the characteristic equation for the infinite helix with an outer layer of loading. We will look at some limit cases in the next section.

2.3 The Unloaded Sheath Helices

The dispersion equation for the unloaded helices can be obtained from (2.60). This is done by putting $\mu = 1$ and $\epsilon = 1$. From (2.4) and (2.7),

$$\gamma = \Gamma = \sqrt{\beta^2 - k^2} \quad (2.61)$$

From (2.61) and (2.38) - (2.45), it is not hard to see that the D's in (2.48) also reduce to zero.

$$D^{sp} = D^{pt} = D^{qt} = D^{sq} = 0 \quad (2.62)$$

Making use of (2.61) and (2.62), (2.60) becomes

$$\begin{aligned} & \frac{\omega^2 \mu_0 \epsilon_0}{\Gamma^2} \cot^2 \psi \left[K'(\Gamma r) I(\Gamma r) - I'(\Gamma a) K(\Gamma r) \right] \frac{K'(\Gamma r)}{I(\Gamma r)} \\ & = \left(1 - \frac{n\beta}{\Gamma_a^2} \cot \psi \right)^2 \left[K(\Gamma r) I'(\Gamma r) - I(\Gamma r) K'(\Gamma r) \right] \frac{K(\Gamma r)}{I'(\Gamma r)} \end{aligned} \quad (2.63)$$

This can be simplified further by recognizing the factor in the square brackets as the Wronskian of the Bessel equation

$$I_n(z) K_n'(z) - I_n'(z) K_n(z) = \frac{-1}{z} \quad . \quad (2.64)$$

Using (2.64), (2.63) reduces to

$$\frac{I'(\Gamma r) K'(\Gamma r)}{I(\Gamma r) K(\Gamma r)} = (-) \frac{(\Gamma^2 a^2 - n\beta a \cot \psi)^2}{k_o^2 a^4 \Gamma^2 a^2 \cot^2 \psi} \quad . \quad (2.65)$$

(2.65) is the unloaded sheath helix dispersion equation found in the literature^{2,5}.

2.4 The Very Slow Wave Approximation

In the case $\beta \gg \sqrt{\mu\epsilon} k_o > k_o$, it is seen $\beta \sim \Gamma \sim \gamma$. If the slow wave approximation, as defined in Rassweiler,

$$\beta = \Gamma = \gamma \quad (2.66)$$

is used, the characteristic equation (2.60) can be simplified a great deal.

$$\left\{ \begin{array}{l} p_1 = q_2 = s_1 = t_2 = 0 \\ p_2 = \frac{j\omega\epsilon_o}{\beta} (1 - \epsilon) K'(\beta b) \\ q_1 = \frac{j\omega\mu_o}{\beta} (\mu - 1) K'(\beta b) \\ s_2 = \frac{j\omega\epsilon_o}{\beta} \frac{\epsilon K(\beta b) I'(\beta b) - K'(\beta b) I(\beta b)}{K(\beta b)} \\ t_1 = \frac{j\omega\mu_o}{\beta} \frac{K'(\beta b) I(\beta b) - \mu I'(\beta b) K(\beta b)}{K(\beta b)} \end{array} \right. \quad (2.67)$$

$$\left\{ \begin{array}{l} D^{pt} = \frac{p_2}{s_2} \\ D^{sp} = D^{qt} = 0 \\ D^{sq} = \frac{q_1}{t_1} \end{array} \right. \quad (2.68)$$

From (2.66) - (2.68), (2.60) becomes

$$(A_1 D^{pt} + A_3) \cdot A_6 - (A_2 D^{sq} + A_4) \cdot A_5 = 0 \quad (2.69)$$

with A_i 's also simplified by (2.66) - (2.68). It can be shown, after lengthy algebra, (2.69) can also be put in the form

$$\frac{I'(\beta a) K'(\beta a)}{I(\beta a) K(\beta a)} = \frac{(-)(\beta a - n \cot \psi)^2}{C^2 k_o^2 a^2 \cot^2 \psi} \quad (2.69a)$$

where

$$C^2 = \mu \frac{K(\beta a) I'(\beta a)}{K'(\beta a) I(\beta a)} \frac{\epsilon \frac{I'(\beta a) + C_1 K'(\beta a)}{I(\beta a) + C_1 K(\beta a)} \frac{I(\beta a)}{I'(\beta a)} - 1}{1 - \frac{1}{\mu} \frac{I(\beta a) + C_2 K(\beta a)}{I'(\beta a) + C_2 K'(\beta a)}} \quad (2.70)$$

$$C_1 = \frac{K'(\beta b) I(\beta b) - \epsilon I'(\beta b) K(\beta b)}{(\epsilon - 1) K(\beta b) K'(\beta b)} \quad (2.71)$$

$$C_2 = \frac{K'(\beta b) I(\beta b) - \mu K(\beta b) I'(\beta b)}{(\mu - 1) K(\beta b) K'(\beta b)} \quad (2.72)$$

(2.69a) is in a form similar to the dispersion equations for the solid core loaded helical antennas and the inner layer loaded helical antennas in Rassweiler⁵.

The factor C in (2.70) would be referred to as the reduction factor using the terminology of the same reference.

It should be pointed out that solutions to the dispersion equations of the helices by various workers mostly fall into the very slow wave category. That is, $\beta \gg \sqrt{\mu\epsilon} k_0$ for the loaded helices and $\beta \gg k_0$ for the unloaded helices. This result is mainly due to the fact that the very high frequency asymptotic solution $\beta = k / \sin \psi$ is used as the starting point for the $k - \beta$ curve. Most workers, however, did not impose the slow wave approximation $\beta = \Gamma = \gamma$ used by Rassweiler.

2.5 Two Bases for the Selection of the Right Branch of Roots

Two ways have been used in this text to single out the right branch of roots that are responsible for the radiation phenomenon of the helical antenna with an outer layer of ferrite loading.

The first is through probing the near fields of the antenna. This is described in Chapter IV, the experimental part of this work.

The second method is an indirect one. The roots found from the characteristic equation can be used to compute the radiation pattern. The calculated patterns are then compared with the experimental patterns. The ones that do not give correct patterns can then be thrown out. Fortunately, for the type of antennas considered in this work, it is found that the pattern calculation can be replaced by the calculation of a relatively simple factor $A(\theta)$ for the purpose of sorting out the correct β that is responsible for the radiation mechanism of the antenna.

2.6 Numerical Solutions to the Characteristic Equations

The numerical solutions to the characteristic equation of the helical antenna with an outer layer of ferrite loading will be presented in this section. All results are based on the following parameters which correspond to the electrical and physical constants associated with the model antennas and the loading material used in this work.

$$\left\{ \begin{array}{l} \mu = 2.2 \\ \epsilon = 3.8 \\ \psi = 6.4^\circ \\ a = 0.054 \text{ m} \\ b = 0.060 \text{ m} \\ n = 1 \end{array} \right. \quad (2.73)$$

Now, the two bases for selecting the right root out of several known roots can as well be used as guide lines to pick proper initial trial values. This was found to result in great saving of computing time.

Results of the near field measurements are presented in Chapter IV. It is found that the near fields of the loaded helical antenna bear a resemblance to those of the unloaded helical antenna. The phase is found to increase almost linearly with distance as the probe goes away from the feeding point. The amplitude is found to decrease as the probe goes away from the feeding point. One way this kind of field can be described is

$$\left(\begin{array}{c} \bar{E} \\ \bar{H} \end{array} \right) \sim e^{-j\beta z} \quad (2.74)$$

with

$$\left\{ \begin{array}{l} \beta = \beta_r + j\beta_i \\ \beta_r < 0 \\ \beta_i < 0 \end{array} \right. \quad (2.75)$$

assuming the feeding point to be $z=0$ and the antenna extends along the positive z -axis. Equation (2.75) immediately puts a restraint on the solutions to the characteristic equation, i.e., β is in the third quadrant on the complex β plane. Furthermore, the approximate value of β_r is found to be near the free space wave number k . The first of the two bases set forth in Section 2.5, therefore, seems to point to a value for β as

$$\begin{cases} \beta \sim -k + j\beta_i \\ \beta_i < 0 \end{cases} \quad (2.76)$$

In Chapter III, it will be seen that the radiation pattern of the antenna is mainly determined by a factor $A(\theta)$, studied in great detail in Appendix C. Extensive calculations of $A(\theta)$ were made using different values of β_r and β_i . It is found that the only values of β that $A(\theta)$ can be backfire is when

$$\beta \sim (-)k \quad (2.77)$$

in the complex β plane. Equation (2.77) can be replaced by a set of two real relations

$$\begin{cases} \beta_r \sim (-)k \\ |\beta_i / \beta_r| \ll 1 \end{cases} \quad (2.77a)$$

On the basis of both (2.76) and (2.77), an initial value of β with

$$\begin{cases} \beta_r = -k \\ \beta_i = -0.1k \end{cases} \quad (2.78)$$

was fed in the program to obtain the propagation constant β at different frequencies. The result is shown in Fig. 2-2. Also shown in Fig. 2-2 is the result when the initial trial value of β is

$$\begin{cases} \beta_r = k \\ \beta_i = -0.1k \end{cases} \quad (2.79)$$

Only β_r is shown in Fig. 2-2, β_i is found to be zero for all values of k that the program was run. Note only part of the roots found with either (2.78) or (2.79) seem to be on the same branch. They are connected by solid straight lines in the order of increasing k . The two groups of connected points are

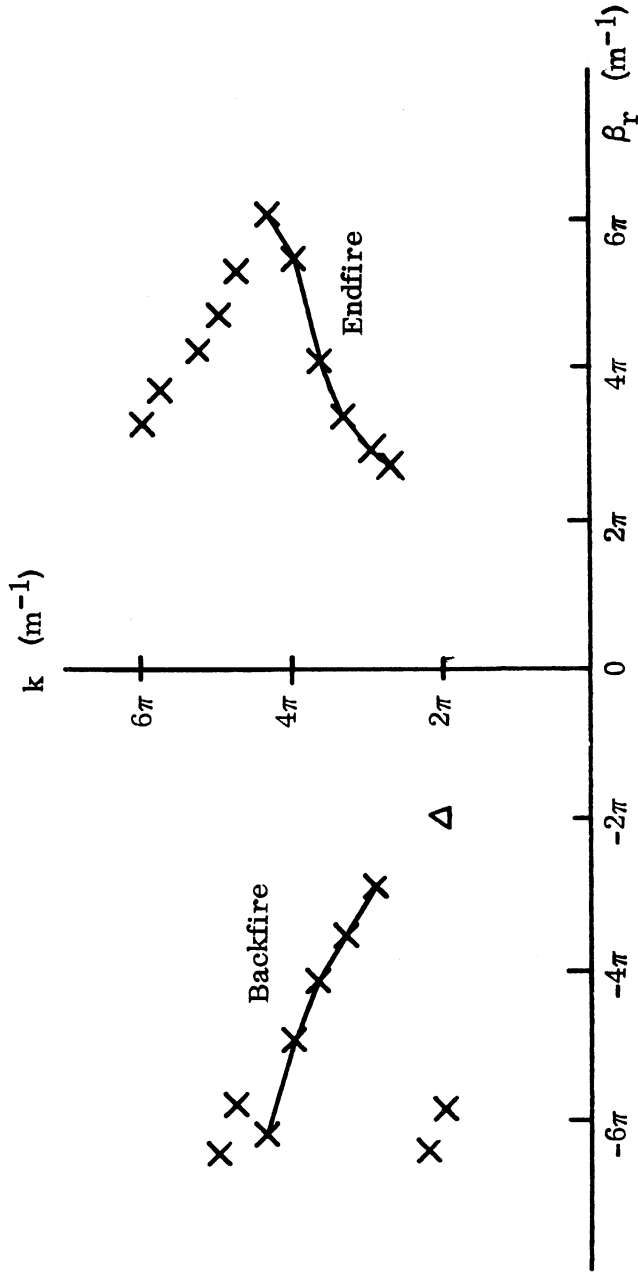


FIG. 2-2: Some Solutions to the Characteristic Equation (2.69) with Parameters as in (2.73). $0 =$ Initial Trial Values $\beta = k - j0.1k$, $X =$ Initial Trial Values $\beta = -k - j0.1k$, $\Delta =$ Initial Trial Value $\beta = -k$.

marked "Backfire" and "Endfire" because they would give these kinds of radiation patterns. The real antenna, as said before, is found to be backfire. Two scattered roots are found with either (2.78) or (2.79) as the initial trial value. Since these points correspond to the two smallest values of k in each case, the question arises as to whether this would indicate the end of the two branches and hence the low frequency cut-off point for each of the two modes. This important question, along with a few others, cannot be answered without going into a study of the numerical techniques used to solve the characteristic equation. One fundamental difficulty with the present program is that it does not ensure any initial trial value would converge to the nearest root in the complex β plane. For instance, for $k=2\pi(m^{-1})$, $\beta=(-)k + j0$ is found to be a root to the characteristic equation. This is indicated by the small triangle in Fig. 2-2. However, also for $k=2\pi(m^{-1})$, an initial trial value given by (2.78) is found to converge to the point $\beta = (-) 18.2 + j0$ instead of $\beta = (-)k + j0$ by the present program. Another interesting question, also of importance, is whether the roots show any symmetry on the complex β plane. For example, would the existence of $\beta = \beta_r + j\beta_i$ as a root imply that $\beta = -\beta_r + j\beta_i$ or $\beta = \beta_r - j\beta_i$ is also a root? Again, no generalized conclusion can be made. Figure 2-3 shows the roots found from some random choices of initial trial values. A straight line is used to connect an initial trial value and the root it converges to. The line, however, has nothing to do with the actual path of convergence in the complex β plane. The program is made to stop if no root is reached after 30 iterations. This was the case with one trial value, although the path was definitely leading to a root. It should be apparent from this figure that, for the most part, better initial trial values save computer time due to the faster converging rate. It should be emphasized at this point that the actual number of roots is likely to be much larger than those shown in Fig. 2-3. No attempt was made to obtain more roots since it was felt that no purpose would be served.

In Chapter III, the radiation patterns will be calculated using the backfire mode shown in Fig. 2-2.

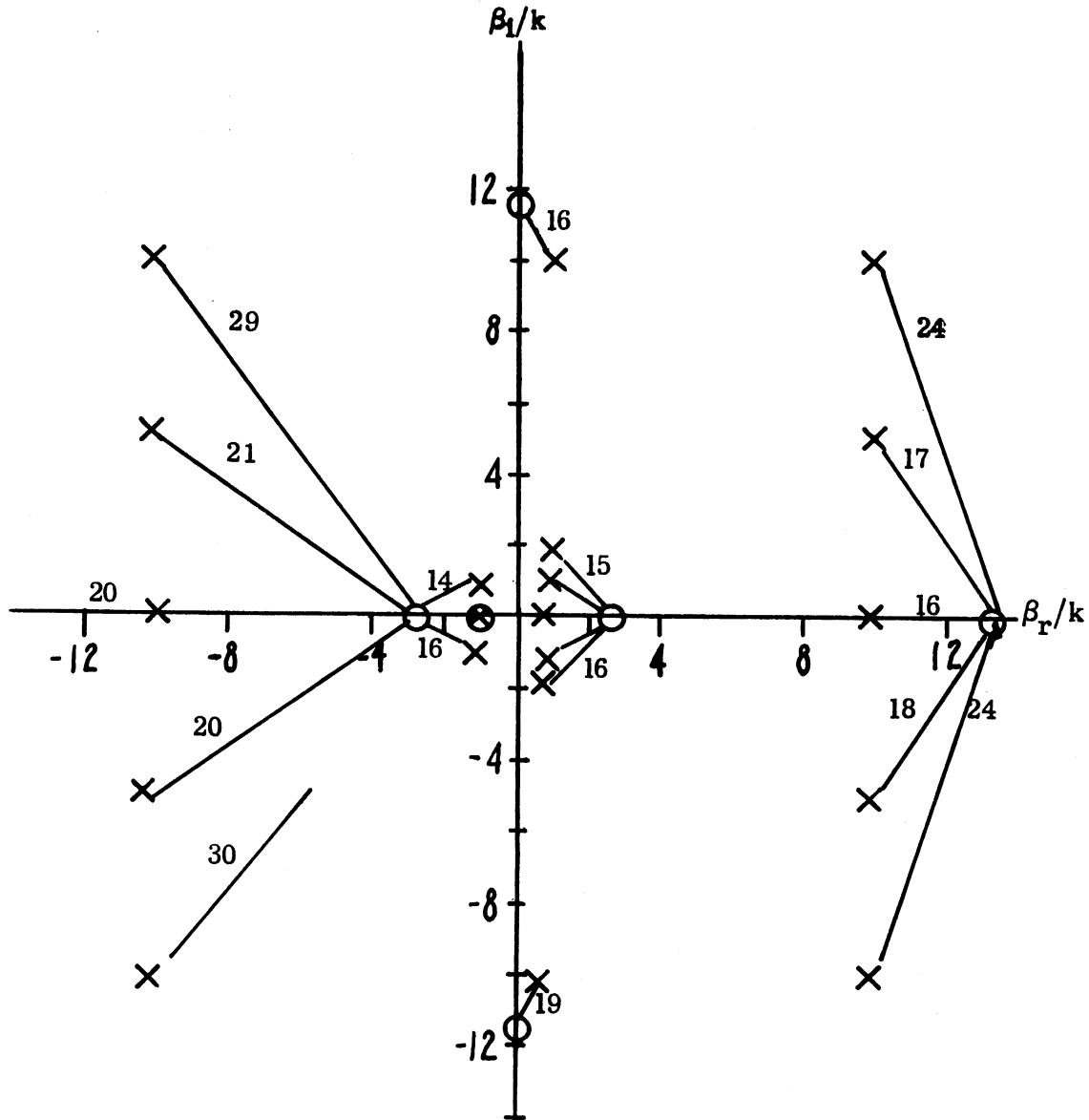


FIG. 2-3: Some Roots to the Characteristic Equation, $k=2\pi(m^{-1})$. An initial trial value and the root it converges to are connected by a straight line. The number by the straight line indicates the number of iterations required for convergence to the root.

III

THE RADIATION PATTERNS OF THE TUBE ANTENNA EXCITED BY A BIFILAR HELIX

3.1 The Equivalence Principle

The radiation patterns of a tube antenna can be evaluated by means of the Equivalence Principle^{6, 7, 8}. The knowledge of the fields on the surface of the antenna is required. The tangential component of the magnetic field on the surface of the antenna is replaced by an equivalent electric surface current

$$\bar{K} = \hat{n} \times \bar{H}' \quad (3.1)$$

where \hat{n} is the outward pointing unit normal vector to the surface. The tangential component of the electric field on the surface is replaced by a fictitious magnetic surface current

$$\bar{K}_m = (-) \hat{n} \times \bar{E}'' \quad (3.2)$$

The Equivalence Principle states that the fields exterior to the antenna surface would remain unchanged if the surface fields \bar{H}' and \bar{E}'' were replaced by the two equivalent surface currents. The two surface currents are to be treated as independent sources. The resultant far fields would be the superposition of the fields generated by each source;

$$\begin{aligned} \bar{E} &= \bar{E}' + \bar{E}'' \\ \bar{H} &= \bar{H}' + \bar{H}'' \end{aligned} \quad (3.3)$$

where \bar{E} , \bar{H} are the resultant fields,

\bar{E}' , \bar{H}' are the fields generated by \bar{K} ,

\bar{E}'' , \bar{H}'' are the fields generated by \bar{K}_m .

The fields \bar{E}' , \bar{H}' are related to the vector potential \bar{A}

$$\bar{A} = \mu_0 \iint \bar{K}(\bar{R}') G(\bar{R}, \bar{R}') ds' \quad (3.4)$$

where $G(\bar{R}, \bar{R}')$ is the free space Green's function

$$G(\bar{R}, \bar{R}') = \frac{e^{-jk|\bar{R}-\bar{R}'|}}{4\pi|\bar{R}-\bar{R}'|} \quad (3.5)$$

The unprimed coordinate variables will be used throughout this Chapter as the field point coordinates. The primed variables will be used as the source point coordinates. The integral (3.4) is over the surface of the antenna,

$$\bar{E}' = (-)j \frac{\omega}{k^2} \nabla_x \nabla_x \bar{A} \quad (3.6)$$

$$\bar{H}' = \frac{1}{\mu_0} \nabla_x \bar{A} \quad (3.7)$$

The fields \bar{E}'' and \bar{H}'' are related to the magnetic vector potential \bar{A}_m

$$\bar{A}_m = \epsilon_0 \iint \bar{K}_m(\bar{R}') G(\bar{R}, \bar{R}') ds' \quad (3.8)$$

$$\bar{E}'' = (-) \frac{1}{\epsilon_0} \nabla_x \bar{A}_m \quad (3.9)$$

$$\bar{H}'' = (-) j \frac{\omega}{k^2} \nabla_x \nabla_x \bar{A}_m \quad (3.10)$$

For the far fields, it can be shown

$$\bar{A} = \mu_0 g_0(R) \bar{N}(\theta, \phi) \quad (3.11)$$

$$\bar{A}_m = \epsilon_0 \eta_0 g_0(R) \bar{M}(\theta, \phi) \quad (3.12)$$

where

$$\bar{N} = \iint \bar{K}(\bar{R}') e^{+jk\bar{R}' \cdot \hat{R}} ds' \quad (3.13)$$

$$\bar{\mathbf{M}} = \frac{1}{\eta_0} \iint \bar{\mathbf{K}}_m(\bar{\mathbf{R}}') e^{+jk\bar{\mathbf{R}}' \cdot \mathbf{R}} ds' \quad (3.14)$$

and $g_0(\mathbf{R})$ is the free space Green's function

$$g_0(\mathbf{r}) = \frac{1}{4\pi} \frac{e^{-jkR}}{R} \quad (3.15)$$

$\bar{\mathbf{N}}$ and $\bar{\mathbf{M}}$ are known as the electric and magnetic radiation vectors respectively. Note that the vector $\bar{\mathbf{M}}$ as defined in (3.14) differs from the Schelkunoff expression by the factor $1/\eta_0$. $\bar{\mathbf{E}}$ and $\bar{\mathbf{H}}$ in the far fields can be expressed in terms of $\bar{\mathbf{M}}$ and $\bar{\mathbf{N}}$,

$$\bar{\mathbf{E}} = jk\eta_0 \left[-\bar{\mathbf{N}}_t + \hat{\mathbf{R}} \times \bar{\mathbf{M}}_t \right] g_0(\mathbf{R}) \quad (3.16)$$

$$\bar{\mathbf{H}} = (-)jk \left[\bar{\mathbf{M}}_t + \hat{\mathbf{R}} \times \bar{\mathbf{N}}_t \right] g_0(\mathbf{R}) \quad (3.17)$$

where $\bar{\mathbf{M}}_t$ and $\bar{\mathbf{N}}_t$ are the components of $\bar{\mathbf{M}}$ and $\bar{\mathbf{N}}$ perpendicular to the direction of propagation $\hat{\mathbf{R}}$. In the following sections, the surface fields pertaining to the infinite tube will be used as the surface fields on the finite tube to find the far field expressions for $\bar{\mathbf{M}}$, $\bar{\mathbf{N}}$, $\bar{\mathbf{E}}$ and $\bar{\mathbf{H}}$.

3.2 Radiation from the Side Surface of a Cylinder

Consider the cylinder in Fig. 3-1. We will look at the radiation due to the cylindrical side surface $r = b$ in this section. The equivalent surface currents are

$$\bar{\mathbf{K}} = (H_\phi \hat{\mathbf{z}} - H_z \hat{\phi}) \Big|_{r=b} \quad (3.18)$$

$$\bar{\mathbf{K}}_m = (-E_\phi \hat{\mathbf{z}} + E_z \hat{\phi}) \Big|_{r=b} \quad (3.19)$$

Using the field expressions (3.3), (3.17) for H_ϕ and H_z in (3.18), it is found

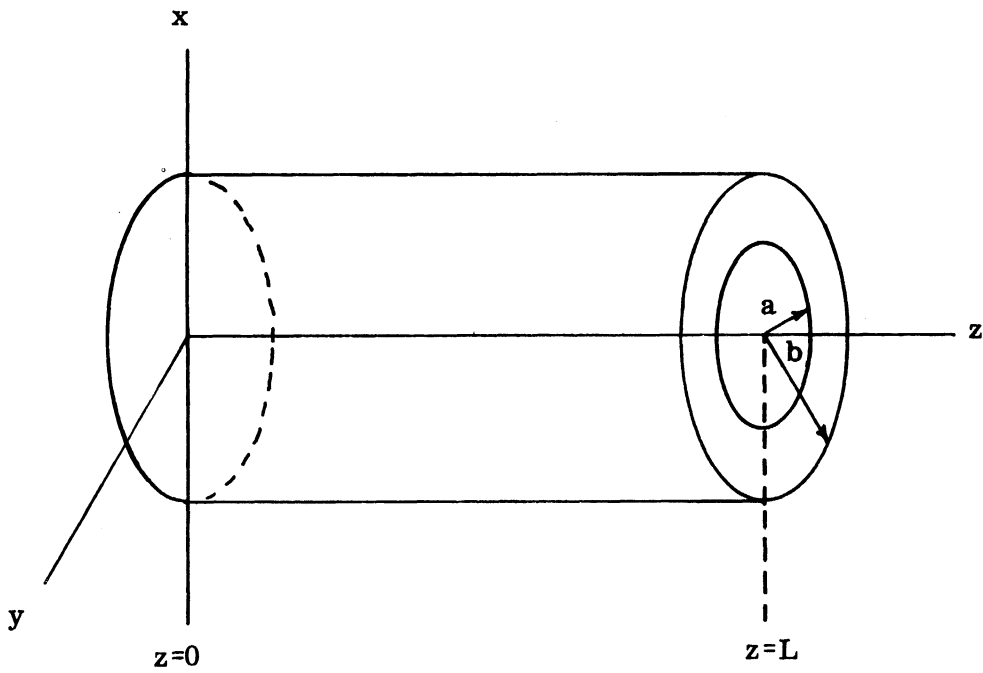


FIG. 3-1: A Helical Antenna Loaded with a Layer of Ferrite.
Radius of the helical wire is a .
Ferrite layer is between $r=a$ and $r=b$.
Antenna length is L .

$$N_x = GK(\mathbf{r}b) \int_0^L \int_0^{2\pi} e^{jk\bar{\mathbf{R}}' \cdot \hat{\mathbf{R}}} e^{j(n\phi' - \beta z')} (\sin\phi') b d\phi' dz' \quad (3.20)$$

$$N_y = -GK(\mathbf{r}b) \int_0^L \int_0^{2\pi} e^{jk\bar{\mathbf{R}}' \cdot \hat{\mathbf{R}}} e^{j(n\phi' - \beta z')} (\cos\phi') b d\phi' dz' \quad (3.21)$$

$$N_z = \left[F \frac{j\omega \epsilon_0}{\Gamma} K'(\mathbf{r}b) - G \frac{n\beta}{\Gamma^2 b} K(\mathbf{r}b) \right] \int_0^L \int_0^{2\pi} e^{jk\bar{\mathbf{R}}' \cdot \hat{\mathbf{R}}} e^{j(n\phi' - \beta z')} b d\phi' dz' \quad (3.22)$$

The components of $\bar{\mathbf{M}}$ can be found similarly. It can be seen

$$\frac{N_x}{\bar{M}_x} = -\eta_0 \frac{G}{F} \quad (3.23)$$

$$\frac{N_y}{\bar{M}_y} = -\eta_0 \frac{G}{F} \quad (3.24)$$

$$\frac{N_z}{\bar{M}_z} = \eta_0 \frac{F \frac{j\omega \epsilon_0}{\Gamma} K'(\mathbf{r}b) - G \frac{n\beta}{\Gamma^2 b} K(\mathbf{r}b)}{F \frac{n\beta}{\Gamma^2 b} K(\mathbf{r}b) + G \frac{j\omega \mu_0}{\Gamma} K'(\mathbf{r}b)} \quad (3.25)$$

It is necessary, therefore, to carry out only three integrations to obtain all six components of $\bar{\mathbf{M}}$ and $\bar{\mathbf{N}}$,

$$\bar{\mathbf{R}}' = (b \cos \phi', b \sin \phi', z') \quad (3.26)$$

$$\hat{\mathbf{R}} = (\sin \theta \cos \phi, \sin \theta \sin \phi, \cos \theta) \quad (3.27)$$

$$\therefore \bar{\mathbf{R}}' \cdot \hat{\mathbf{R}} = b \sin \theta \cos(\phi - \phi') + z' \cos \theta \quad (3.28)$$

Using (3.28), each of the three integrations (3.20) — (3.22) can be expressed as a product of two factors ;

$$N_\alpha = A(\theta) C_\alpha(\theta, \phi) \quad (3.29)$$

where α can be x, y or z.

The factor $A(\theta)$ results from the z' integration

$$A(\theta) = \frac{j}{L} \int_0^L e^{jkz' \cos \theta} e^{-j\beta z'} dz' \quad (3.30)$$

$A(\theta)$ may be viewed as the array factor in the array theory. The factor $C_\alpha(\theta, \phi)$ results from the ϕ' integration and may be viewed as the individual element pattern in the array theory.

$$C_x(\theta, \phi) = (-j) \beta L G K(\Gamma b) \int_0^{2\pi} e^{jk b \sin \theta \cos(\phi - \phi')} e^{jn\phi'} \sin \phi' d\phi' \quad (3.31)$$

$$C_y(\theta, \phi) = j \beta L G K(\Gamma b) \int_0^{2\pi} e^{jk b \sin \theta \cos(\phi - \phi')} e^{jn\phi'} \cos \phi' d\phi' \quad (3.32)$$

$$C_z = \left[F \frac{\omega \epsilon_0}{\Gamma} K'(\Gamma b) + j G \frac{n \beta}{\Gamma^2 b} K(\Gamma b) \right] b L \cdot \int_0^{2\pi} e^{jk b \sin \theta \cos(\phi - \phi')} e^{jn\phi'} d\phi' \quad (3.33)$$

Carrying out the integration, (3.30) becomes

$$A(\theta) = \frac{1 - e^{-ju(\theta)}}{u(\theta)} \quad (3.34)$$

where

$$u(\theta) = \left(\frac{\beta}{k} - \cos \theta \right) k L \quad (3.35)$$

The integrations for the C_α 's can be carried out by using the Bessel-Fourier series,

$$e^{jk b \sin \theta \cos \phi} = J_0(k b \sin \theta) + \sum_{m=1}^{\infty} 2(j)^m J_m(k b \sin \theta) \cos m \phi \quad (3.36)$$

and the orthogonality property of the sinusoidal functions,

$$\int_0^{2\pi} \sin m\phi \cos n\phi d\phi = 0$$

$$\int_0^{2\pi} \cos m\phi \cos n\phi d\phi = \pi \delta_{mn}, \quad m \neq 0 \quad (3.37)$$

$$\int_0^{2\pi} \sin m\phi \sin n\phi d\phi = \pi \delta_{mn}, \quad m \neq 0$$

where δ_{mn} is the Kronecker delta.

For example,

$$C_x(\theta, \phi) = (-)jbLGK(\Gamma b) \cdot \int_0^{2\pi} e^{jkbsin\theta \cos(\phi - \phi')} \cdot \frac{1}{2} \left[\sin(n+1)\phi' - \sin(n-1)\phi' \right. \\ \left. - j\cos(n+1)\phi' + j\cos(n-1)\phi' \right] d\phi' = (-)j^{n+1}\pi bLGK(\Gamma b) \cdot \\ \cdot \left[J_{n+1}(kbsin\theta)e^{j(n+1)\phi} + J_{n-1}(kbsin\theta)e^{j(n-1)\phi} \right]. \quad (3.38)$$

Similarly,

$$C_y(\theta, \phi) = (-)j^n \pi bLGK(\Gamma b) \left[J_{n+1}(kbsin\theta)e^{j(n+1)\phi} - J_{n-1}(kbsin\theta)e^{j(n-1)\phi} \right] \quad (3.39)$$

$$C_z(\theta, \phi) = \left[F \frac{\omega \epsilon_0}{\Gamma} K'(\Gamma b) + jG \frac{n\beta}{\Gamma^2 b} K(\Gamma b) \right] \cdot j^n 2\pi bL \cdot J_n(kbsin\theta)e^{jn\phi}, \quad (3.40)$$

and (3.38) - (3.40) are valid also when $n = 0, \pm 1$. This can be seen by actually doing the integrations for these values of n .

In order for the antenna to be endfire, both $A(\theta)$ and $C_\alpha(\theta, \phi)$ would have to be endfire. It is obvious from (3.38) - (3.40) that

$$n = \pm 1 \quad (3.41)$$

are the only cases the antenna would be endfire. Along the axis $\theta=0$, \bar{M}_t

and \bar{N}_t are composed of C_x and C_y only. Both of these are non-zero only when $n = \pm 1$, since

$$J_n(0) = \delta_{n0} \quad (3.42)$$

In order that the $n = \pm 1$ mode can be excited, it is a common practice to make the circumference of the antenna the order of one free space wavelength. Thus, for the type of antennas under consideration, we have

$$kb \sim 1 \quad (3.43)$$

Figure 3-2 shows the normalized patterns for C_x and C_y in the plane $\phi = 0$ under conditions (3.41) and (3.43). The antenna axis $\theta = 0$ is shown in Fig. 3-2a. This will not be shown for other figures in the text. It is seen for the range of kb indicated by (3.43), that C_x and C_y have almost no preferred direction of radiation.

The endfire condition of $A(\theta)$ is less well known. Extensive study of this factor by analytical and numerical means was made in Appendix C. After examination of the factor for all possible values of the parameters β_r, β_i and L , it may be concluded that the endfire condition for $A(\theta)$ is

$$\beta \sim k \quad (3.44)$$

Since the β in (3.44) is complex, (3.44) can be replaced by a set of two real relations

$$\begin{aligned} \beta_r &\sim k \\ \left| \beta_i / \beta_r \right| &\ll 1 \end{aligned} \quad (3.44a)$$

It should be noted here that neither (3.44) nor (3.44a) is an identity relation. How close β_r should be to k depends on the length L of the antenna, and the value of β_i / β_r . A more elaborate endfire condition can be found in Appendix C as

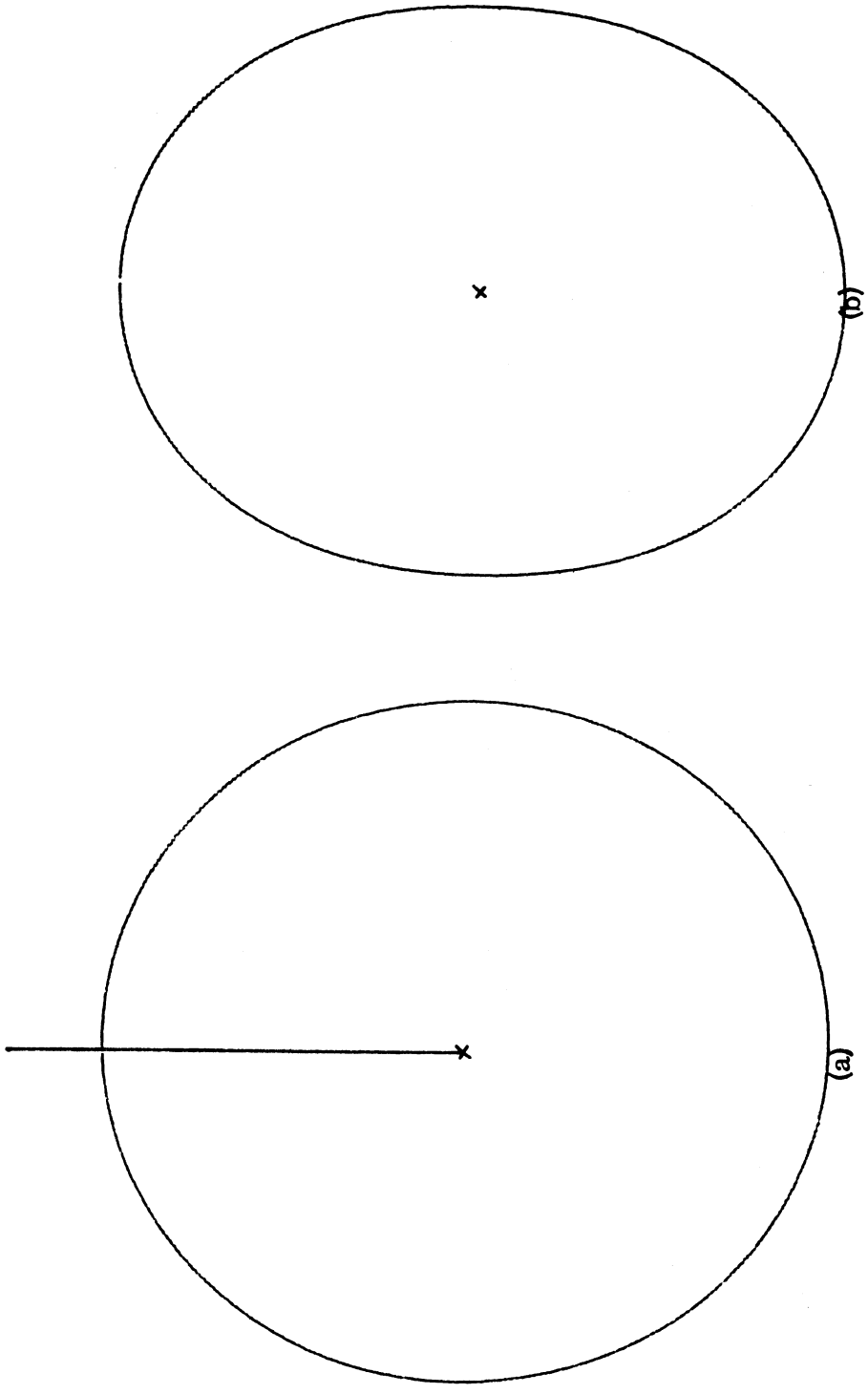


FIG. 3-2: $C_x(kb \sin \theta)$ and $C_y(kb \sin \theta)$, $\phi = 0$. (a) $C_x, kb = 0.8$, (b) $C_y, kb = 0.8$.

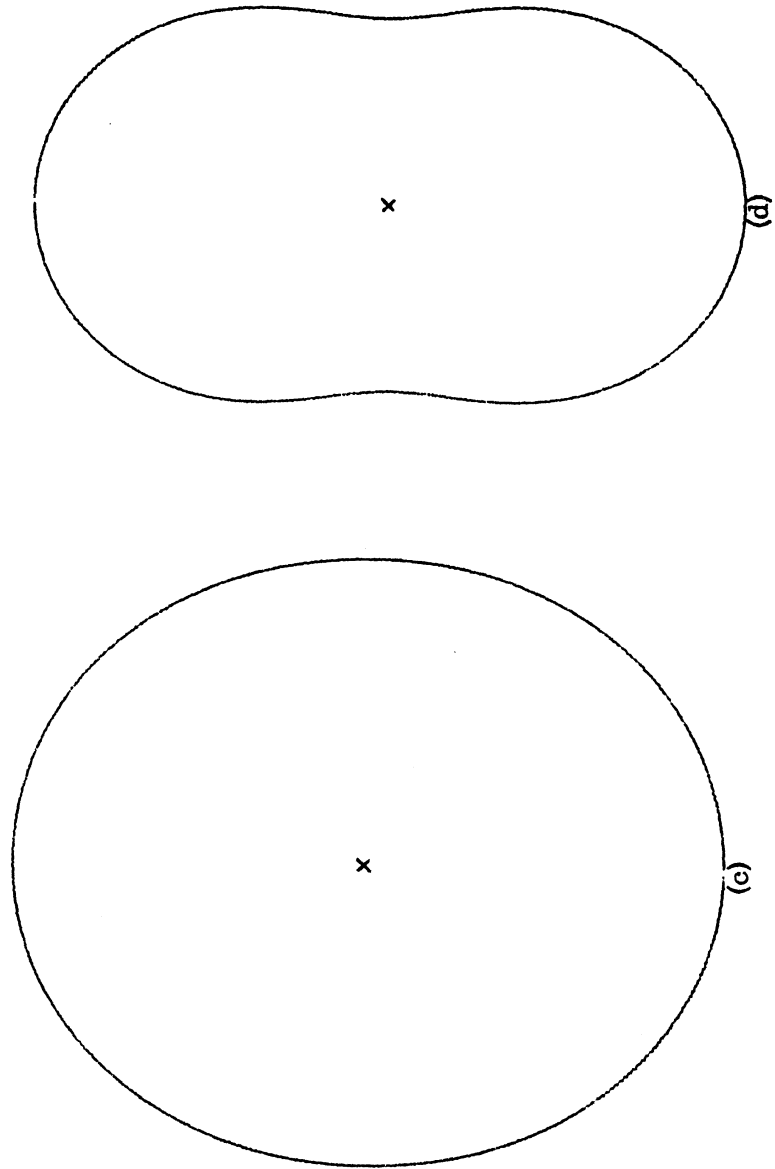


FIG. 3-2 (continued): (c) C_x , $kb = 1.2$, (d) C_y , $kb = 1.2$.

$$\left(\frac{\beta}{k} - 1\right) \frac{kL}{2} \sim 0 \quad (\text{C. 41})$$

where β is the complex propagation constant. The relation (3.44) or (3.44a) however, is sufficient when the length L is a few wavelengths. Figure 3-3 shows $|A(\theta)|$ for different values of β_r , when $\beta_i=0$ and $L=6\lambda$. The only end-fire case is seen to be when $\beta_r \sim k$. Figures for cases with non-zero β_i can be found in Appendix C.

The conclusion (3.44) is very important. It lends a decisive clue as to what is the correct branch of roots of the characteristic equation that would account for the end-fire operation. As was seen in Chapter II, the characteristic equation has many different branches of roots. In fact, Eq. (3.44) would serve as the basis for selecting initial trial values of β in the numerical process, since most programs to solve the transcendental characteristic equation would definitely be iteration processes.

In summary, the radiation patterns determined by the product factors $C_\alpha(\theta, \phi) A(\theta)$, are mainly determined by the factor $A(\theta)$. The propagation constant β does not appear in the factors C_α . It is, however, the single most important factor determining the radiation pattern through its great influence on the factor $A(\theta)$. The endfire conditions for antennas with a source function of the form $F(x, y)e^{-j\beta z}$ are (3.41), (3.43) and (3.44).

It should be pointed out that the condition (3.44) has been used in the calculation of the radiation patterns of rod antennas and tube antennas⁹. It was not known, however, that (3.44) gives the only values of β that antennas with the aforementioned source distribution function would endfire. In Chapter IV it will be seen that current probe measurements on a loaded helical antenna operating in the endfire mode, indeed, bear out a propagation constant β as indicated by (3.44).

So far, it has tacitly been assumed that the side cylindrical surface is the more important radiator in the endfire operation of the antenna.

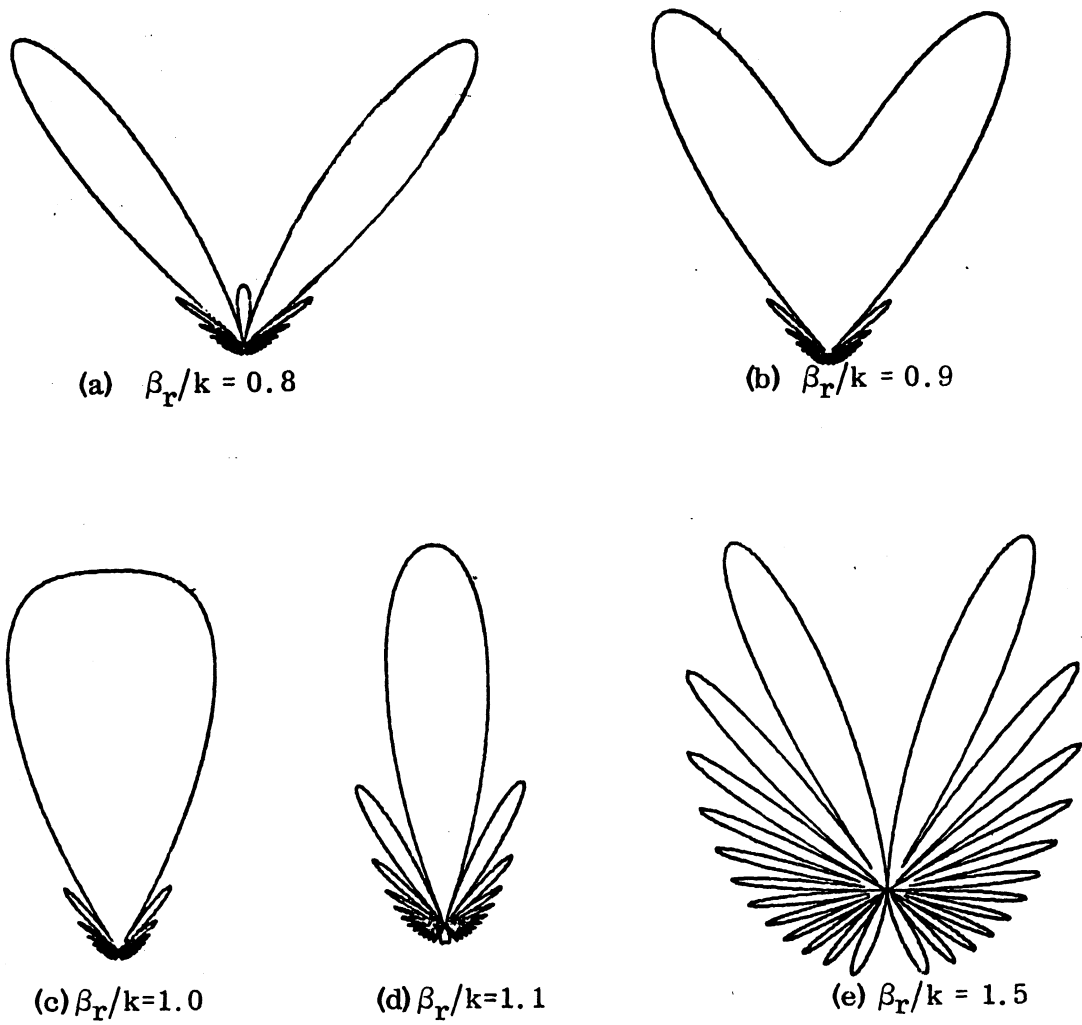


FIG. 3-3: $|A(\theta)|$ for Different Values of β_r ; $\beta_i = 0$, $kL = 12\pi$.

This is partially justified by noting that under the endfire condition (3.44), the radiation in the $\theta=0$ direction from any source point on the cylindrical surface $r=b$ is in phase. Also, the total area of the cylindrical surface is substantially larger than the area of the ends. Therefore, the radiation from the cylindrical side surface is much more important than the radiation from the ends. The only exceptions are short antennas for which the area of the end faces is comparable with the side cylindrical surface area.

3.3 Radiation from the Ends of a Cylinder

First, consider the end $z = 0$.

$$\bar{\mathbf{R}}' = (r' \cos \phi', r' \sin \phi', 0) \quad (3.45)$$

$$\hat{\mathbf{R}} = (\sin \theta \cos \phi, \sin \theta \sin \phi, \cos \theta) \quad (3.46)$$

$$\bar{\mathbf{R}}' \cdot \hat{\mathbf{R}} = r' \sin \theta \cos (\phi - \phi') \quad (3.47)$$

$$\bar{\mathbf{K}}_m = (E_r \hat{\phi} - E_\phi \hat{r}) \Big|_{z=0} \quad (3.48)$$

$$\bar{\mathbf{K}} = (-H_r \hat{\phi} - H_\phi \hat{r}) \Big|_{z=0} \quad (3.49)$$

For the area $0 < r' < a$

$$\begin{aligned} M_x^{(3)} = \frac{1}{\eta_0} \int_0^a \int_0^{2\pi} & \left[(-E_r^{(3)} \sin \phi' - E_\phi^{(3)} \cos \phi') \Big|_{z=0} \right] \\ & \cdot e^{jkr' \sin \theta \cos (\phi - \phi')} r' d\phi' dr' \quad (3.50) \end{aligned}$$

Using the field expressions (2.22) and (2.23) for $E_r^{(3)}$ and $E_\phi^{(3)}$, and Euler's formula

$$\begin{aligned} \sin \phi &= \frac{1}{2j} (e^{j\phi} - e^{-j\phi}) \\ \cos \phi &= \frac{1}{2} (e^{j\phi} + e^{-j\phi}) \end{aligned} \quad (3.51)$$

and the recursion formulas for Bessel function $I_n(z)$

$$I'_n(z) - \frac{n}{z} I_n(z) = I_{n+1}(z) \quad (3.52)$$

$$I'_n(z) + \frac{n}{z} I_n(z) = I_{n-1}(z) \quad (3.53)$$

Eq. (3.50) reduces to, after some algebra

$$\begin{aligned} M_x^{(3)} = & \frac{\pi}{\eta_o \Gamma} (-\beta F^{(3)} + j\omega \mu_o G^{(3)}) e^{j(n+1)\phi_j} L_{I(n+1)}^{(3)} \\ & + \frac{\pi}{\eta_o \Gamma} (\beta F^{(3)} + j\omega \mu_o G^{(3)}) e^{j(n-1)\phi_j} L_{I(n-1)}^{(3)} \end{aligned} \quad (3.54)$$

where $L_{I(n+1)}^{(3)}$ and $L_{I(n-1)}^{(3)}$ are the Lommel integrals for the region $0 \leq r \leq a$. These are defined in this text as

$$L_{In}^{(3)} = \int_0^a I_n(Ir') J_n(kr' \sin\theta) r' dr' \quad (3.55)$$

where I_n and J_n are Bessel functions. The Lommel integrals for $a \leq r \leq b$ are similarly defined as

$$L_{Zn}^{(2)} = \int_a^b Z_n(\gamma r') J_n(kr' \sin\theta) r' dr' \quad (3.56)$$

where Z_n can be I_n or K_n . The Lommel integrals can be integrated out in terms of Bessel functions,

$$L_{In}^{(2)} = \frac{r'}{\gamma^2 + k^2 \sin^2 \theta} \left[-k \sin\theta I_n(\gamma r') J_{n-1}(kr' \sin\theta) + \gamma J_n(kr' \sin\theta) I_{n-1}(\gamma r') \right] \Bigg|_{r'=a}^{r'=b} \quad (3.57)$$

$$L_{Kn}^{(2)} = \frac{-r'}{\gamma + k \sin^2 \theta} \left[k \sin \theta K_n(\gamma r') J_{n-1}(kr' \sin \theta) + \gamma J_n(kr' \sin \theta) K_{n-1}(\gamma r') \right] \Bigg|_{r'=a}^{r'=b} \quad (3.58)$$

$$L_{In}^{(3)} = \frac{a}{\Gamma + k \sin^2 \theta} \left[-k \sin \theta I_n(\Gamma a) J_{n-1}(ka \sin \theta) + \Gamma J_n(ka \sin \theta) I_{n-1}(\Gamma a) \right] \quad (3.59)$$

These can be derived easily. The case when $n = 1$ can be obtained from Chen's thesis⁹ on ferrite tube antennas. The same derivation also applies to all other integer values of n . M_x for the region $a \leq r \leq b$ can now be obtained simply by making the following substitutions in (3.54)

$$\left\{ \begin{array}{l} \mu_0 \\ \epsilon_0 \\ \Gamma \\ a \\ 0 \\ F_{In}^{(3)} \\ G_{In}^{(3)} \\ F_{L_{I(n \pm 1)}}^{(3)} \\ G_{L_{I(n \pm 1)}}^{(3)} \end{array} \right\} \longrightarrow \left\{ \begin{array}{l} \mu \mu_0 \\ \epsilon \epsilon_0 \\ \gamma \\ b \\ a \\ f I_n + f C_1 K_n \\ g I_n + g C_2 K_n \\ f L_{I(n \pm 1)}^{(2)} - f C_1 L_{K(n \pm 1)}^{(2)} \\ g L_{I(n \pm 1)}^{(2)} - g C_2 L_{K(n \pm 1)}^{(2)} \end{array} \right\} \quad (3.60)$$

Using (3.54) and (3.60), M_x for the region $a \leq r \leq b$ is found as

$$\begin{aligned}
M_x^{(2)} = & \frac{\pi}{\gamma \eta_0} e^{j(n+1)\phi} j^{n+1} \left\{ (-\beta) \left[fL_{I(n+1)}^{(2)} - fC_{1L}^{(2)} L_{K(n+1)}^{(2)} \right] \right. \\
& + j\omega\mu\mu_0 \left[gL_{I(n+1)}^{(2)} - gC_{2L}^{(2)} L_{K(n+1)}^{(2)} \right] \left. \right\} \\
& + \frac{\pi}{\gamma \eta_0} e^{j(n-1)\phi} j^{n-1} \cdot \left\{ \beta \left[fL_{I(n-1)}^{(2)} - fC_{1L}^{(2)} L_{K(n-1)}^{(2)} \right] \right. \\
& \left. + j\omega\mu\mu_0 \left[gL_{I(n-1)}^{(2)} - gC_{2L}^{(2)} L_{K(n-1)}^{(2)} \right] \right\} \quad (3.61)
\end{aligned}$$

The sum of (3.54) and (361) then gives M_x for the end $z = 0$,

$$M_x = M_x^{(2)} + M_x^{(3)} \quad (3.62)$$

Similarly, M_y for $z = 0$ is the sum of $M_y^{(2)}$ and $M_y^{(3)}$ due, respectively, to the regions $a \leq r \leq b$ and $r \leq a$,

$$M_y = M_y^{(2)} + M_y^{(3)} \quad (3.63)$$

where

$$\begin{aligned}
M_y^{(3)} = & \frac{\pi}{\eta_0 \Gamma} (j\beta F^{(3)} + \omega\mu_0 G^{(3)}) j^{n+1} e^{j(n+1)\phi} L_{I(n+1)}^{(3)} \\
& + \frac{\pi}{\eta_0 \Gamma} (j\beta F^{(3)} - \omega\mu_0 G^{(3)}) j^{n-1} e^{j(n-1)\phi} L_{I(n-1)}^{(3)} \quad (3.64)
\end{aligned}$$

$$\begin{aligned}
M_y^{(2)} = & \frac{\pi}{\eta_0 \gamma} j^{n+1} e^{j(n+1)\phi} \left\{ j\beta \left[fL_{I(n+1)}^{(2)} - fC_{1L}^{(2)} L_{K(n+1)}^{(2)} \right] \right. \\
& + \omega\mu\mu_0 \left[gL_{I(n+1)}^{(2)} - gC_{2L}^{(2)} L_{K(n+1)}^{(2)} \right] \left. \right\} + \frac{\pi}{\eta_0 \gamma} j^{n-1} e^{j(n-1)\phi} \cdot \\
& \cdot \left\{ j\beta \left[fL_{I(n-1)}^{(2)} - fC_{1L}^{(2)} L_{K(n-1)}^{(2)} \right] - \omega\mu\mu_0 \left[gL_{I(n-1)}^{(2)} - gC_{2L}^{(2)} L_{K(n-1)}^{(2)} \right] \right\} \quad (3.65)
\end{aligned}$$

M_z is zero, since both \bar{J} and \bar{J}_m have no z component on the end $z = 0$.

$$M_z = 0 \quad (3.66)$$

The components of the vector \bar{N} are found from \bar{J} in a similar way;

$$N_x = N_x^{(2)} + N_x^{(3)} \quad (3.67)$$

$$N_y = N_y^{(2)} + N_y^{(3)} \quad (3.68)$$

$$N_z = 0, \quad (3.69)$$

where

$$\begin{aligned} N_x^{(3)} &= \frac{\pi}{\Gamma} (j\omega \in_o F^{(3)} + \beta G^{(3)}) e^{j(n+1)\phi_j} \phi_j^{n+1} L_{I(n+1)}^{(3)} \\ &+ \frac{\pi}{\Gamma} (j\omega \in_o F^{(3)} - \beta G^{(3)}) e^{j(n-1)\phi_j} \phi_j^{n-1} L_{I(n-1)}^{(3)} \end{aligned} \quad (3.70)$$

$$\begin{aligned} N_y^{(3)} &= \frac{\pi}{\Gamma} (\omega \in_o F^{(3)} - j\beta G^{(3)}) e^{j(n+1)\phi_j} \phi_j^{(n+1)} L_{I(n+1)}^{(3)} \\ &- \frac{\pi}{\Gamma} (\omega \in_o F^{(3)} + j\beta G^{(3)}) e^{j(n-1)\phi_j} \phi_j^{(n-1)} L_{I(n-1)}^{(3)} \end{aligned} \quad (3.71)$$

$N_x^{(2)}$ and $N_y^{(2)}$ are obtained by making the substitution (3.60) in (3.70) and (3.71) respectively.

$$\begin{aligned} N_x^{(2)} &= \frac{\pi}{\gamma} e^{j(n+1)\phi_j} \phi_j^{n+1} \left\{ j\omega \in_o \left[fL_{I(n+1)}^{(2)} - fC_1 L_{K(n+1)}^{(2)} \right] \right. \\ &+ \beta \left[gL_{I(n+1)}^{(2)} - gC_2 L_{K(n+1)}^{(2)} \right] \left. \right\} + \frac{\pi}{\gamma} e^{j(n-1)\phi_j} \phi_j^{n-1} \cdot \\ &\cdot \left\{ j\omega \in_o \left[fL_{I(n-1)}^{(2)} - fC_1 L_{K(n-1)}^{(2)} \right] - \beta \left[gL_{I(n-1)}^{(2)} - gC_2 L_{K(n-1)}^{(2)} \right] \right\} \end{aligned} \quad (3.72)$$

$$\begin{aligned}
N_y^{(2)} = \frac{\pi}{\gamma} e^{j(n+1)\phi} j^{n-1} & \left\{ \omega \epsilon \epsilon_0 (fL_{I(n+1)}^{(2)} - fC_{1K(n+1)}^{(2)}) \right. \\
& \left. - j\beta (gL_{I(n+1)}^{(2)} - gC_{2K(n+1)}^{(2)}) \right\} - \frac{\pi}{\gamma} e^{j(n-1)\phi} j^{n-1} \\
& \cdot \left\{ \omega \epsilon \epsilon_0 (fL_{I(n-1)}^{(2)} - fC_{1K(n-1)}^{(2)}) + j\beta (gL_{I(n-1)}^{(2)} - gC_{2K(n-1)}^{(2)}) \right\}. \quad (3.73)
\end{aligned}$$

The vectors \bar{M} and \bar{N} due to the other end $z = L$ can now be considered.

$$\bar{R}' \Big|_{z=L} = (r' \cos \phi', r' \sin \phi', L) \quad (3.74)$$

$$\hat{R} = (\sin \theta \cos \phi, \sin \theta \sin \phi, \cos \theta) \quad (3.75)$$

$$\bar{R}' \cdot \hat{R} \Big|_{z=L} = r' \sin \theta \cos(\phi - \phi') + L \cos \theta = \bar{R}' \cdot \hat{R} \Big|_{z=0} + L \cos \theta. \quad (3.76)$$

The equivalent surface currents on $z=L$ is the same as those on $z=0$, except for a factor $(-)e^{-j\beta L}$. The factor $e^{-j\beta L}$ is the delay factor of the wave on the antenna. The minus sign arises because the two planes have opposite normal vectors.

$$\begin{aligned}
\bar{K}_m \Big|_{z=L} &= -(E_r \hat{\phi} - E_\phi \hat{r}) \Big|_{z=L} = (E_r \hat{\phi} - E_\phi \hat{r}) \Big|_{z=0} (-e^{-j\beta L}) \\
&= (\bar{K}_m \Big|_{z=0}) (-e^{-j\beta L}). \quad (3.77)
\end{aligned}$$

The vectors \bar{M} and \bar{N} due to $z=L$ can therefore be related to \bar{M} and \bar{N} due to $z=0$. For example

$$\begin{aligned}
\bar{M} \Big|_{z=L} &= \frac{1}{\eta_0} \iint (\bar{K}_m e^{jk \bar{R}' \cdot \hat{R}}) \Big|_{z=L} ds' = \frac{1}{\eta_0} \iint (\bar{K}_m e^{jk \bar{R}' \cdot \hat{R}}) \Big|_{z=0} ds' \\
&\cdot \begin{bmatrix} -jkL \left(\frac{\beta}{k} - \cos \theta \right) \\ -e \end{bmatrix} = (\bar{M} \Big|_{z=0}) \begin{bmatrix} -jkL \left(\frac{\beta}{k} - \cos \theta \right) \\ -e \end{bmatrix}. \quad (3.78)
\end{aligned}$$

The combined contribution of the two ends $z=0$ and $z=L$ to \bar{M} is

$$\bar{M} = \bar{M}\Big|_{z=0} + \bar{M}\Big|_{z=L} = (\bar{M}\Big|_{z=0}) B(\theta) \quad (3.79)$$

where

$$B(\theta) = 1 - e^{-ju(\theta)} \quad (3.80)$$

$$u(\theta) = \left(\frac{\beta}{k} - \cos\theta\right)kL \quad (3.35)$$

The other radiation vector \bar{N} due to the two ends can be expressed similarly as

$$\bar{N} = (\bar{N}\Big|_{z=0}) B(\theta) \quad (3.81)$$

The vectors $\bar{M}\Big|_{z=0}$ and $\bar{N}\Big|_{z=0}$ in (3.79) and (3.81) are given by (3.62), (3.63), (3.66) - (3.69) and may again be looked upon as the element factor, while $B(\theta)$ may be looked upon as the array factor for the two ends. The θ dependence of \bar{M} and \bar{N} , which determines the far fields, is in the Lommel integrals (3.57) - (3.59). These integrals vary slowly with θ through the Bessel functions of the first kind $J_n(ka \sin\theta)$ and $J_n(kb \sin\theta)$. A comparison of these integrals with the element factors $C_\alpha(\theta, \phi)$ for the cylindrical surface shows that the functional dependence of the Lommel integrals (3.57) - (3.59) on θ is analogous to that of the factors $C_\alpha(\theta, \phi)$ in (3.38) - (3.40). Hence, it may be concluded that the element pattern for the ends are not very directional provided ka and kb are both close to unity as in (3.43). The result is not surprising when one recalls that the ϕ variation of the source function for the ends is the same as that for the cylindrical side surface.

We will now look at the array factor $B(\theta)$. In the case $\beta_1=0$,

$$|B(\theta)| = 2|\sin(x(\theta))| \quad (3.82)$$

where

$$x(\theta) = \frac{1}{2} u(\theta) = \left(\frac{\beta}{k} - \cos\theta\right) \frac{kL}{2} \quad (3.83)$$

It is shown in Appendix C that Eq. (3.83) maps the interval $[0, \pi]$ for θ onto $[x(0), x(\pi)]$, continuously and monotonically where

$$\begin{aligned} x(0) &= \left(\frac{\beta}{k} - 1\right) \frac{kL}{2} \\ x(\pi) &= \left(\frac{\beta}{k} + 1\right) \frac{kL}{2} \end{aligned} \quad (3.84)$$

Thus, $|B(\theta)|$ on $[0, \pi]$ may be plotted out point by point from $2\sin x$ on $[x(0), x(\pi)]$. The number of lobes of $B(\theta)$ on $[0, \pi]$ is equal to the number of maxima of $|\sin x|$ on $[x(0), x(\pi)]$, or, roughly

$$\frac{1}{\pi} [x(\pi) - x(0)] = \frac{\beta L}{\pi} \quad (3.85)$$

Since long endfire antennas are usually a few free space wavelengths in length, (3.85) shows $B(\theta)$ would have several lobes at least, assuming the endfire condition $\beta \sim k$. Furthermore, all these lobes have the same magnitude. The pattern for $B(\theta)$, therefore, cannot be endfire. Figure 3-4 shows this multi-lobe situation for $B(\theta)$ for different lengths of the antenna assuming $\beta_r = k$ and $\beta_i = 0$. The patterns for $B(\theta)$ in the presence of a non-zero β_i are shown in Figs. 3-5 and 3-6. Although these are different from Fig. 3-4, the conclusion that $B(\theta)$ is not endfire can be seen to remain unchanged.

3.4 The Backfire Bifilar Helix

In Section 3.2, the endfire condition for a wave $F(r, \theta)e^{-j\beta z}$ was introduced in Eq.(3.44). The bifilar helix, however, usually operates on a peculiar mode known as the backfire mode. This was not mentioned in Section 3.2 so as to avoid undue confusion. The situation will be clarified now before we look at the calculated patterns.

For the purposes of illustration, it will be assumed in this section that the feeding point of the antenna is at $z=0$ and the physical structure of the antenna extends along the positive z -axis. Ordinary endfire mode corresponds to a source distribution whose phase decreases along the antenna, relative to the feeding point. This situation can be represented by $e^{-j\beta z}$

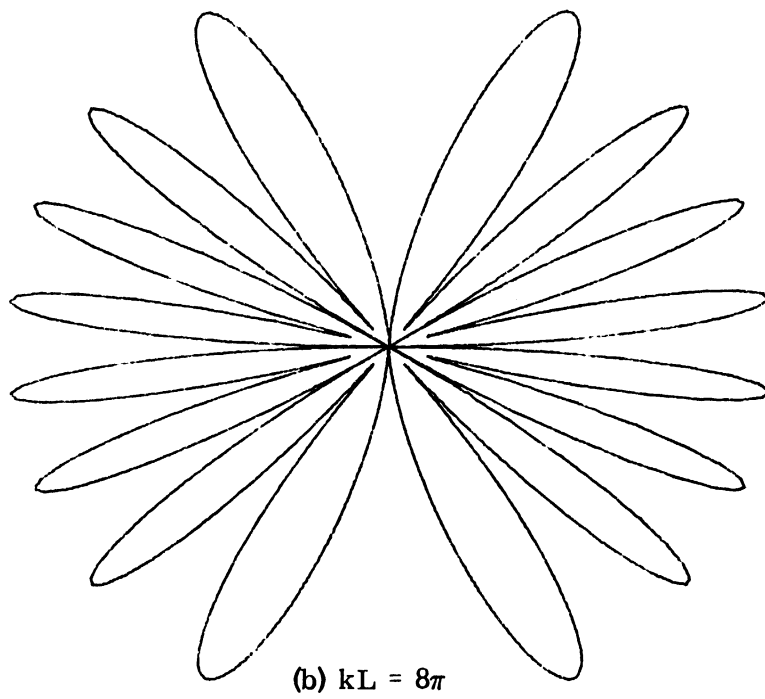
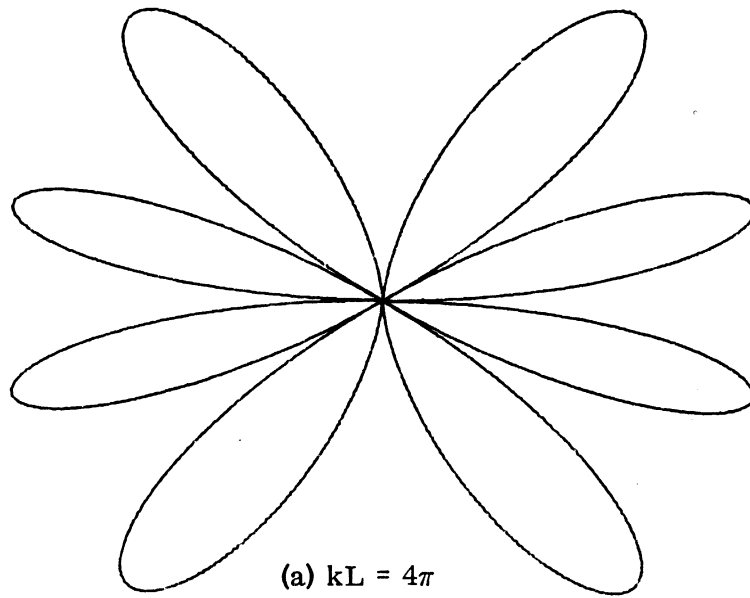


FIG. 3-4: $|B(\theta)|$ for $\beta_r = k$, $\beta_i = 0$.

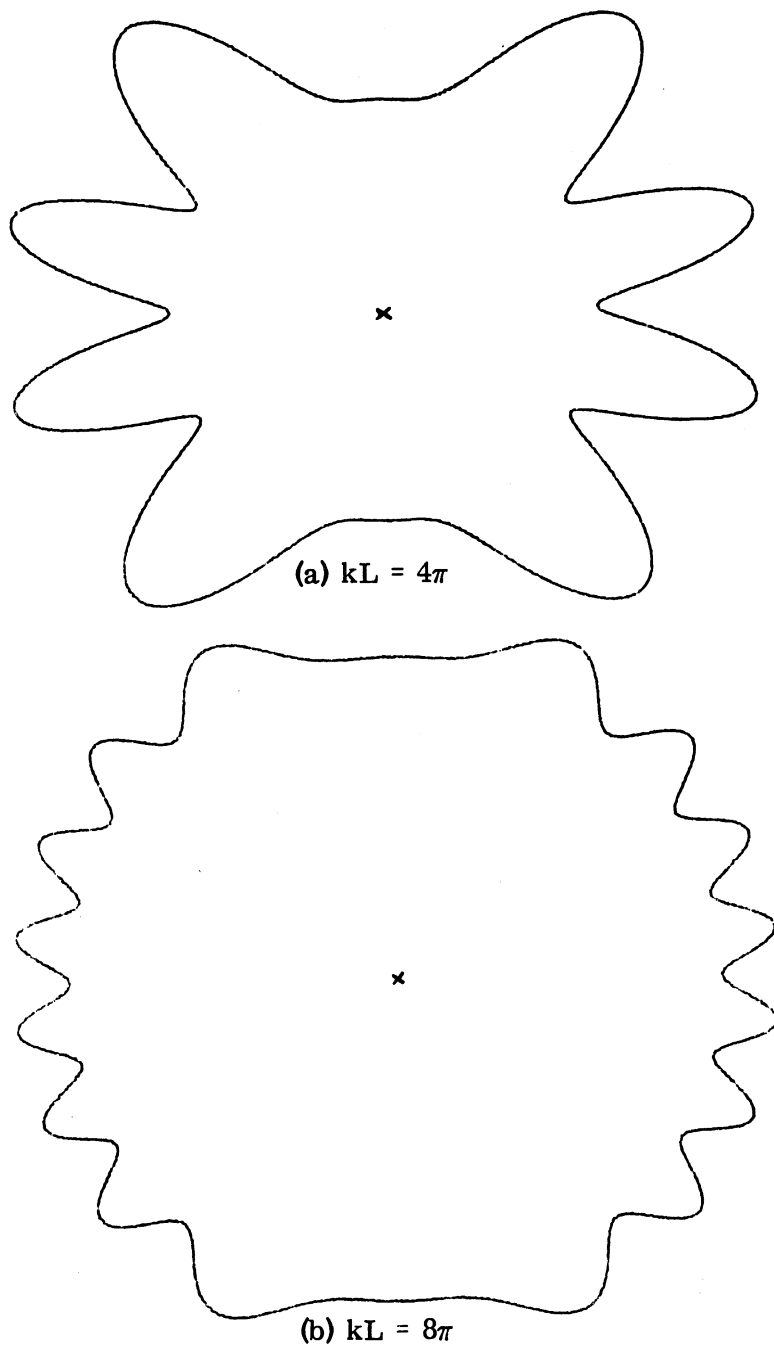


FIG. 3-5: $|B(\theta)|$ for $\beta_r = k$, $\beta_i = -0.1k$.

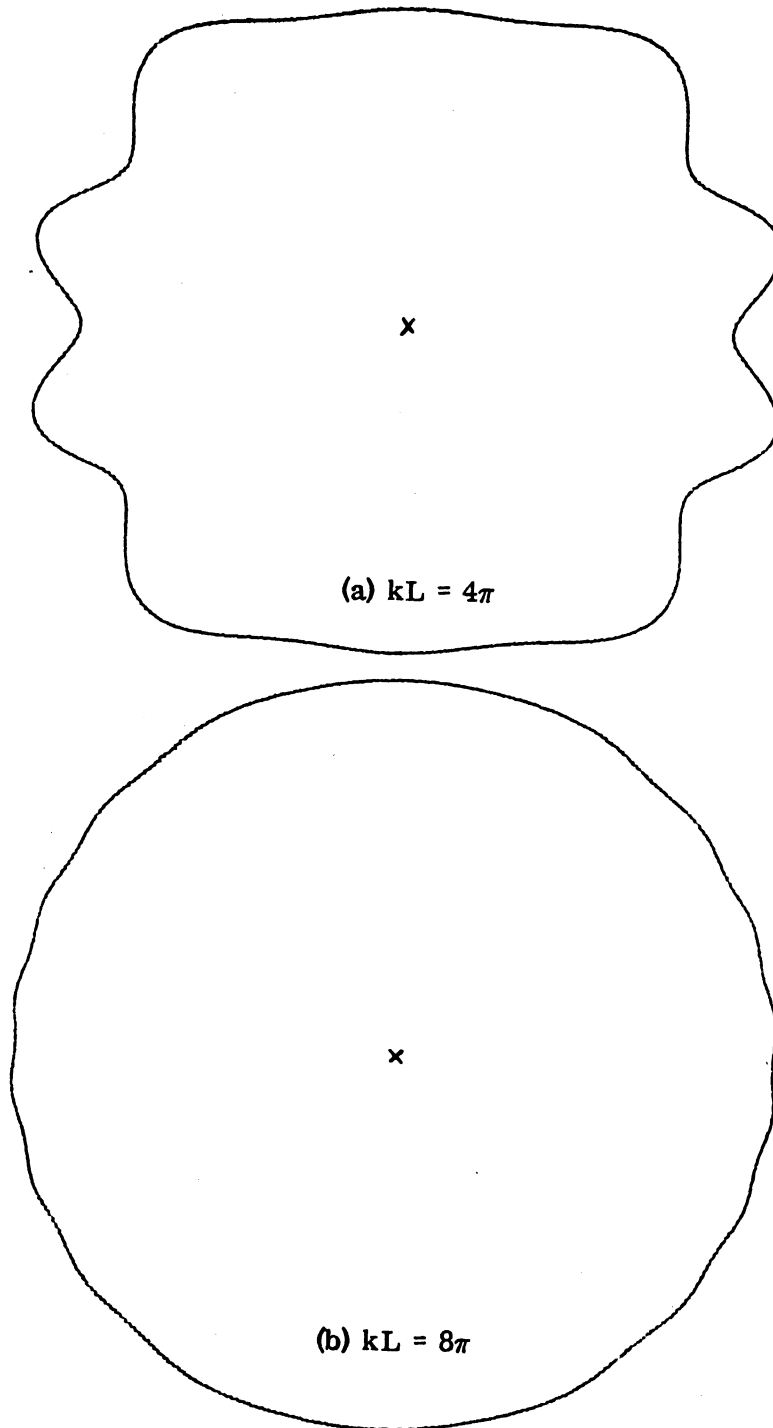


FIG. 3-6: $|B(\theta)|$ for $\beta_r = k$, $\beta_i = -0.2k$.

with $\beta_r > 0$, or, by $e^{j\beta z}$ with $\beta_r < 0$. The backfire bifilar helix, on the other hand, has a source distribution whose phase increases along the antenna structure. This can be represented by $e^{-j\beta z}$ with $\beta_r < 0$ or, by $e^{j\beta z}$ with $\beta_r > 0$. For consistency, the $e^{-j\beta z}$ representation has been used throughout this text. There is, of course, no fundamental objection against the use of the $e^{j\beta z}$ representation. The main difference in the radiation patterns of the two cases comes from the factor $A(\theta)$. In Appendix C, it is shown that $|A(\theta)|$ on $[0, \pi]$ is given by $|f(x)|$ on $[x(0), x(\pi)]$, where

$$\begin{aligned} x(0) &= \left(\frac{\beta}{k} - 1\right) \frac{kL}{2} \\ x(\pi) &= \left(\frac{\beta}{k} + 1\right) \frac{kL}{2} \end{aligned}$$

It is also shown in Appendix C that the endfire condition is

$$x(0) \sim 0 \quad . \quad (C.41)$$

Note that since $\beta_r > 0$, both $x(0)$ and $x(\pi)$ are greater than zero. The interval $[x(0), x(\pi)]$ is to the right of $x = 0$. This is shown by the interval $[a, b]$ in Fig. C-2. A backfire condition can likewise be established. Since now, $\beta_r < 0$,

$$x(0) < x(\pi) < 0$$

the interval $[a, b]$ in Fig. C-2 would be displaced to the left of the origin $x=0$. Suppose

$$x(\pi) \sim 0 \quad , \quad (3.86)$$

the interval $[x(0), x(\pi)]$ would then be like the interval $[c, d]$ in Fig. C-2. This obviously shows that $|A(\theta)|$ is backfire. Equation (3.86) can therefore be regarded as the backfire condition. For antennas whose length is a few free space wavelengths, (3.86) can be replaced by

$$\begin{aligned} \beta_r &\sim -k \\ \left| \frac{\beta_i}{\beta_r} \right| &\ll 1 \end{aligned} \quad (3.86a)$$

by analogy with the endfire case. It should be clear from Fig. C-2, that $|A(\theta)|$ for the backfire case is exactly the same as $|A(\theta)|$ for the endfire case except for a 180° rotation in the physical space. Or, $|A(\theta)|$ for the endfire antenna has its main lobe at $\theta=0$ and $A(\theta)$ for the backfire antenna has its main lobe at $\theta=\pi$.

In establishing the backfire condition (3.86), the factors $B(\theta)$, $L_{zn}(\theta, \phi)$ and $C_\alpha(\theta, \phi)$ were completely neglected. No more justification will be given since it would simply be a reproduction of the previous work leading to the establishment of (C.44) as the endfire condition.

Finally, it is worth noting that the word 'backfire' as used in backfire antennas describes a totally different phenomenon from that described by the word 'backward' as used in backward wave tubes. By definition (probably by microwave tube people), a forward wave is one whose phase and group velocities are in the same direction. A backward wave is one whose group velocity is in the opposite direction to its phase velocity. The wave on a backfire antenna would be a forward wave since its group and phase velocities are in the same direction, along the negative z-axis for our antenna.

3.5 Numerical Results of the Pattern Calculation

The radiation patterns in the x-z plane, or $\phi=0$ plane, are calculated for the case $n = 1$. The coordinate transformation formulas

$$\begin{aligned} A_\theta &= (A_x \cos\phi + A_y \sin\phi)\cos\theta - A_z \sin\theta \\ A_\phi &= (-)A_x \sin\phi + A_y \cos\phi \end{aligned} \quad (3.87)$$

are used in obtaining the θ and ϕ components of \bar{M} and \bar{N} from the x, y, z components. \bar{M} , of course, is the sum of the two \bar{M} 's found from the two equivalent surface currents \bar{K} and \bar{K}_m . \bar{N} is the sum of the two \bar{N} 's found from \bar{K} and \bar{K}_m . The electric field \bar{E} and the magnetic field \bar{H} are then calculated from \bar{M} and \bar{N} using (3.16) and (3.17).

Two different lengths, 0.381 m. (15") and 0.635 m. (25"), and three different frequencies, 400 to 600 MHz at 100 MHz intervals, are used in the calculation. The lengths correspond to the lengths of the actual model antennas. The frequencies correspond to the range where the actual models have the best backfire performance.

The backfire mode in Fig. 2-2 is used to calculate the radiation pattern. Calculations are also made using values of β that are slightly different from the β given by the characteristic equation. This is done to confirm our previous assumption that small variations in the value of β would not affect the far field patterns to any significant extent. The use of the sheath model is therefore adequate for the description of the far fields.

It is important to note that $\beta_r < 0$, $\beta_i \leq 0$ in reading the patterns below. These choices for β_r and β_i are consistent with the facts that the physical antenna extends from $z=0$ to $z=L$ and the feeding point is at $z=0$. Since we have adopted the $e^{-j\beta z}$ representation in this text, such choices of β_r and β_i would indicate a source function with increasing phase but decreasing amplitude going away from the feeding point, in accord with experiments.

Figure 3-7 gives a comparison of the field components $E_\theta^{(c)}$, $E_\phi^{(c)}$, E_θ , E_ϕ and $A(\theta)$, where $E_\theta^{(c)}$ and $E_\phi^{(c)}$ are the calculated field components due to the radiation of the cylindrical surface alone. These are found from the vectors \bar{M} and \bar{N} due to the cylindrical surface. E_θ and E_ϕ are the field components when the radiation of the ends are also taken into consideration. The striking similarity of these patterns is no coincidence. It reflects the important role the cylindrical surface plays in the backfire operation of the antenna. Above all, it shows the dominant influences of the factor $A(\theta)$ on the radiation patterns of the antenna.

Figure 3-8 shows the influence on the radiation patterns due to small variations of β_r . Figure 3-9 shows the effects on the radiation patterns due to small variations of β_i . It should be evident from these figures that the

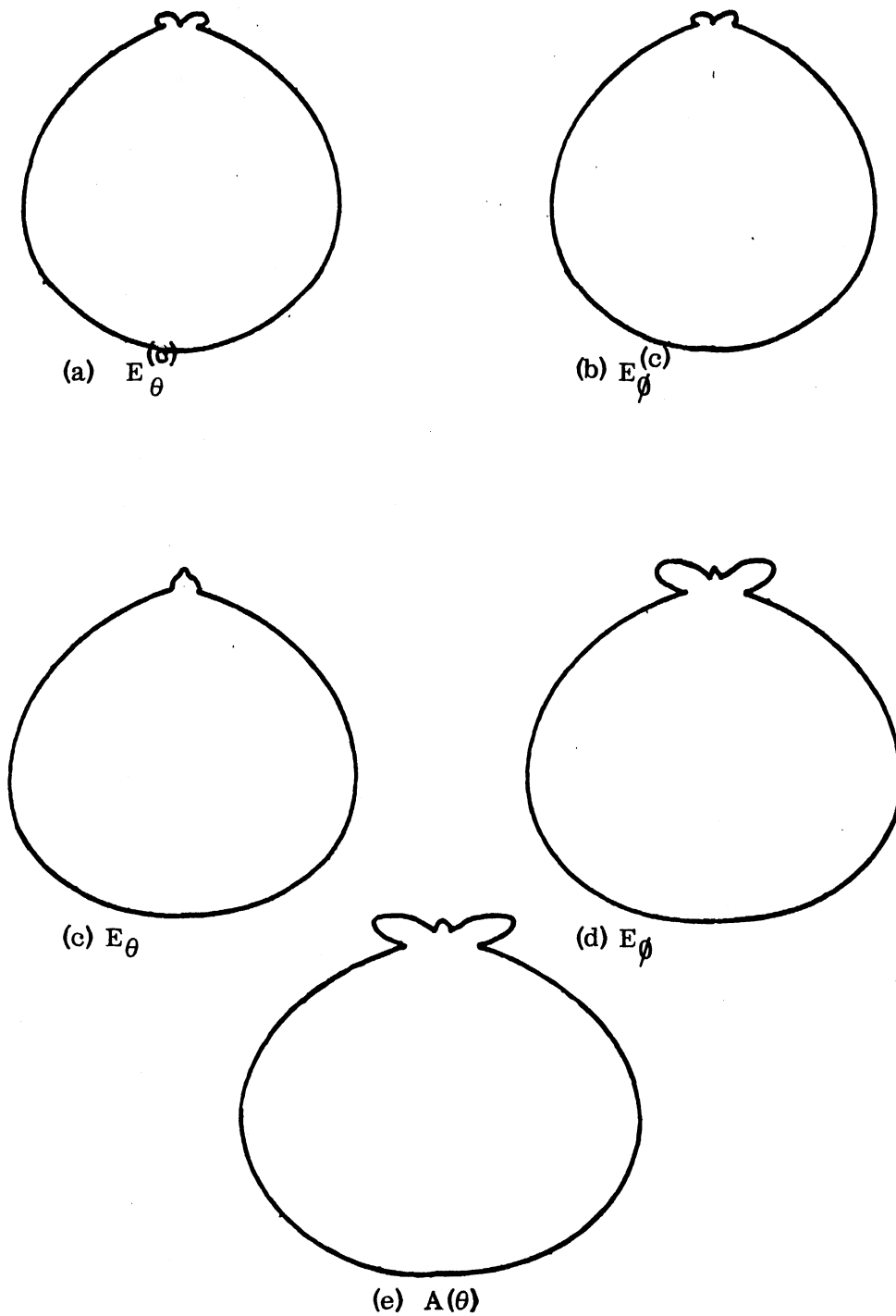


FIG. 3-7: Calculated Patterns; $f=500$ MHz, $L=0.635$ m. (25 in.),
 $\beta_r = -1.0$ k, $\beta_i = -0.1$ k .

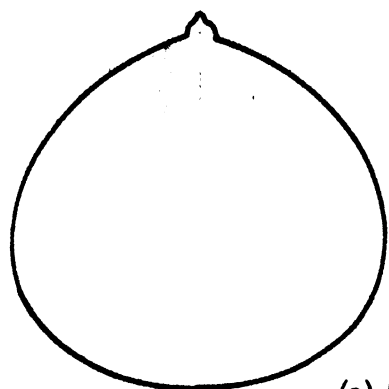
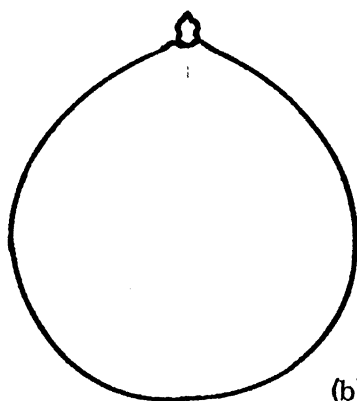
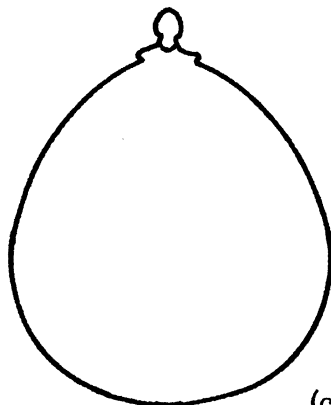
(a) $\beta_r = -1.0 k$ (b) $\beta_r = -1.1 k$ (c) $\beta_r = -1.2 k$

FIG. 3-8: Influences of β_r on the Patterns.
 E_θ , $f=500$ MHz, $L=0.635$ m (25 in.), $\beta_i = -0.1 k$.

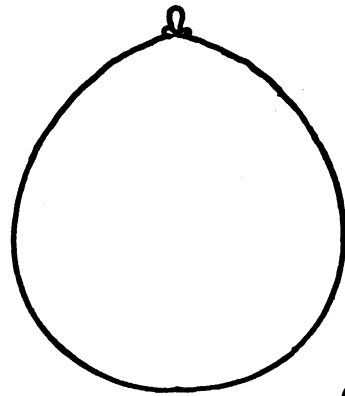
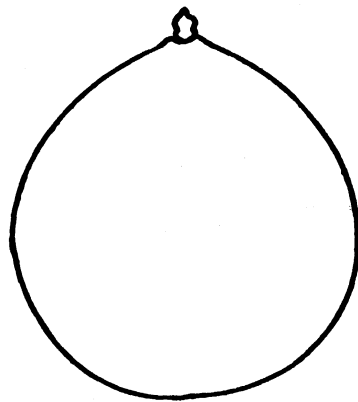
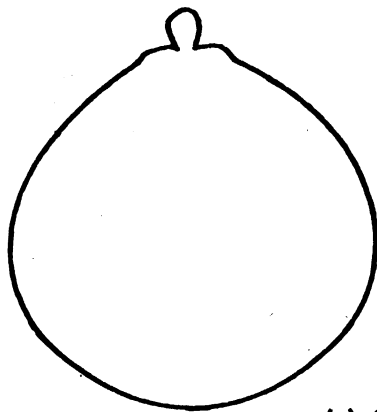
(a) $\beta_i = 0k$ (b) $\beta_i = -0.1k$ (c) $\beta_i = -0.2k$

FIG 3-9: Influence of β_i on the Patterns. E_θ ,
 $f = 500$ MHz, $L = 0.635$ m. (25 in.), $\beta_r = -1.1k$.

radiation patterns are indeed quite insensitive to small changes in the values of β_r and β_i .

A comparison between the calculated patterns and the measured patterns will be given in Chapter IV.

IV EXPERIMENTS

In this chapter, the experimental results are presented. Some technical data on designing practical antennas are supplied. Perhaps more importantly, measurements have been made to support assumptions and to confirm results of the theoretical work.

4.1 The Model Antennas

Many models had to be built to find the proper values for the various parameters of the antenna. These include the radius of the helical winding a , the thickness of the loading material ($b-a$), the pitch angle ψ and the length L . Of these, the pitch angle ψ is the most critical parameter affecting the performance of the antenna. The ferrite used as the loading material is E.A.F.2 with $\mu_r = 2.2$ and $\epsilon_r = 3.8$ as supplied by the manufacturer. Models with pitch angles equal to 6.4° , 12.5° , 25° were built and tested. For the particular loading material used, only the ones with $\psi = 6.4^\circ$ give good backfire radiation over a wide band. Four antennas with $\psi = 6.4^\circ$ but of different length are made in order to study the effects of the length. A comparison of the radiation patterns between these antennas of different length can be found in Section 4.3. All models are bifilar helices with infinite balun feeding. The thickness of the loading layer is 0.5 in. This is made as thin as possible to reduce the loss in the ferrite. All measurements presented in the subsequent sections are based on the following parameter values:

$$\psi = 6.4^\circ ,$$

$$a = 2 \frac{1}{8} \text{ in. } ,$$

$$b = 2 \frac{5}{8} \text{ in. } ,$$

$$L = 9", 15", 25",$$

$$\mu = 2.2,$$

$$\epsilon = 3.8.$$

4.2 The Near Field Measurements

Two near field measurements were performed in the anechoic chamber. Both E and H field probes are used. As the probe moves parallel to the axis of the antenna at a certain height, the amplitude and phase are read on a vector voltmeter. The probe height over the antenna is of vital importance in obtaining good data. Many of the error sources can be minimized by a proper probe height. Error arises due to the inability to align the probe in proper direction or failure to maintain the probe at a constant height over the antenna at different locations along the antenna. The discontinuity of the physical structure at both ends and the reflection from the chamber walls also causes disturbances in the measurements. Except for the reflection from the walls, all the errors above can be minimized by using an appreciable separation between the probe and the antenna. However, the input signal to the vector voltmeter would be weaker for higher probe altitude. This would lead to internal error in the vector voltmeter. The best compromise probe height is found to be around a quarter wavelength above the antenna surface.

Figure 4-1 shows the result of the first near field measurement. The antenna, with a length of 15", sits horizontally in the chamber. An E-field probe hangs down vertically from the ceiling of the chamber and moves along the axial direction of the antenna at a height of 5 1/2". Although taken at $f=500$ MHz, Fig. 4-1 represents a typical near field measurement. This is the case for all frequencies that the antenna operates on the backfire mode. The amplitude of the field decays away from the feeding point. The phase, on the other hand, increases as the probe moves away from the feeding point. Further, the phase increase is seen to be almost linear. The measurement may, therefore, be viewed as the foundation of the assumption that the surface field of the antenna can be represented by a wave $e^{-j\beta z}$ with $\beta_r < 0$, $\beta_i < 0$. Ideally, one would be able to figure out the guided wavelength λ_g along the z-axis by the length

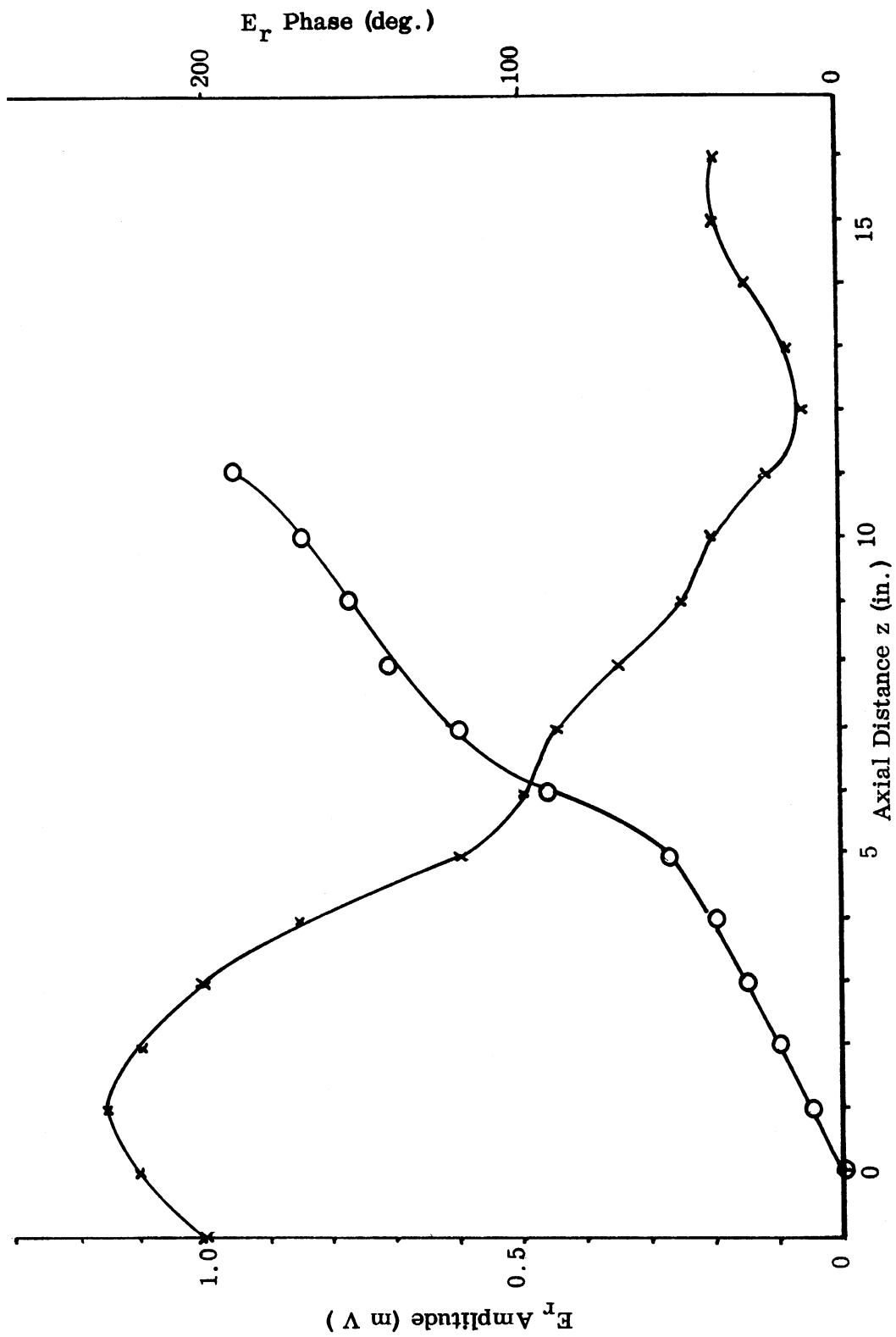


FIG. 4-1: Near Field Measurements of E_r . $f = 500$ MHz. Feeding End, $z=0$, Open End, $z=15$.
(x = Amplitude) (o = Phase).

that the wave has a 360° phase shift. β_r could then be calculated by

$$\beta_r = \frac{2\pi}{\lambda_g} \quad . \quad (4.1)$$

Unfortunately, this is not possible in the case of the ferrite loaded helical antenna. The phase reading in Fig. 4-1 stops at $z = 11$ inches. This is because the amplitude of the wave has decreased to the point that no stable phase reading can be obtained from the vector voltmeter. The total phase shift of about 190° from $z = 0$ to $z = 11$ inches falls much short of the 360° that would be required to calculate β_r . As the real part β_r of the propagation constant β is of vital importance in determining the correct root of the characteristic equation and in the calculation of the radiation pattern, a second near field measurement was done, following Barlow and Brown¹⁰. The set-up is shown in Fig. 4-2. Two vertical 4' x 4' metal plates were placed in the chamber, parallel to each other. The antenna was at a position about half way in between the two metal plates, with its axis passing through the center of each metal plate if extended. For a fixed separation of the two metal plates, the frequency was varied at 20 MHz intervals. The amplitude of the near field was again probed along the axial direction of the antenna. When, at some frequency, the separation between the two plates became a multiple of one half the guided wavelength, a resonance would occur. The vector voltmeter would then record a standing wave pattern. The peak to peak distance is equal to one half the guided wavelength at the resonant frequency. β_r at that particular frequency is calculated from (4.1). The separation was then changed and the process repeated to obtain β_r at some other frequency. Figure 4-3 shows the result of such a measurement when the separation between the two plates is 22 inches. The resonance is seen to be not very sharp and occurs at $f = 480, 500, 520$ MHz. This is due to the fact that the metal plates are relatively small in terms of

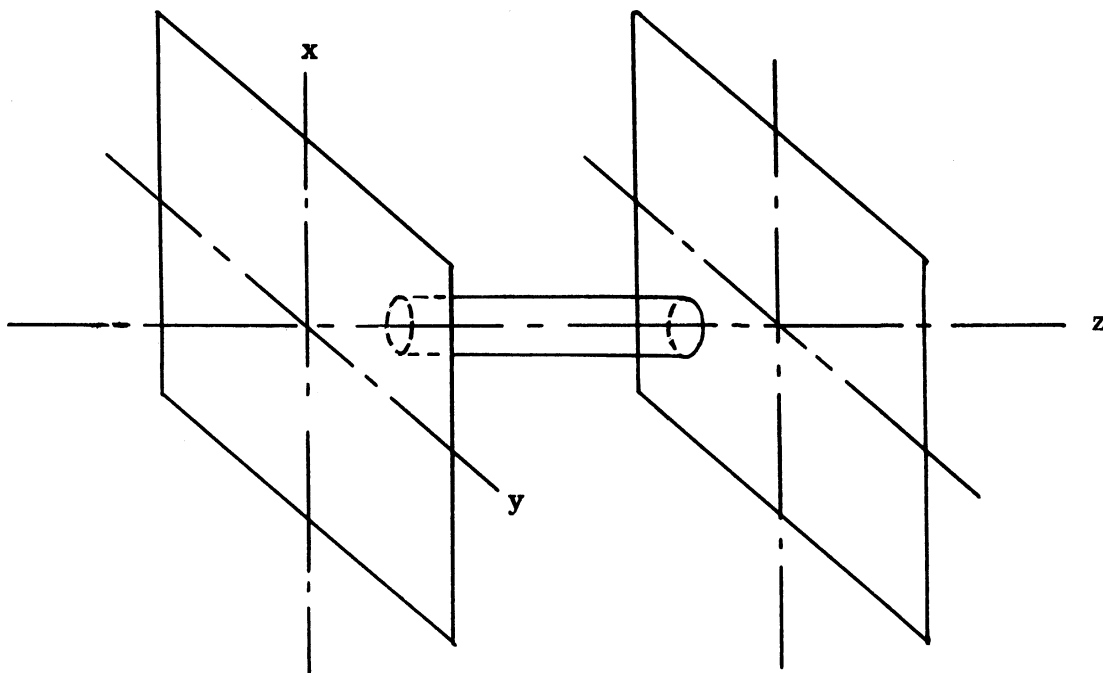


FIG. 4-2: The Set-up for Measurement of β_r . The E-field probe, which is not shown on the figure, hangs down vertically (along the x axis) and probes E_r along the z axis.

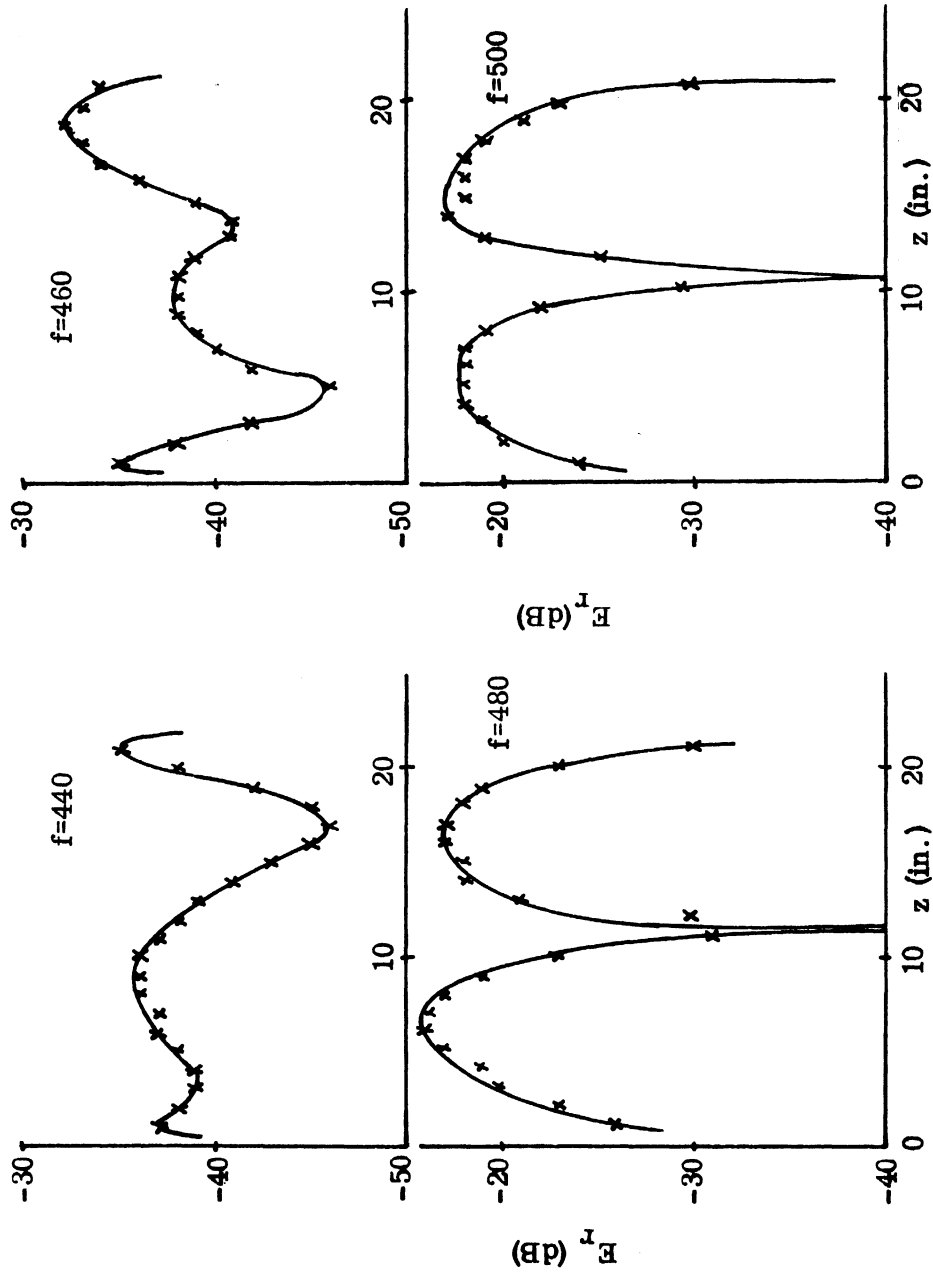
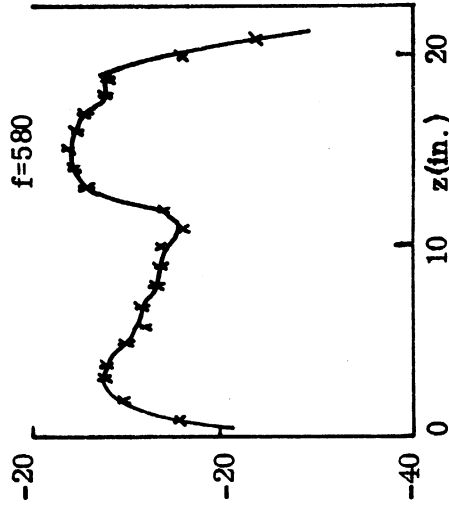
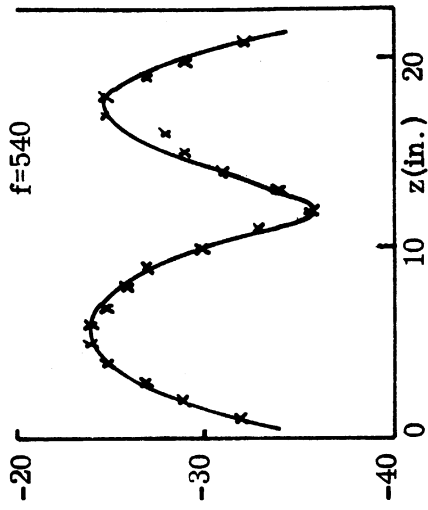
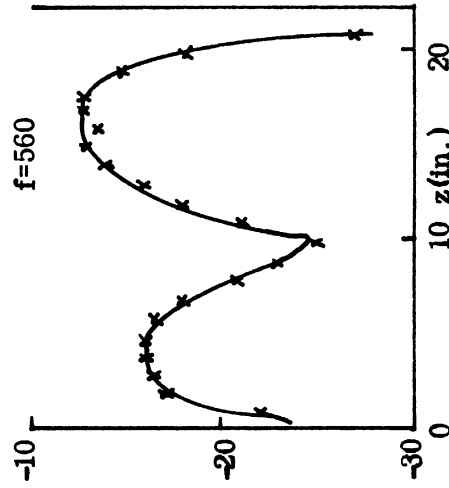
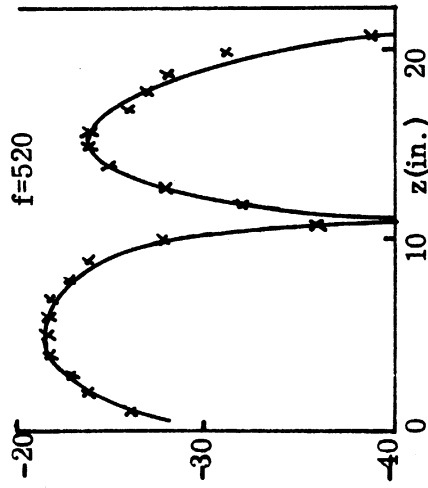


FIG. 4-3: Measurements of the Guided Wavelength Along the Antenna. The E-field probe is 8 inches above the antenna surface. Plate-to-plate separation is 22 inches. f is in MHz.



E_r (dB)



E_r (dB)

FIG. 4-3: Continued.

wavelength. The average of the frequencies where near resonance is observed will be taken as the resonant frequency for the plate-to-plate separation which was used. The error in the computed value for β_r using this average resonant frequency is only a few percent. This is more than sufficient for the purpose of determining the correct branch of roots to the characteristic equation that lead to backfire radiation, as the roots are quite far apart from one another. For instance, if $f = 500$ MHz is taken to be the resonant frequency for a plate-to-plate separation of 22 inches, or 0.56m, β_r can be calculated by

$$\beta_r = \frac{\lambda_o}{\lambda_g} k \quad . \quad (4.2)$$

This gives $\beta_r = 1.07 k$. If either $f = 480$ MHz or 520 MHz is instead, the difference in percentage is 20/500 or just 4 percent. In addition to Fig. 4-3, measurements were also taken with the two metal plates separated by 19 inches and 25 inches. The result is summarized in Table 4-1.

Separation (in.)	19	22	25
Separation (m.)	0.482	0.560	0.635
f = MHz	540	500	460
k (m ⁻¹)	11.3	10.5	9.65
β_r/k	1.15	1.07	1.02
β_r (m ⁻¹)	13	11.2	9.85

TABLE 4-1

It may therefore be concluded that the magnitude of β_r is near k , the free space wave number

$$|\beta_r| \sim k \quad (4.3)$$

Figure 4-1 seems to point to the need of a non-zero β_1 in the $e^{-j\beta z}$ representation for the surface fields. This non-zero imaginary part of β is not provided by the solution to the characteristic equation. The discrepancy is at least partly due to the values $\mu = 2.2$, $\epsilon = 3.8$ used in the computation. It is only reasonable to expect that complex values should be used with these electric constants of the ferrite to account for the loss in the material.

4.3 The Radiation Pattern

The radiation patterns for antennas with parameter values as shown in Section 4.1 are given below. Figure 4-4 shows the patterns for $L = 15$ inches. Figure 4-5 shows the patterns for $L = 25$ inches. Only $|E_\theta|$ is shown as the patterns for $|E_\phi|^2$ are similar to the ones shown here for $|E_\theta|^2$. All patterns are in the x-z plane, or $\phi = 0$ plane.

Also shown on Figs. 4-4 and 4-5 are the calculated patterns based on the roots to the characteristic equation. The calculation takes into account the contribution due to both ends as well as the cylindrical surface. It is made only for $f = 500$ MHz and 600 MHz. The agreement between the calculated patterns and the experimental patterns is seen to be fairly good. The most important source contributing to the disagreement between the calculation and the measurement is probably the use of real values for μ and ϵ in the calculation which ignores the loss in the ferrite material.

Figure 4-6 shows the radiation patterns of the 25-inch antenna without loading. It is seen that the unloaded antenna operates on the backfire mode at much higher frequencies. This indicates a substantial reduction in the diameter of the antenna. For instance, Kraus' formula for the low frequency limit of the unloaded mono-filar helix is

$$f_m = \frac{0.7 c}{2 \pi b} \quad (4.4)$$

where c is the free space light velocity. For $2b = 5$ inches, which is the outer diameter of the ferrite loaded antennas used in this work, (4.4) gives

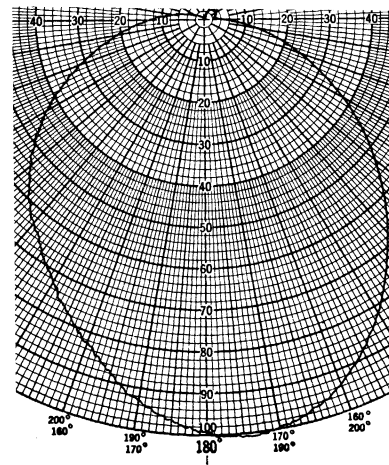
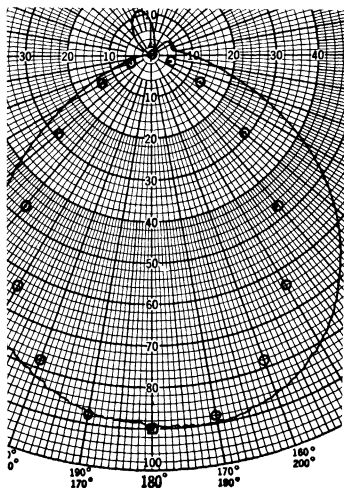
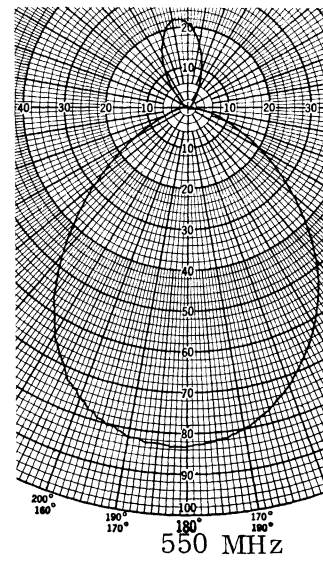
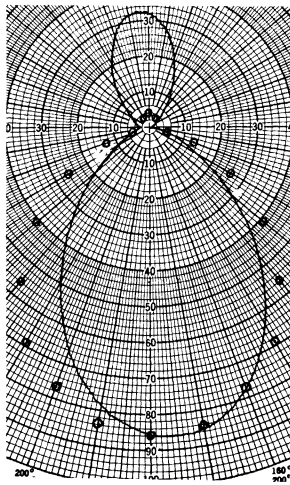
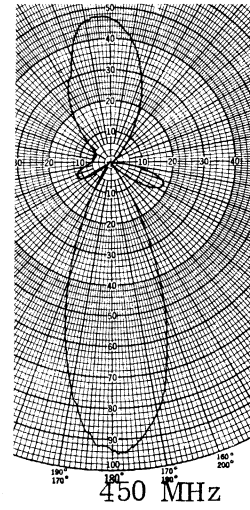
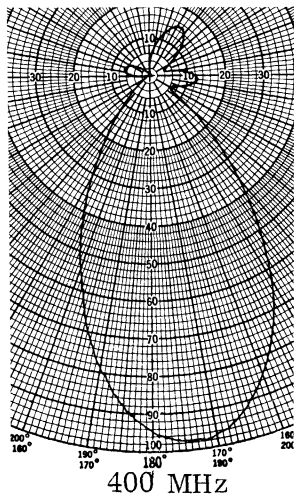


FIG. 4-4: The Measured Patterns of the Bifilar Helical Antenna with an Outer Layer of Ferrite. $L=15$ in. Circles indicated calculated patterns based on solution to the characteristic equation.

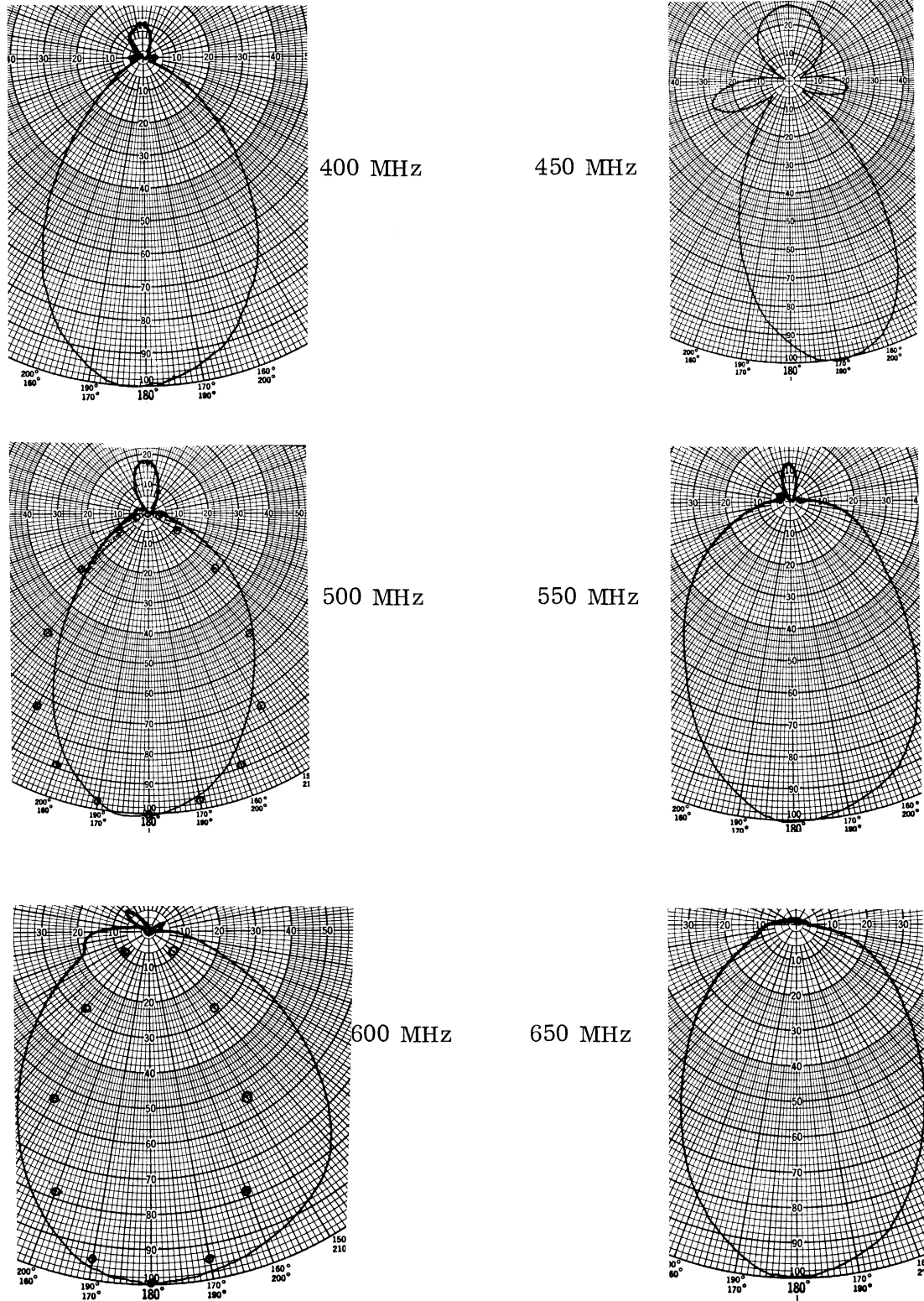


FIG. 4-5: Measured Patterns of Bifilar Helical Antenna with Outer Layer of Ferrite. $L=25$ in. Circles indicate calculated patterns based on solution to characteristic equation.

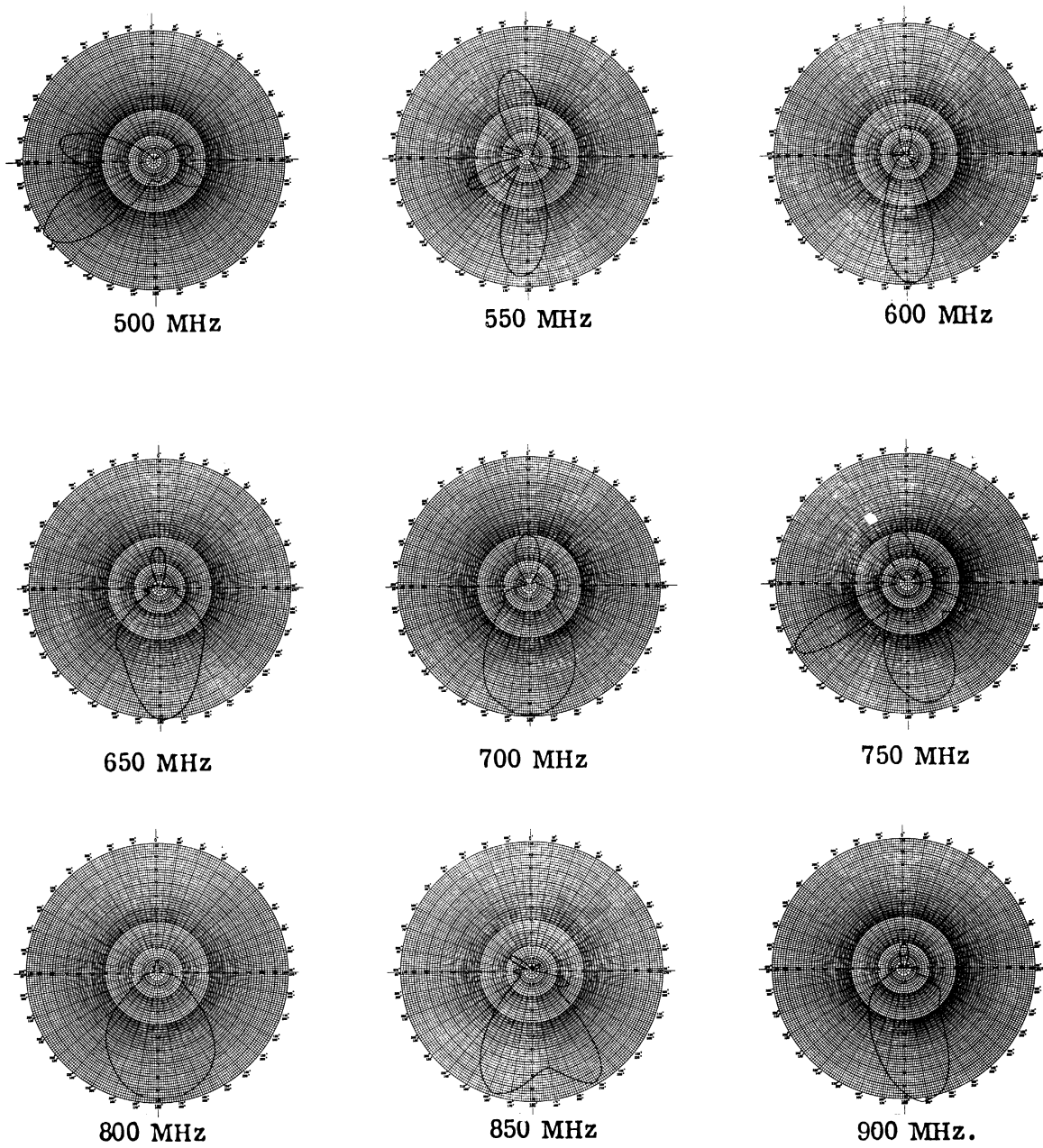


FIG. 4-6: The Measured Patterns of the Unloaded Bifilar Helical Antenna. $L = 25$ in.

$f_m = 530$ MHz. This is more than 30 percent higher than the low frequency limit for the loaded antennas seen from Figs. 4-4 and 4-5.

For the same diameter, the operating frequencies of the helical antenna with an outer layer of ferrite are also considerably lower than those of the ferrite tube antennas. This can be seen by direct comparison of the radiation patterns of the two kinds of antennas⁹.

CONCLUSIONS AND RECOMMENDATIONS

5.1 General

A large part of the present work can be applied to explain the radiation phenomenon of tube antennas and rod antennas operating in the end-fire mode. Assuming an axial dependence of $e^{-j\beta z}$, it is found that the radiation patterns are largely determined by the factor $A(\theta)$,

$$A(\theta) = \frac{1 - e^{-ju(\theta)}}{u(\theta)} \quad , \quad (5.1)$$

$$u(\theta) = \left(\frac{\beta}{k} - \cos \theta \right) kL \quad . \quad (5.2)$$

The end-fire condition is given by

$$x(0) = \frac{1}{2} u(0) = \left(\frac{\beta}{k} - 1 \right) \frac{kL}{2} \sim 0 \quad . \quad (5.3)$$

The backfire condition is given by

$$x(\pi) = \frac{1}{2} u(\pi) = \left(\frac{\beta}{k} + 1 \right) \frac{kL}{2} \sim 0 \quad . \quad (5.4)$$

For L equal to a few wavelength, (5.3) and (5.4) can be replaced by

$$\beta \sim k \quad , \quad (5.3a)$$

$$\beta \sim (-) k \quad , \quad (5.4a)$$

respectively. Note that β is complex.

On the characteristic equation, the following conclusions may be given:

- (1) The characteristic equation has many different roots.
- (2) Initial trial values and the iteration program used have much to do with the values of β eventually obtained.

- (3) The results of near field measurements may be used as a basis to determine the correct branch of roots that account for the radiation phenomenon of the antenna.
- (4) If the radiation patterns of the antenna are endfire, (5.3) may be used to furnish initial trial values for the characteristic equation. If the radiation patterns are backfire, (5.4) may be used to give the initial trial values.

On the radiation patterns, the following conclusions may be given:

- (1) The important contribution to either the backfire radiation or the endfire radiation is from the cylindrical surface for antennas with a surface field described by (5.3a) or (5.4a), provided the antenna length is over one free space wavelength.
- (2) The pattern is relatively insensitive to small variations in β_r and β_i .

5.2 Conclusions Pertaining to the Helical Antenna with an Outer Layer of Ferrite

(1) The near field measurements of the helical antenna with an outer layer of ferrite show that the surface fields of the antenna can be approximated by $e^{-j\beta z}$.

(2) The real part β_r of the propagation constant is found to be near $(-)k$.

The minus sign arises due to the fact that the phase of the surface field increases as the probe moves away from the feeding end toward the open end of the antenna.

(3) One branch of roots to the characteristic equation is

$$\beta \sim (-) k .$$

(4) Calculated patterns based on the branch of roots above show good agreement with the experimental patterns, which are backfire.

(5) For the same diameter, the bifilar helical antenna with an outer layer of ferrite operates at considerably lower frequencies than either the unloaded helical antenna or the ferrite tube antenna.

5.3 Suggestions for Future Efforts

There appear to be many worthwhile undertakings with the characteristic equations. For simplicity, it is suggested that the unloaded sheath helix be used for the study.

(1) Investigation of the conditions that conjugate roots to the characteristic equation exist.

(2) Investigation of the number of complex roots in a certain region, e.g., the number of roots with $|\beta| \leq 2$.

(3) Study of the existing iteration programs in connection with the solution of complex roots to any equation. In particular, the possibility that these programs may be modified to control the iteration process in some desirable fashion, e.g., an initial trial value always goes to the nearest root.

On the radiation patterns of the unloaded helical antenna, there are also a few problems of fundamental importance that can be explored further. The present work finds that the branch $\beta_r \sim (-)k$ gives the correct roots that are responsible for the backfire radiation of the bifilar helix with an outer layer of ferrite. While this is consistent with the general experiences on the rod and tube antennas, it differs from the branch $\beta \sim (-)k / \sin \psi$ commonly accepted as the correct branch of roots for the unloaded backfire bifilar helix. The easiest answer to this would appear to be that the loaded antenna operates on a mode that is different from that of the unloaded antenna. It is worth noting that there has been little work on calculation of the far field patterns, making use of the solutions to the characteristic equation, in the case of the unloaded helical antenna. Some efforts along this line appear to be well justified. In particular, it is recommended that the following subjects be explored further:

(4) Whether the Equivalence Principle approach used in the present analysis is applicable to the case of unloaded helical antennas.

(5) Actual calculation of the current on the winding of the helix, starting from the solution to the characteristic equation.

REFERENCES

1. S. Sensiper, "Electromagnetic Wave Propagation on Helical Conductors," MIT Research Laboratory, Cambridge, Mass., Technical Report No. 194 (1951).
2. S. Sensiper, "Electromagnetic Wave Propagation on Helical Structures: A Review and Survey of Present Programs," Proc. IRE, 43, pp. 149-161 (February 1955).
3. R. Mittra, "Wave Propagation on Helices," Trans. IRE, AP-11, pp. 585-586 (September 1963).
4. P. Klock, "A Study of Wave Propagation of Helices," University of Illinois Antenna Laboratory, Urbana, Illinois, Technical Report No. 68 (March 1963).
5. G. Rassweiler, "Helical and Log Conical Helical Antennas Loaded with an Isotropic Material," Ph. D. Thesis, The University of Michigan Radiation Laboratory Report 7848-3-Q, AD 806094 (1966).
6. C. T. Tai, "Lecture Notes on Antennas," The University of Michigan, Ann Arbor, Michigan
7. S. A. Schelkunoff, Electromagnetic Waves, D. Van Nostrand Company, New York (1943).
8. R. F. Harrington, Time Harmonic Electromagnetic Fields, McGraw-Hill Book Company, New York (1961).
9. C-C Chen, "An Analysis of the Behavior of the HE₁₁ Mode Ferrite Tube Antenna," Ph. D. Thesis, The University of Michigan Radiation Laboratory Report 1770-1-T, AD 849707 (March 1969).
10. H. Barlow and J. Brown, Radio Surface Waves, Oxford Clarendon Press (1962).
11. H. C. Pocklington, "Electrical Oscillations in Wires," Proc. Camb. Philo. Soc., 9, p. 324 (1897).
12. J. D. Kraus and Williamson, "Characteristics of the Helical Antennas Radiating in the Axial Mode," J. Appl. Phys., 19, p. 87 (1948).
13. W. T. Patton, "The Backfire Bifilar Helical Antenna," The University of Illinois Antenna Laboratory, Urbana, Illinois, Technical Report No. 61 (September 1962).
14. G. N. Watson, A Treatise on the Theory of Bessel Functions, Cambridge University Press, Second Edition, 1966.

APPENDIX A

SOME USEFUL RELATIONS INVOLVING THE BESSEL FUNCTIONS WITH COMPLEX ARGUMENT

The Bessel functions $I_n(z)$ and $K_n(z)$ used in this text are as defined in Watson. Some of the relations that are used involving these functions are given below.

1. Bessel-Fourier series:

$$e^{jkb \sin \theta \cos \phi} = J_0(kb \sin \theta) + \sum_{m=1}^{\infty} 2(j)^m J_m(kb \sin \theta) \cos m\phi \quad (\text{A.1})$$

2. Some reduction formulas:

$$I'_n - \frac{n I_n}{z} = I_{n+1} \quad (\text{A.2})$$

$$I'_n + \frac{n I_n}{z} = I_{n-1} \quad (\text{A.3})$$

$$K'_n - \frac{n K_n}{z} = (-) K_{n+1} \quad (\text{A.4})$$

$$K'_n + \frac{n K_n}{z} = (-) K_{n-1} \quad (\text{A.5})$$

3. Lommel integrals:

$$\begin{aligned}
& \int_a^b z Z_n(\alpha z) J_n(\beta z) dz \quad (a, b, \alpha, z \text{ complex}) \\
&= \frac{z}{\alpha^2 - \beta^2} \left[\beta Z_n(\alpha z) J_n'(\beta z) - \alpha J_n(\beta z) Z_n'(\alpha z) \right] \Big|_a^b \\
&= \frac{z}{\alpha^2 - \beta^2} \left[\beta Z_n(\alpha z) J_{n-1}(\beta z) - \alpha J_n(\beta z) Z_{n-1}(\alpha z) \right] \Big|_a^b \quad (A.6)
\end{aligned}$$

where

$$Z_n = J_n, N_n, H_n^{(1)}, H_n^{(2)} .$$

Using the relation,

$$I_n(z) = (-j)^n J_n(jz) \quad (A.7)$$

$$K_n(z) = \frac{\pi}{2} j^{(n+1)} H_n^{(1)}(jz) \quad (A.8)$$

between different kinds of Bessel functions, the following Lommel's integrals for $I_n(z)$ and $K_n(z)$ may be obtained

$$\begin{aligned}
& \int z I_n(\alpha z) J_n(\beta z) dz \\
&= \frac{z}{\alpha^2 + \beta^2} \left[-\beta I_n(\alpha z) J_{n-1}(\beta z) + \alpha J_n(\beta z) I_{n-1}(\alpha z) \right] \quad (A.9)
\end{aligned}$$

$$\begin{aligned}
& \int z K_n(\alpha z) J_n(\beta z) dz \\
&= \frac{-z}{\alpha^2 + \beta^2} \left[\beta K_n(\alpha z) J_{n-1}(\beta z) + \alpha J_n(\beta z) K_{n-1}(\alpha z) \right] \quad (A.10)
\end{aligned}$$

4. Other integrals:

$$\int_0^{2\pi} e^{jkb \sin \theta \cos (\phi - \phi')} e^{jn\phi'} \sin \phi' d\phi$$

$$= j^n \pi \left[J_{n+1}(kb \sin \theta) e^{j(n+1)\phi} + J_{n-1}(kb \sin \theta) e^{j(n-1)\phi} \right] \quad (\text{A.11})$$

$$\int_0^{2\pi} e^{jkb \sin \theta \cos \phi} e^{jn(\phi - \phi')} \cos \phi' d\phi'$$

$$= j^{n-1} \pi \left[J_{n-1}(kb \sin \theta) e^{j(n-1)\phi} - J_{n+1}(kb \sin \theta) e^{j(n+1)\phi} \right] \quad (\text{A.12})$$

$$\int_0^{2\pi} e^{jkb \sin \theta \cos (\phi - \phi')} e^{jn\phi'} d\phi'$$

$$= 2\pi j^n J_n(kb \sin \theta) e^{jn\phi} \quad (\text{A.13})$$

APPENDIX B

EVALUATION OF THE UNDETERMINED COEFFICIENTS IN CONNECTION WITH THE FIELDS ON THE ANTENNA

The coefficients f , g , F , G , etc., are needed in the calculation of the far field patterns. These are evaluated after the value of β is obtained from the characteristic equation. Since (2.52) and (2.53) are homogeneous equations for (fC_1) and (gC_2) , one of these two coefficients can be set arbitrarily. Let

$$f C_1 = 1 \quad . \quad (B.1)$$

Then, from (2.53),

$$g C_2 = -A_5/A_6 \quad . \quad (B.2)$$

From (2.46),

$$f = D^{pt} - \frac{A_5}{A_6} D^{qt} \quad . \quad (B.3)$$

From (2.47),

$$g = D^{sp} - \frac{A_5}{A_6} D^{sq} \quad . \quad (B.4)$$

F , G are obtained from (2.34) and (2.35) respectively,

$$F = \frac{1}{K(\Gamma b)} \left[f I(\gamma b) + f C_1 K(\gamma b) \right] \quad (B.5)$$

$$G = \frac{1}{K(\Gamma b)} \left[I(\gamma b) g + K(\gamma b) g C_2 \right] \quad . \quad (B.6)$$

Finally, from (2.31),

$$F^{(3)} = \frac{1}{I(\Gamma a)} \left[f I(\gamma a) + f C_1 K(\gamma a) \right] \quad (B.7)$$

and from (2.30) and (2.31),

$$\begin{aligned}
 G^{(3)} = & \frac{-\Gamma}{j\omega\mu_0\Gamma'(\Gamma a)} \left\{ \frac{n\beta}{a} \left(\frac{1}{\Gamma^2} - \frac{1}{\gamma^2} \right) I(\gamma a) f \right. \\
 & + \frac{n\beta}{a} \left(\frac{1}{\Gamma^2} - \frac{1}{\gamma^2} \right) K(\gamma a) f C_1 \\
 & - \frac{j\omega\mu_0}{\gamma} \Gamma'(\gamma a) g \\
 & \left. - \frac{j\omega\mu_0}{\gamma} K'(\gamma a) g C_2 \right\} \tag{B.8}
 \end{aligned}$$

APPENDIX C
A FACTOR $A(\theta)$ FOR THE FAR FIELDS
OF SOME LONG ANTENNAS

C.1 Introduction

In considering the far field patterns of long antennas with a source distribution of the form $F(r, \phi) e^{-j\beta z}$, a factor $A(\theta)$ appears after integration of the above source function. The two factors in the source function are separable in the integration process. The factor $A(\theta)$ comes out of the $e^{-j\beta z}$ integration and may be viewed as the array factor in the array theory. The integration of the transverse distribution factor $F(r, \phi)$ may be viewed as the element factor in the array theory. The total pattern is then found as the product of the individual element factor and the array factor. The factor $A(\theta)$ is often a very directional factor, or, $A(\theta)$ changes a great deal with θ . This is the case, for example, when the long antennas are operating in the endfire mode. It is, therefore, the dominant factor determining the far field pattern in many cases.

C.2 The Factor $A(\theta)$

The factor $A(\theta)$ is a complex composite function of θ

$$A(\theta) = \frac{1 - e^{-j u(\theta)}}{u(\theta)} \quad (C.1)$$

where

$$u(\theta) = \left(\frac{\beta}{k} - \cos \theta\right) kL \quad (C.2)$$

$$\beta = \beta_r + j\beta_i$$

k = free space wave number

L = length of the antenna

θ = angle measured from the axis of the antenna.

$A(\theta)$ may be written as a product of an amplitude function and a phase function. Let

$$v(\theta) = \left(\frac{\beta_r}{k} - \cos \theta \right) kL \quad , \quad (\text{C.3})$$

then

$$u = v + j \beta_i L \quad . \quad (\text{C.4})$$

Note v is a real function of θ .

$$A(\theta) = \left| f \left(\frac{1}{2} v(\theta) \right) \right| e^{jg(v(\theta))} \quad (\text{C.5})$$

Both the amplitude function $\left| f \left(\frac{1}{2} v(\theta) \right) \right|$ and the phase function $g(v(\theta))$ are real functions.

$$\left| f \left(\frac{v}{2} \right) \right| = \sqrt{\frac{\frac{1}{4} \left(1 - e^{\beta_i L} \right)^2 + e^{\beta_i L} \sin^2 \frac{v}{2}}{\left(\frac{v}{2} \right)^2 + \left(\frac{\beta_i L}{2} \right)^2}} \quad (\text{C.6})$$

$$g(v) = \tan^{-1} \left[\frac{\frac{\beta_i L}{e^{\beta_i L} \sin v} - \frac{\beta_i L}{v}}{\frac{1 - e^{\beta_i L} \cos v}{1 + \frac{\beta_i L \sin v}{\beta_i L} - \frac{\beta_i L}{v}}} \right] \quad . \quad (\text{C.7})$$

An important case is when β is real. Then,

$$\begin{aligned} \beta &= \beta_r \\ \beta_i &= 0 \\ u = v &= \left(\frac{\beta}{k} - \cos \theta \right) kL \end{aligned} \quad (\text{C.8})$$

$$f \left(\frac{v}{2} \right) = \frac{\sin \frac{v}{2}}{\frac{v}{2}} \quad (\text{C.9})$$

$$g(v) = \frac{\pi}{2} - \frac{v}{2} \quad (\text{C.10})$$

For convenience, we will introduce a new variable x .

$$x(\theta) = \frac{v(\theta)}{2} \quad (\text{C.11})$$

Then,

$$|A(\theta)| = |f(x(\theta))| \quad (\text{C.12})$$

Before going into the pattern study, it is necessary to study the function $f(x)$ in detail.

C.3 Properties of the Real Function $f(x)$.

$$f(x) = \frac{\sin x}{x} \quad (\text{C.13})$$

The function $f(x)$ has the following properties:

- 1.) $f(x)$ is even,
- 2.) The absolute maximum of $f(x)$ is 1 at $x = 0$,

$$f(0) = 1 \quad (\text{C.14})$$

- 3.) Other extremums of $f(x)$ occurs at the roots to the equation

$$x = \tan x, \quad (\text{C.15})$$

other than $x = 0$ which is the absolute maximum.

Fig. C-1 shows the roots to the equation graphically. It is seen from the figure that there is one and only one root in the interval

$$\left[\frac{2n-1}{2} \pi, \frac{2n+1}{2} \pi \right], \quad \text{where } n = \pm 1, \pm 2, \pm 3, \dots$$

This root will be written as x_n . The only exception is the interval $[-\pi, \pi]$, where there is the root $x = 0$. This root will be written as x_0 .

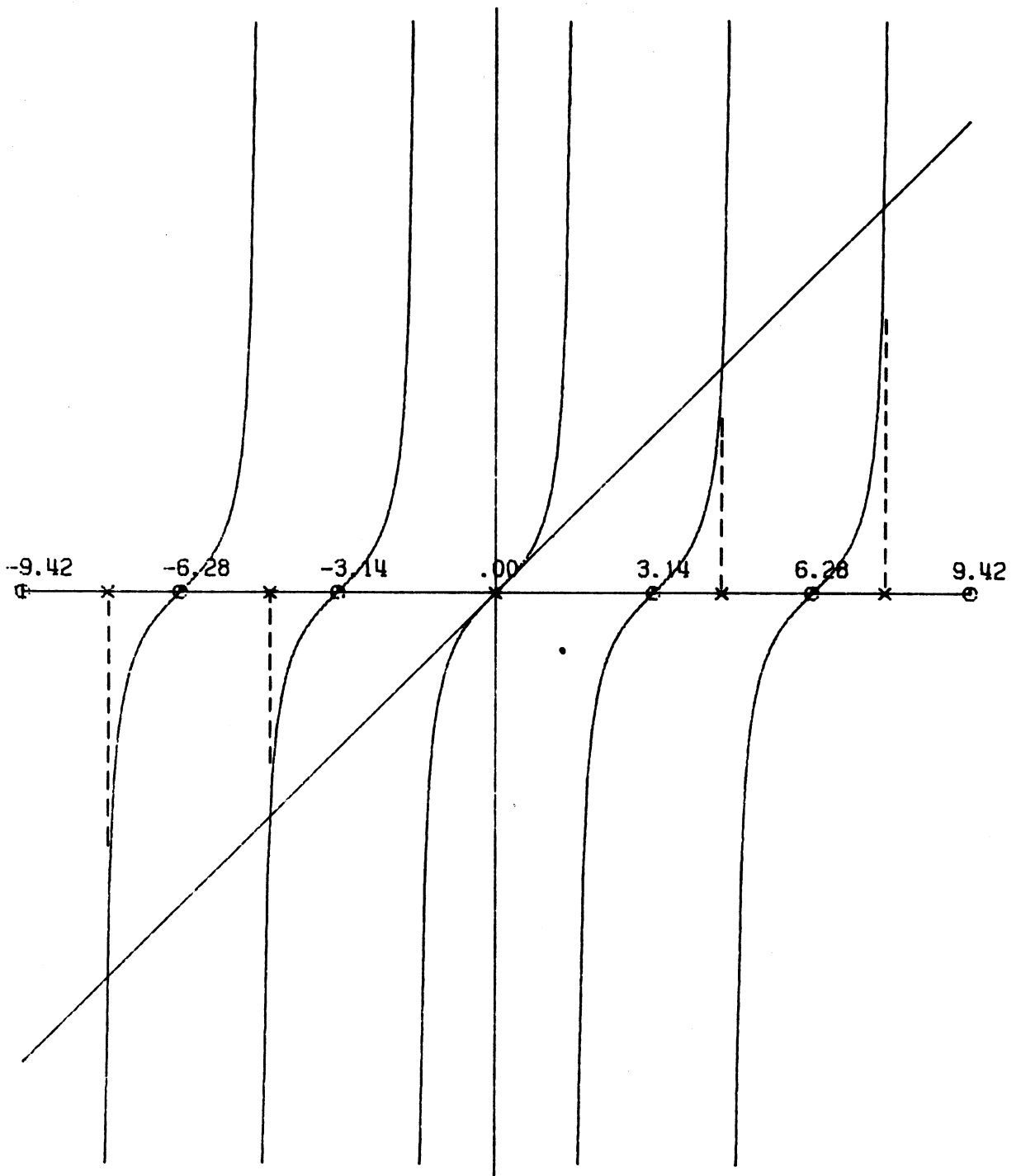


FIG. C-1: Graphical Solution of the Equation $x = \tan x$. Maximums of $|f(x)|$ are indicated by crosses; zeros by circles.

The following properties of the roots are obvious from Fig. C-1.

$$\dots < x_{-n} < x_{-n+1} < \dots < x_{-1} < x_0 < x_1 < \dots < x_{n-1} < x_n < \dots \quad (\text{C.16})$$

$$x_{-n} = -x_n \quad (\text{C.17})$$

$$x_n \sim n\pi + \frac{\pi}{2} \text{ for large } n \quad (\text{C.18})$$

The first few positive roots are

$$\begin{cases} x_1 = 4.493 \\ x_2 = 7.725 \\ x_3 = 10.90 \\ x_4 = 14.07 \\ x_5 = 17.22 \end{cases} \quad (\text{C.19})$$

For $n = 5$, the large n approximation for x_5 gives $x_5 \sim 5.5\pi = 17.30$ compared with the correct value of $x_5 = 17.22$. The value of the function $f(v)$ at these extremums is

$$f(x_n) = \frac{\sin x_n}{x_n} = \frac{(-1)^n}{\sqrt{1+x_n^2}} \quad (\text{C.20})$$

$$f(x_n) \sim \frac{(-1)^n}{x_n} \sim \frac{(-1)^n}{\left(n + \frac{1}{2}\right)\pi} \text{ large } n \quad (\text{C.21})$$

The first few $f(x_n)$ are

$$\begin{cases} f(x_1) = (-) 0.217 \\ f(x_2) = 0.128 \\ f(x_3) = (-) 0.0915 \\ f(x_4) = 0.0711 \\ f(x_5) = (-) 0.0581 \end{cases} \quad (\text{C.22})$$

For $n = 5$, the formula for large n yields $f(x_5) \sim \frac{(-1)^5}{5.5\pi} = (-) 0.0579$, compared with the correct value of $f(x_5) = (-) 0.0581$. The values of $f(x)$ at the roots x_n have the property

$$|f(x_0)| > |f(x_1)| > \dots > |f(x_{n-1})| > |f(x_n)| > \dots, \quad (\text{C.23})$$

as a result of (C.16) and (C.20).

4.) Zeros of $f(x)$ are the roots to the equations

$$\begin{cases} \sin x = 0 \\ x \neq 0 \end{cases} \quad (\text{C.24})$$

The roots are $x = n\pi$, where n is any integer other than zero.

The roots will be denoted by y_n .

$$\begin{cases} y_n = n\pi \\ n = \text{any integer other than } 0. \end{cases} \quad (\text{C.25})$$

5.) The zeros and extremums of $f(x)$ are interlaced in the following way:

$$\dots < x_{-n} < y_{-n} < x_{-n+1} \dots < y_{-1} < x_0 < y_1 < \dots < x_{n-1} < y_n < x_n < \dots \quad (\text{C.26})$$

Fig. C-2 shows $|f(x)|$ as a function of x . The inequality (C.26) is also shown graphically in Fig. C-1.

C.4 The Mapping $x(\theta)$ and its Inverse for a Real β

We will investigate the properties of the mapping $x(\theta)$,

$$x(\theta) = \frac{1}{2} v(\theta) = \left(\frac{\beta}{k} - \cos \theta \right) \frac{kL}{2} \quad (\text{C.11})$$

The domain of x is $\{\theta | \theta \in [0, \pi]\}$. The range is $R_1 = \{x | x \text{ real}\}$. Since $\cos \theta$ is continuous and monotonically decreasing on $[0, \pi]$, the mapping $x : \theta \rightarrow x$ is continuous and monotonically increasing, or,

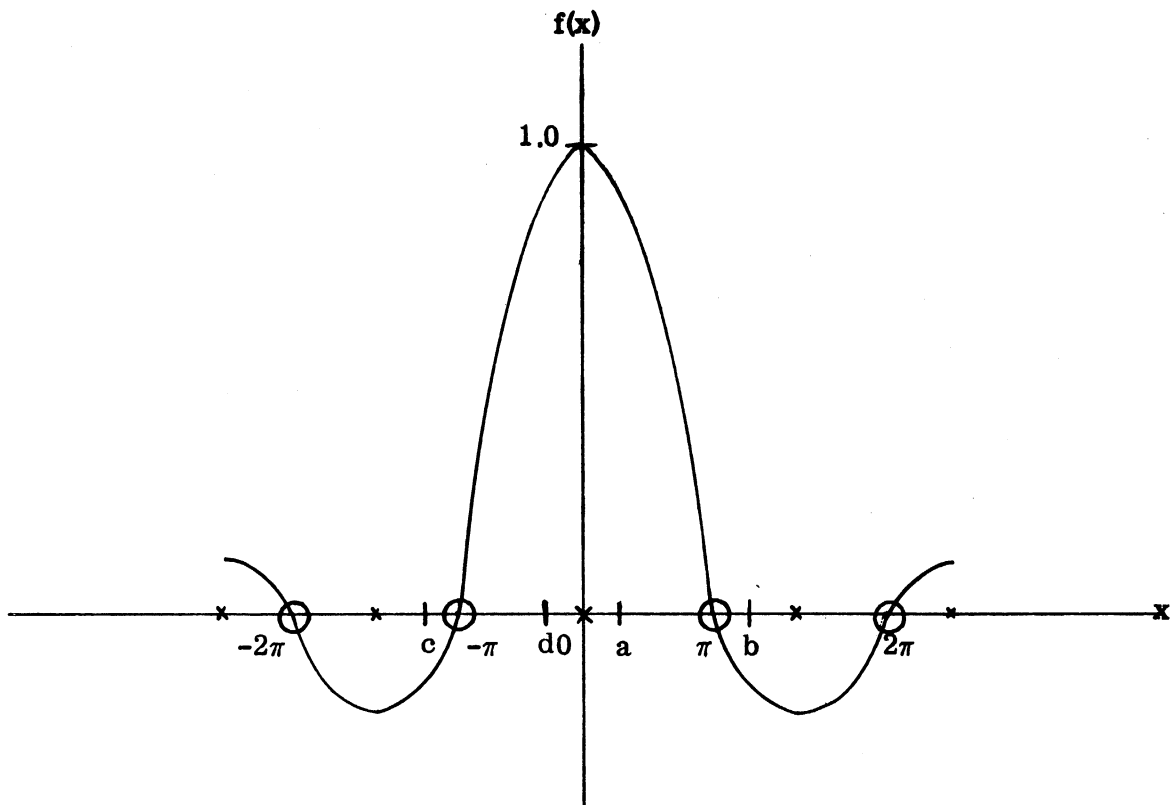


FIG. C-2: $f(x) = \frac{\sin x}{x}$ and Its Zeros and Extremums.

Circles show positions of zeros $y_n = n\pi$, $n \neq 0$. Crosses show positions of extremums x_n , $n \neq 0$ and the absolute maximum $x = 0$.

$$\theta_1 > \theta_2 \implies x_1 = x(\theta_1) > x_2 = x(\theta_2) \dots \quad (\text{C.27})$$

Furthermore, $[0, \pi]$ is mapped into another closed interval $[x(0), x(\pi)]$, where

$$\begin{cases} x(0) = \left(\frac{\beta}{k} - 1\right) \frac{kL}{2} \\ x(\pi) = \left(\frac{\beta}{k} + 1\right) \frac{kL}{2} \end{cases} \quad (\text{C.28})$$

We can therefore define an inverse mapping

$$\begin{aligned} \theta &: x \rightarrow \theta \\ x &\in [x(0), x(\pi)] \in R_1 \\ \theta &\in [0, \pi] \end{aligned}$$

by

$$\theta = \cos^{-1} \left(\frac{\beta}{k} - \frac{2x}{kL} \right). \quad (\text{C.29})$$

The inverse mapping is also continuous and monotonically increasing,

$$x_1 > x_2 \implies \theta_1 = \theta(x_1) > \theta_2 = \theta(x_2) \quad (\text{C.30})$$

The mapping properties of $x(\theta)$ and its inverse are very useful. The shape of the factor $|A(\theta)|$ for any pair of β/k and kL can be determined graphically using these properties and Fig. C-2. This is because $\{\theta \mid \theta \in [0, \pi]\}$ will be mapped to a closed interval $\{x \mid x \in [x(0), x(\pi)]\}$ by the mapping properties. The shape of $|A(\theta)|$ is then determined by $|f(x)|$ on this closed interval. For instance, if $[0, \pi]$ is mapped onto $[a, b]$ on Fig. C-2, this would represent an endfire pattern. The main lobe level would be $|f(a)|$. The back lobe would be the only minor lobe and its level would be $|f(b)|$.

We are now in a position to estimate the number of lobes of $A(\theta)$. Obviously, the number of lobes of $A(\theta)$ is equal to the number of maximums of $|f(x)|$ on $[x(0), x(\pi)]$. While it is possible to give precise formulas governing different cases, it will suffice here by presenting a simple but revealing

approximate formula. The exact number of lobes is not of much concern in most cases. Figure C-2 shows there is one maximum x_n in any interval Δx of length π , except near $x = 0$. The number of x_n 's in $[x(0), x(\pi)]$ is therefore approximately $(1/\pi)[x(\pi) - x(0)]$. Using (C.28), the number of lobes N of $A(\theta)$ is

$$N \sim \frac{kL}{\pi} + \begin{pmatrix} 0 \\ 1 \\ 2 \end{pmatrix} \quad (\text{C.31})$$

The choice of 0, 1, 2 is determined by considerations as to whether any or all of the two end points $x(0)$ and $x(\pi)$ are maximums and the inaccuracy of the kL/π term. For long antennas,

$$N \sim \frac{kL}{\pi} + 1 \quad (\text{C.31a})$$

appears to be adequate for an estimation in most cases. (C.31) and (C.31a) clearly indicate that the number of lobes of $A(\theta)$ is almost entirely determined by the length L , with longer antennas having more lobes. The value of β affects the positions of $x(0)$ and $x(\pi)$. Its effect on N is only in the choice of 0, 1, or 2 in (C.31).

C.5 The Factor $A(\theta)$ for a Real Propagation β

In the case $\beta = \beta_r, \beta_i = 0$

$$x(\theta) = \frac{v(\theta)}{2} = \left(\frac{\beta}{k} - \cos \theta \right) \frac{kL}{2} \quad (\text{C.11})$$

$$A(\theta) = \left| f(x(\theta)) e^{jg(v(\theta))} \right| \quad (\text{C.5})$$

$$\left| A(\theta) \right| = \left| f(x(\theta)) \right| \quad (\text{C.12})$$

$$f(x) = \frac{\sin x}{x} \quad (\text{C.13})$$

The phase function $g(v(\theta))$ will not affect the shape of the pattern. We will now look into the composite amplitude function $\left| f(x(\theta)) \right|$ in detail.

1.) The function $f(x(\theta))$ has an absolute maximum equal to 1 at $x(\theta) = 0$.

This happens at an angle

$$\theta_0 = \cos^{-1} \frac{\beta}{k} . \quad (\text{C.32})$$

It is seen that θ_0 can be found only for the case $\beta < k$. The angle θ_0 is independent of the antenna length L .

2.) The other maximums for $|A(\theta)|$ occur at angles θ such that $f(x(\theta))$ has an extremum (maximum or minimum),

$$x(\theta) = x_n$$

where x_n 's are the roots to (C.15). From (C.29), we have,

$$\begin{cases} \theta_{xn} = \cos^{-1} \left(\frac{\beta}{k} - \frac{2x_n}{kL} \right) \\ n = \pm 1, \pm 2, \pm 3 \dots \end{cases} \quad (\text{C.33})$$

Since the argument of the function arc-cosine is between -1 and 1, only a finite number of x_n 's would yield an angle θ by (C.33) for a certain pair of β/k and kL . These angles, unlike θ_0 , depend on the length of the antenna as well as the propagation constant β . The values of these extremums are given by (C.20) to (C.22). The largest of these relative extremums is $|f(x_1)| = 0.217$ as compared with $f(0) = 1$ for the absolute maximum.

$$|A(\theta_{xn})| = |f(x_n)| \quad (\text{C.34})$$

3.) The zeros of $|A(\theta)|$ are found by

$$|A(\theta)| = |f(x(\theta))| = 0.$$

From (C.25), for the zeros of $f(x)$, and (C.29)

$$\begin{cases} \theta_{yn} = \cos^{-1} \left(\frac{\beta}{k} - \frac{2y_n}{kL} \right) = \cos^{-1} \left(\frac{\beta}{k} - \frac{2n\pi}{kL} \right) \\ n = \pm 1, \pm 2, \pm 3, \dots \end{cases} \quad (\text{C.35})$$

Again, only a finite number of θ can be found by (C.35) for a given pair of β/k and kL . All these zeros are dependent on the antenna length L and the propagation constant β .

$$|A(\theta_{y_n})| = |f(y_n)| = 0 \quad (\text{C.36})$$

4.) The angle θ_{x_n} at which $A(\theta)$ has maximums are interlaced with the angles at which $|A(\theta)| = 0$ in the following way:

$$\begin{aligned} 0 \leq \theta_{x(-n)} < \theta_{y(-n)} < \theta_{x(-n+1)} < \dots < \theta_{y(-1)} < \theta_0 < \theta_{y1} < \dots \\ < \dots < \theta_{x(n-1)} < \theta_{y_n} < \theta_{x_n} < \dots \leq \pi \end{aligned} \quad (\text{C.37})$$

(C.37) is a direct result of the inequality (C.26) and the order preserving property of the inverse mapping $\theta : x \rightarrow \theta$ as given (C.30). The end values 0 and π in (C.37) are the lower and upper bound of the inverse mapping .

Figure C-3 shows the relative positions of the angles θ_{x_n} 's and θ_{y_n} 's. It should be cautioned again that only a finite number of the θ_{x_n} 's and θ_{y_n} 's can be found for given values of β/k and kL . An important observation with (C.37) is that if two θ 's in (C.37) are known to exist, then every θ between the two in the sequence of (C.37) also exists. Figure C-4 shows the relative levels of $|A(\theta)|$ at θ_{x_n} 's and θ_{y_n} 's.

C.6 Classification of Waves

A wave of the form $F(x, y) e^{-j\beta z}$ along the z -axis is often referred to as a fast wave if $\beta < k$ or a slow wave if $\beta > k$. It is generally accepted that fast waves radiate mainly at an angle $\theta_0 = \cos^{-1}\left(\frac{\beta}{k}\right)$ given by (C.32) and slow waves radiate mainly along the z -axis. The directivity of such a traveling wave antenna is thought to be better for longer antennas. The real picture is more complicated, as will be seen in the following sections.

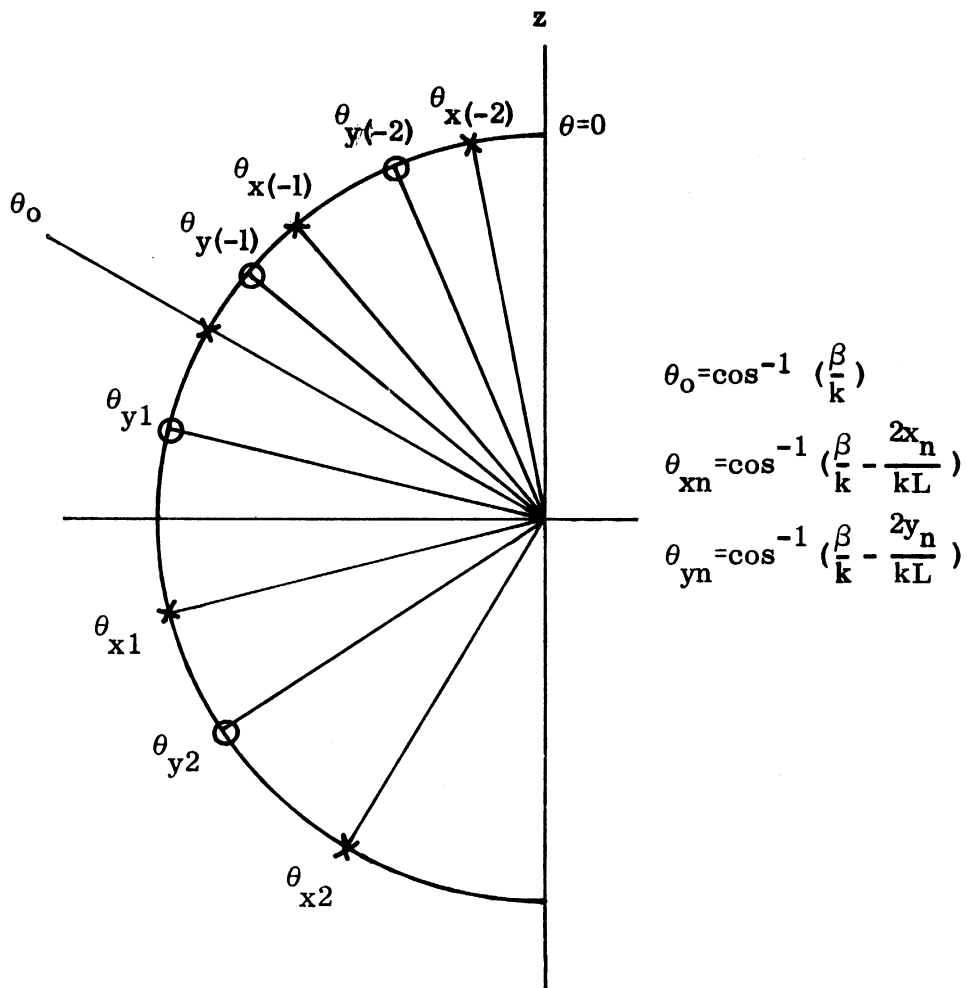


FIG. C-3: Relative Positions of Maxima and Zeros of $|A(\theta)|$.
 Maxima are indicated by crosses; zeros by circles.
 The spacing between θ 's is not the real spacing.

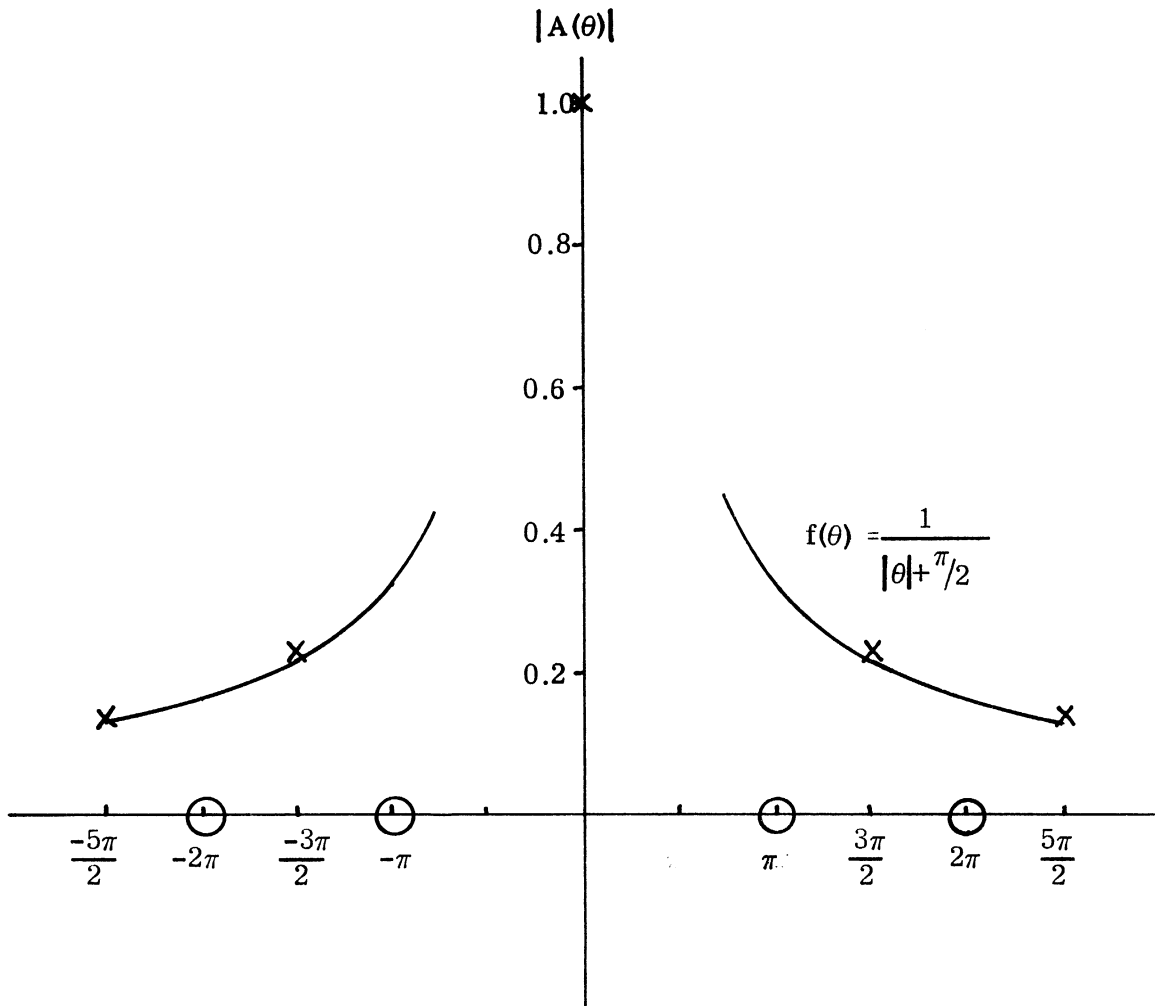


FIG.C-4: Relative Levels of $|A(\theta)|$.

A maximum is represented by a cross; a zero by a circle.

C.7 Fast Waves with a Real Propagation Constant β

The direction of maximum radiation of fast waves $\left(\frac{\beta}{k} < 1\right)$ is along

$$\theta_0 = \cos^{-1} \left(\frac{\beta}{k} \right) \quad (\text{C.32})$$

The zeros about θ_0 are θ_{-1} and θ_1 , from (C.35),

$$\begin{cases} \theta_{y1} = \cos^{-1} \left(\frac{\beta}{k} - \frac{2\pi}{kL} \right) \\ \theta_{y(-1)} = \cos^{-1} \left(\frac{\beta}{k} + \frac{2\pi}{kL} \right) \end{cases} \quad (\text{C.38})$$

For antennas with a length of one free space wavelength ($kL = 2\pi$) or longer, θ_{y1} always exists. The existence of $\theta_{y(-1)}$ would require a longer antenna (for the same β/k) as can be seen from (C.38). Figure C-5a shows the case where only θ_{y1} exists. The region (θ_{y1}, π) , marked S. L. in the figure, indicates the region where minor lobes exist. Figure C-5b shows the case when both θ_{y1} and $\theta_{y(-1)}$ exist. There are two regions that minor lobes can exist in this case. These are $(0, \theta_{y(-1)})$ and (θ_{y1}, π) . The minor lobes are found by (C.33) and zeros by (C.35). They are ordered by (C.37),

$$\theta_{xn} = \cos^{-1} \left(\frac{\beta}{k} - \frac{2x_n}{kL} \right) \quad (\text{C.33})$$

$$\theta_{yn} = \cos^{-1} \left(\frac{\beta}{k} - \frac{2y_n}{kL} \right) \quad (\text{C.35})$$

$$0 < \theta_{y(-1)} < \theta_0 < \theta_{y1} < \theta_{x1} < \theta_{y2} < \dots < \pi \quad (\text{C.37})$$

The minor lobe level is given by

$$\left| A(\theta_{xn}) \right| = \left| f(x_n) \right| \quad (\text{C.34})$$

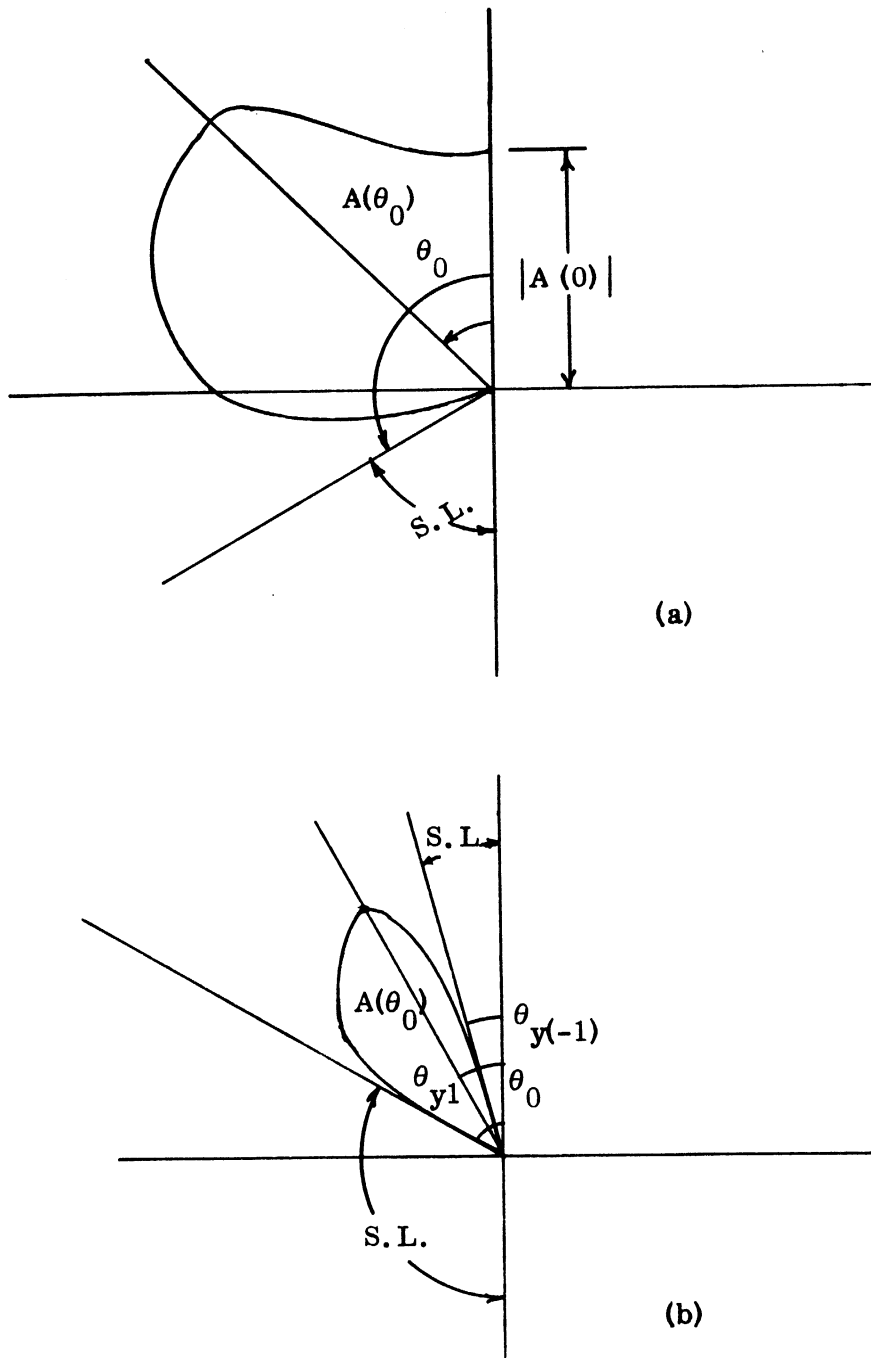


FIG. C-5: Factor $|A(\theta)|$ for fast waves.

The largest minor lobe level is

$$|f(x_1)| = |f(x_{-1})| = 0.217$$

for θ_{x1} and $\theta_{x(-1)}$. This compares with the main lobe level of $|f(0)| = 1$. The end points $\theta = 0$ and $\theta = \pi$ may also be minor lobes. It is obvious that if the smallest of the θ_{xn} 's and θ_{yn} 's is a θ_{yn} , then $\theta = 0$ is also a minor lobe. Likewise, if the largest of the θ_{xn} 's and θ_{yn} 's is a θ_{yn} , then $\theta = \pi$ is also a minor lobe. Whether $\theta = 0$ and $\theta = \pi$ are minor lobes or not, it can be shown the following is always true:

$$\begin{cases} |A(\theta_0)| > |A(\theta_{x1})| > \dots > |A(\theta_{xp})| \geq |A(\pi)| \\ |A(\theta_0)| > |A(\theta_{x(-1)})| > \dots > |A(\theta_{x(-q)})| \geq |A(0)| \end{cases} \quad (\text{C.39})$$

where θ_{xp} is the largest of the θ_{xn} 's, $\theta_{x(-q)}$ is the smallest of the θ_{xn} 's. p, q are non-negative integers. (C.39) ensures that the largest minor lobe level is only 0.217 time of the main lobe level. A numerical example of the preceding result is given below.

If $\beta/k = 0.6$, $kL = 2\pi$ ($L = \lambda$), then,

$$x(0) = \left(\frac{\beta}{k} - 1\right) \frac{kL}{2} = -1.26,$$

$$|f(x(0))| = \left| \frac{\sin(-1.26)}{-1.26} \right| = 0.76,$$

$$x(\pi) = \left(\frac{\beta}{k} + 1\right) \frac{kL}{2} = 5.03,$$

$$|f(x(\pi))| = \left| \frac{\sin(5.03)}{5.03} \right| = 0.19,$$

$$\theta_0 = \cos^{-1} \left(\frac{\beta}{k} \right) = 53^\circ,$$

$$\theta_{y1} = \cos^{-1} \left(\frac{\beta}{k} - \frac{2y_1}{kL} \right) = 116^\circ,$$

$$\theta_{x1} = \cos^{-1} \left(\frac{\beta}{k} - \frac{2x_1}{kL} \right) = 146^\circ .$$

These are the only θ_{xn} 's and θ_{yn} 's that can be found for the values of β/k and kL given. The results may now be tabulated.

θ	0°	53°	116°	146°	180°
$ A(\theta) $	0.76	1	0	0.217	0.19

Figure C-6 shows $|A(\theta)|$ for $\beta/k = 0.6$ and four different kL 's. The numerical example above with $kL = 2\pi$ corresponds to Fig. C-6a. One can see clearly in these figures how the length of the antenna affects the beam width of the main lobe and the number of minor lobes. Incidentally, the beamwidth of the main lobe for long antennas is found by

$$\theta_{y1} - \theta_{y(-1)} = \cos^{-1} \left(\frac{\beta}{k} - \frac{2\pi}{kL} \right) - \cos^{-1} \left(\frac{\beta}{k} + \frac{2\pi}{kL} \right), \quad (C.40)$$

if it is defined as the angle between the two nulls adjacent to the beam. It is not hard to see from (C.40) that the main lobe beam width decreases with increasing length of the antenna.

Finally, it may be remarked that fast waves can be essentially endfire. This is the case when β approaches k and the angle of maximum radiation $\theta_0 = \cos^{-1} \left(\frac{\beta}{k} \right)$ becomes smaller and smaller.

C.8 Slow Waves with a Real Propagation Constant β

For the slow waves ($\beta > k$), the angle

$$\theta_0 = \cos^{-1} \left(\frac{\beta}{k} \right)$$

does not exist. Since

$$x(0) = \left(\frac{\beta}{k} - 1 \right) \frac{kL}{2} > 0 ,$$

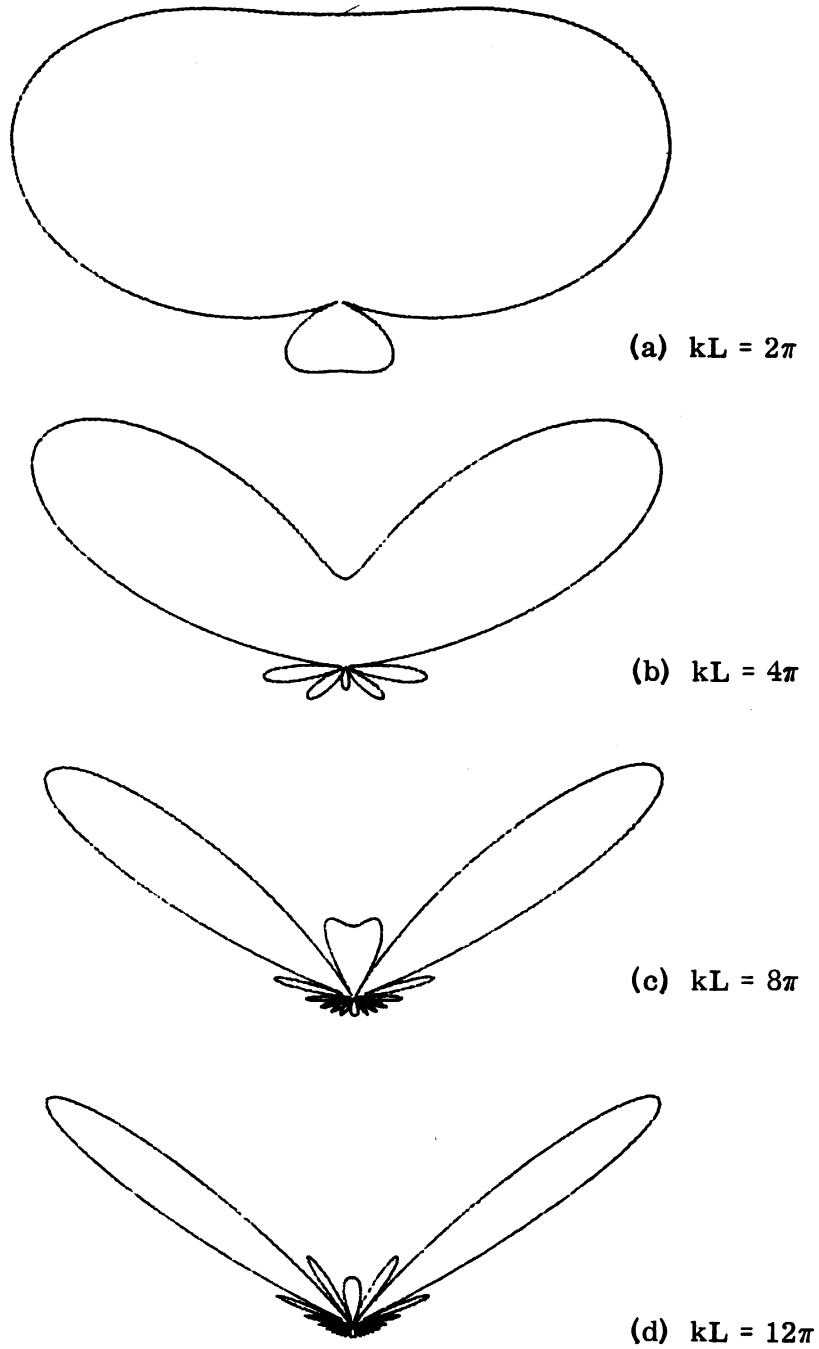


FIG. C-6: $|A(\theta)|$ for Fast Waves, $\beta/k = 0.6$.

the interval $[x(0), x(\pi)]$ is to the right of the origin $x = 0$ on x-axis. From Fig. C-2, it can be seen that the only case $|A(\theta)|$ has just one main lobe is when

$$x(0) = \left(\frac{\beta}{k} - 1\right) \frac{kL}{2} \approx 0 \quad (C.41)$$

In this case,

$$|A(0)| = |f(x(0))| \approx 1$$

and $\theta = 0$ is the absolute maximum on $[0, \pi]$. The highest side lobe level is $|f(x_1)| = 0.217$ at $\theta = \theta_{x1}$. The factor $A(\theta)$ is therefore endfire. Equation (C.41) may therefore be looked upon as the endfire condition for $A(\theta)$. The case (C.41) is satisfied will henceforth be referred to as the endfire slow wave case. The case (C.41) is not satisfied will be referred to as the non-endfire slow wave case. We will look into these two cases separately. Again, an antenna length of at least one free space wavelength will be assumed.

1. Endfire slow waves:

When the endfire condition (C.41) is satisfied, the main beam is in the endfire direction, $\theta = 0$. The beamwidth is

$$2\theta_{y1} = 2 \cos^{-1} \left(\frac{\beta}{k} - \frac{2\pi}{kL} \right) \quad (C.42)$$

For antennas with a length of at least one free space wavelength, the angle θ_{x1} always exists. This is also the side lobe with the highest side lobe level. The end point $\theta = \pi$ is a back lobe if the largest of the θ_{xn} 's and θ_{yn} 's is a θ_{yn} . Whether $\theta = \pi$ is a minor lobe or not,

$$0 < \theta_{x1} < \theta_{x2} < \dots < \theta_{xp} < \pi \quad (C.37)$$

$$|A(0)| > |A(\theta_{x1})| > \dots > |A(\theta_{xp})| \geq |A(\pi)| \quad (C.43)$$

$$|A(\theta_{x_n})| = |f(x_n)| \quad (\text{C.34})$$

where θ_{x_p} is the largest of the θ_{x_n} 's. Equation (C.43) can be normalized,

$$1 > \frac{|A(\theta_{x_1})|}{|A(0)|} > \dots > \frac{|A(\theta_{x_p})|}{|A(0)|} \geq \frac{|A(\pi)|}{|A(0)|} \quad (\text{C.43a})$$

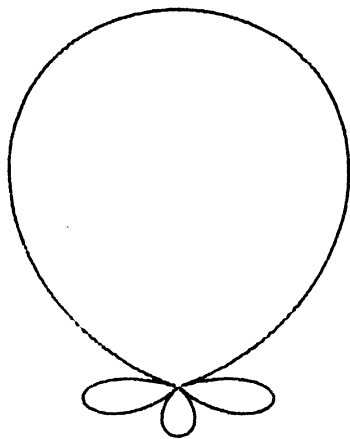
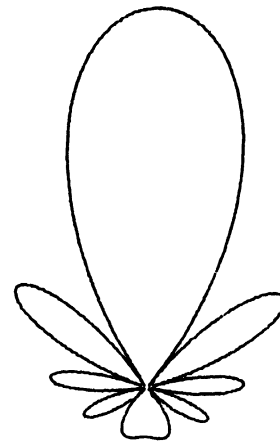
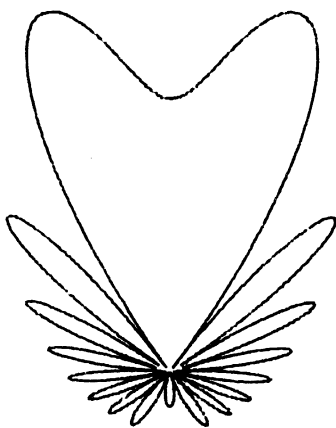
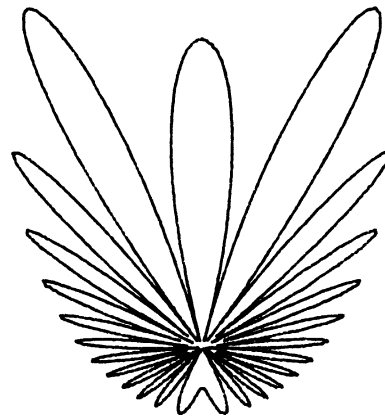
Since $A(0) < 1$, the highest side lobe level $0.217/|A(0)|$ is now greater than 0.217 after normalization. How well the highest side lobe level can be held close to this value depends on how well the endfire condition (C.41) is satisfied.

Length of the antenna: We will now consider the long-standing question whether better directivity can be achieved through the use of longer antennas. The following points all have a bearing in determining the length of the antenna.

- (a). A longer antenna would have a narrower beamwidth for the main lobe. This is seen from (C.42).
- (b). A longer antenna would have more side lobes. This is seen from (C.31).
- (c). A longer antenna would have higher side lobe levels. This is seen from (C.43a). A larger L leads to a larger $x(0)$ and hence a smaller $|f(x(0))|$.
- (d). In the case $\beta_i \neq 0$, the wave on the antenna would attenuate along the structure.

While (a) favors a longer antenna for better directivity, (b) and (c) are against a very long antenna for better directivity. (d) simply says there is little sense in making the antenna longer after it reaches a certain length. It would appear, therefore, that there should be a limit to the length of the antenna for optimum endfire operation. This limit, however, depends very much on the value of β/k , as will be seen later. For $\beta/k \sim 1$, it will also be seen that the limit is very large.

Figure (C-7) shows $|A(\theta)|$ for slow waves. Figures (C-7a) and (C-7b) show the case when the endfire condition (C.41) is satisfied. (C-7d) shows a

(a) $kL = 2\pi$ (b) $kL = 4\pi$ (c) $kL = 8\pi$ (d) $kL = 12\pi$ FIG. C-7: $|A(\theta)|$ for Slow Waves $\beta/k = 1.3$.

typical pattern for $|A(\theta)|$ where (C.41) is violated. Figure (C-7c) is an in-between case. One can see clearly from these figures the effects of increasing the antenna length, specifically in regard to the number of side lobes, the side lobe levels and the beamwidth of the main beam.

2. Non-endfire Slow Waves:

If the endfire condition (C.41) is not satisfied, $|A(\theta)|$ is multi-lobed for antennas with a length at least one free space wavelength. This happens when β/k increases to a certain value depending on kL . The interval $[x(0), x(\pi)]$ now contains some of the maximums, the x_n 's, for $|f(x)|$. Each of these forms a lobe for $|A(\theta)|$. In addition, $\theta = 0$ and $\theta = \pi$ can also be lobes depending on whether they are next to a θ_{yn} or a θ_{xn} .

Relative magnitude of lobes: Assume the θ_{xn} 's that can be found are

$$\theta_{xm} < \theta_{x(m+1)} < \dots < \theta_{x(M-1)} < \theta_{xM} ,$$

then the level of the lobe at θ_{yn} is

$$|f(x_n)| = \frac{1}{\sqrt{1+x_n^2}} .$$

The front lobe level $|A(0)|$ satisfies

$$0 \leq |A(0)| < |f(x_{m-1})| .$$

The back lobe level $|A(\pi)|$ satisfies

$$0 \leq |A(\pi)| < |f(x_{M+1})| .$$

The maximum lobe is therefore either $|A(0)|$ or $|f(x_m)|$. In any case, the largest lobe will be only slightly larger than the first few other lobes. This is therefore a multi-lobe situation. Figure (C-7d) shows a typical pattern for

$|A(\theta)|$ when $x(0) = \left(\frac{\beta}{k} - 1\right) \frac{kL}{2}$ is not near 0. The value of β/k is 1.3 in this particular figure. For larger values of β/k , the shape of $|A(\theta)|$ is strikingly similar to Fig. C-7d, provided the value of kL remains unchanged. This is due to the fact that the number of lobes as predicted by (C.31) is essentially independent of β/k . Figure C-8 shows $|A(\theta)|$ for some different values of β/k . These should be compared with Fig. C-7d.

Propagation constant β : The endfire condition (C.41) puts a restraint also on the value of β . For antennas whose lengths are not too short, (C.41) implies

$$\beta \sim k \quad (C.44)$$

as the endfire condition for slow waves. Since this same limit also implies essentially endfire radiation for fast waves, it appears that the transition region from fast waves to slow waves $\beta \sim k$ in (C.44) is the endfire range for β . The ideal endfire operation from the point of view of the factor $A(\theta)$ would be when $\beta = k$. In this case, $x(0) \equiv 0$ regardless of the value of kL . In theory, the beamwidth of the main lobe for $A(\theta)$ could be made arbitrarily small by using very long antennas. The maximum side lobe level would remain at 0.213 the main lobe level, though the number of side lobes would increase, with increasing length L .

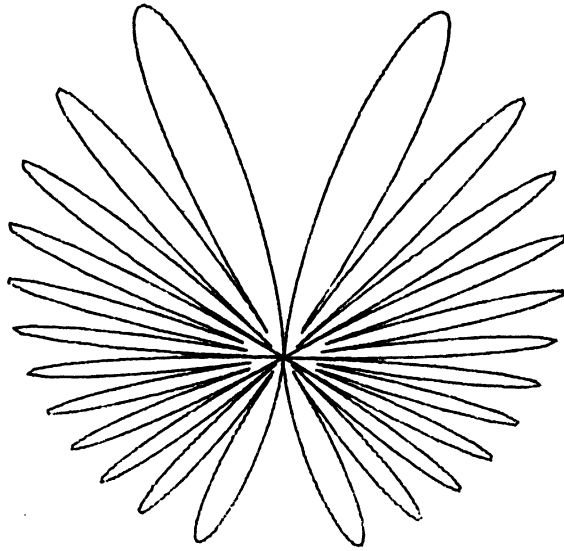
Figure C-9 shows $|A(\theta)|$ for $kL = 12\pi$ and different values of β/k . It should be evident from the figures that the transition region $\beta \sim k$ is indeed the range for endfire operation.

C.9 The Factor $A(\theta)$ with a Complex Propagation Constant $\beta = \beta_r + j\beta_i$

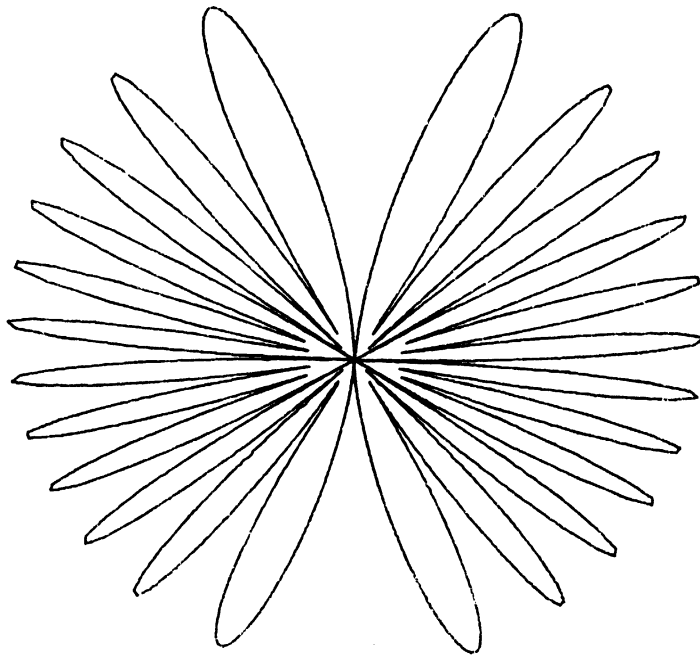
In the case $\beta = \beta_r + j\beta_i$, $\beta_i \neq 0$, the amplitude function $|f(x)|$ becomes

$$|f(x, y)| = \sqrt{\frac{1 + e^{2y} - 2e^y \cos 2x}{4x^2 + y^2}} \quad (C.6)$$

where $y = \beta_i L$. This function, owing to its complicated form, can best be



(a) $\beta/k = 3.0$



(b) $\beta/k = 10.0$

FIG. C-8: $A(\theta)$ for Slow Waves $kL = 12\pi$.

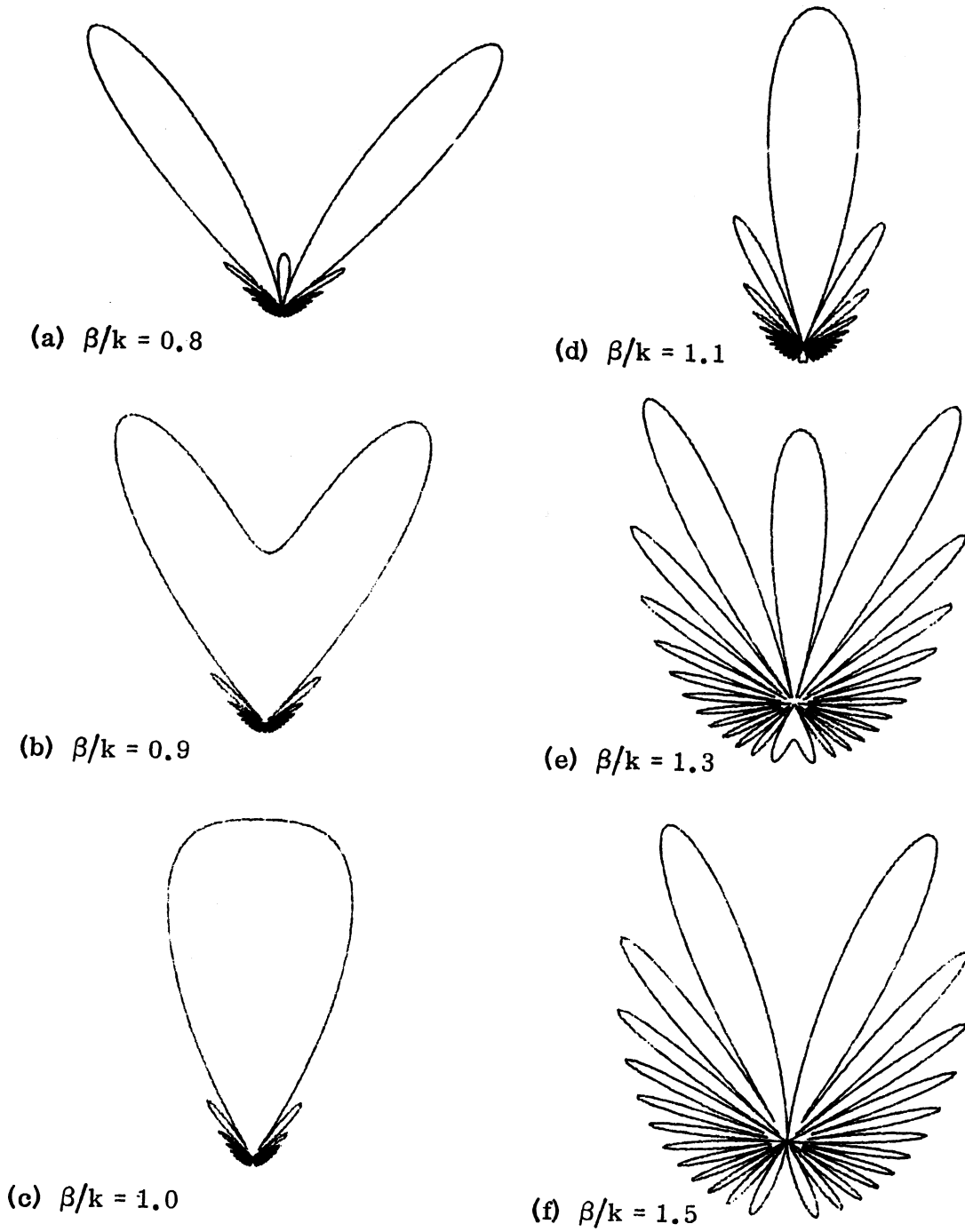


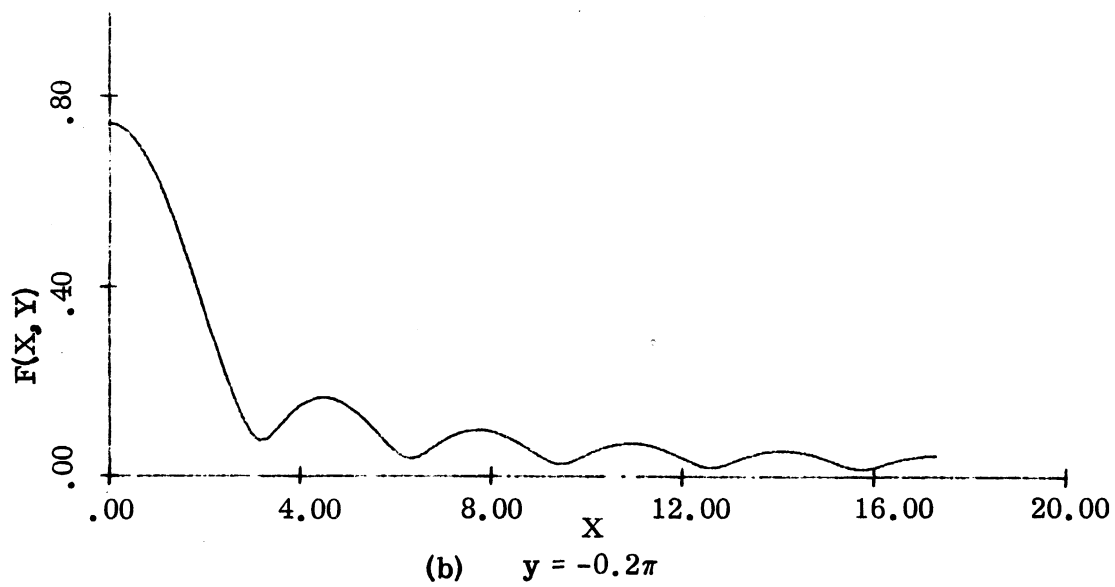
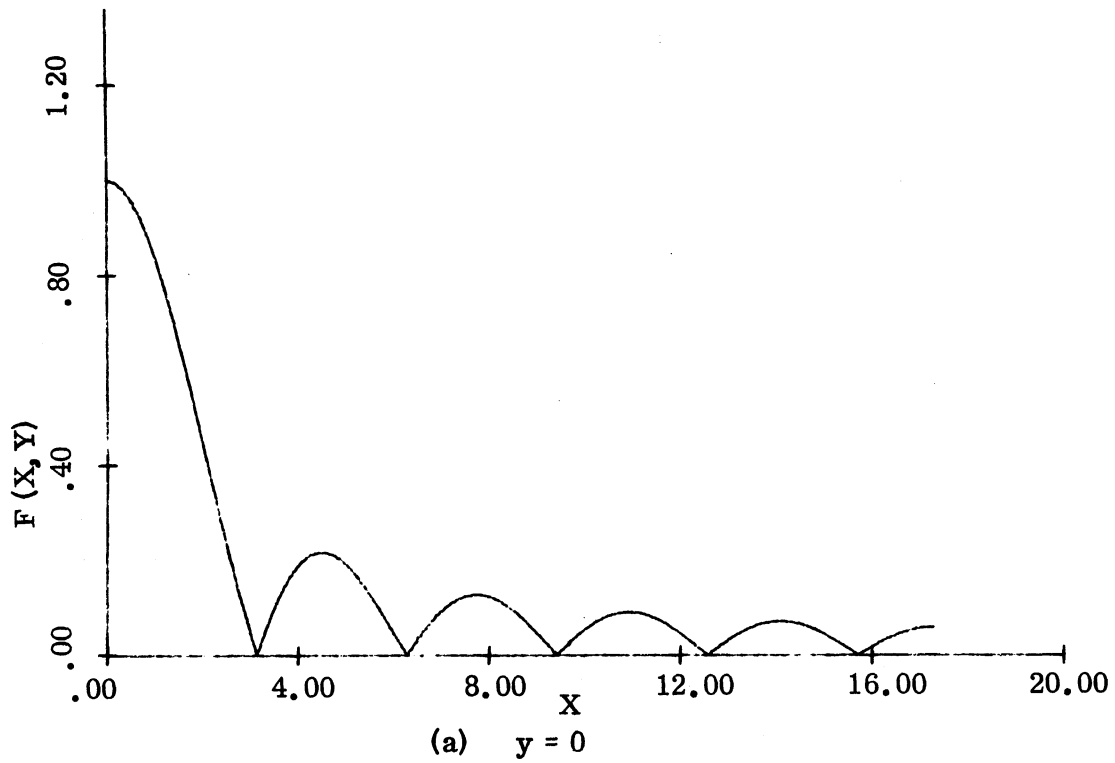
FIG. C-9: Effects of β/k on $|A(\theta)|$, $kL = 12\pi$.

studied graphically. Figure C-10 shows the function $f(x)$ with y as a parameter. It is seen from these figures that the main effect of β_i is to fill the nulls and bring down the peaks.

By means of Fig. C-10 and the mapping function

$$v = \left(\frac{\beta}{k} \right) - \cos \theta \quad (\text{C.3})$$

it is possible to study the pattern $|A(\theta)|$ graphically. The interval $[0, \pi]$ is mapped continuously onto $[x(0), x(\pi)]$. For small values of $|\beta_i L|$, it is seen from Fig. C-10 that the effects of β_i on fast waves and endfire slow waves are small. On the other hand, the effect of the same small $|\beta_i|$ on $|A(\theta)|$ for non-endfire slow wave waves may be quite dramatic. Figure C-11 - C-13 shows some effects of β_i on $|A(\theta)|$ for the various cases discussed above. Figure C-11 shows $|A(\theta)|$ for fast waves. Figure C-12 shows the transition case $\beta = k$. Figure C-13 shows the case for slow waves when the endfire condition is not satisfied. It can be concluded that the only range of β that $|A(\theta)|$ is endfire is still around $(k, 0)$ in the complex β plane.

FIG. C-10: The Function $F(x, y)$ in Eq. (C.6).

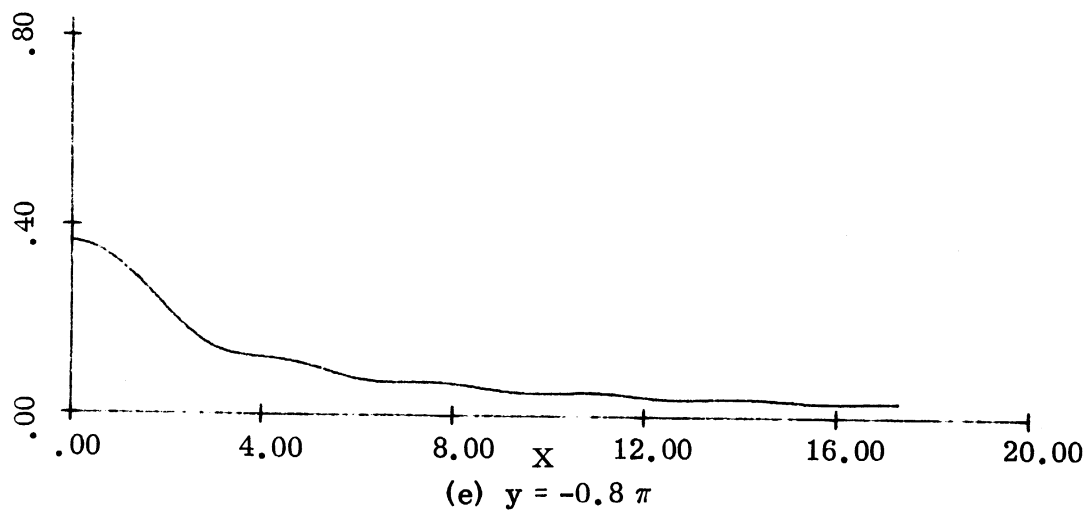
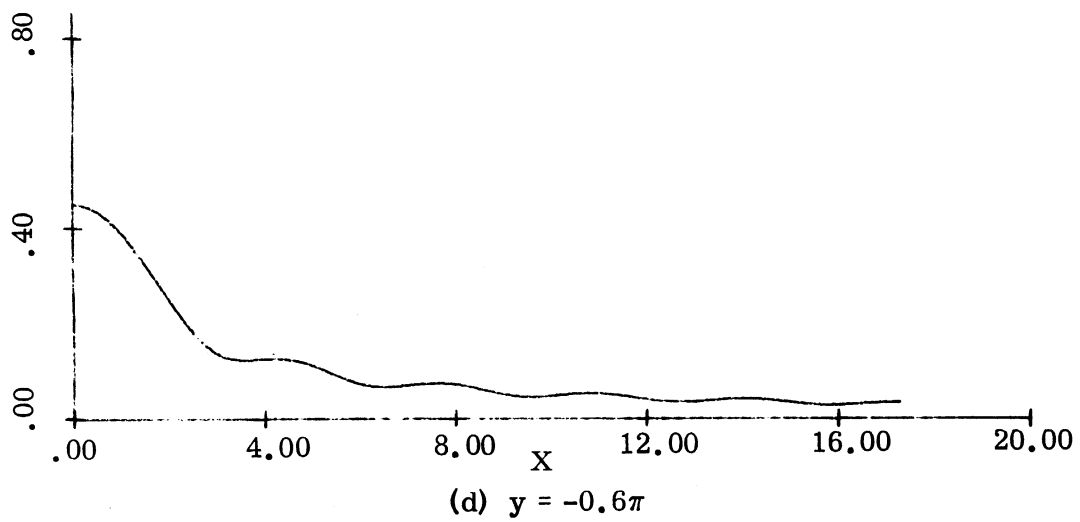
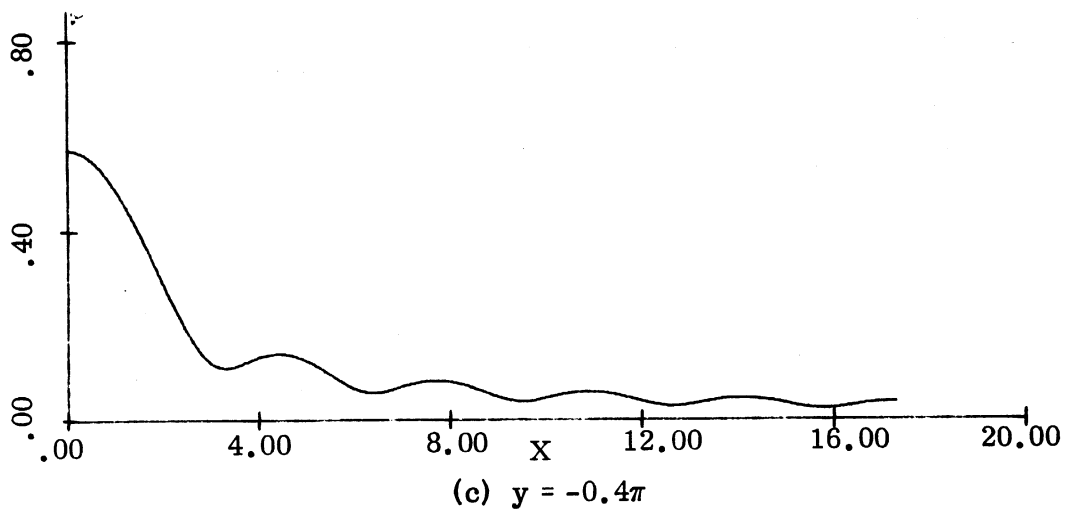


FIG. C-10: Continued.

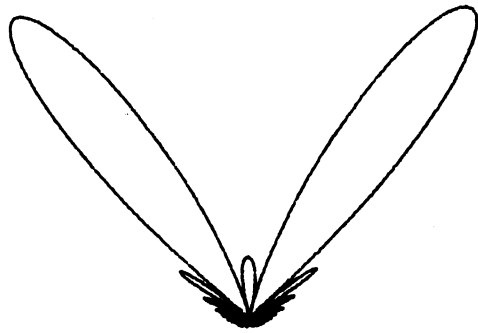
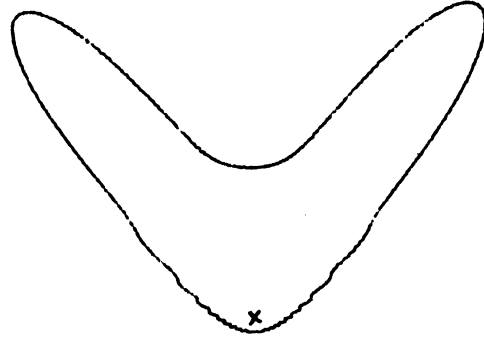
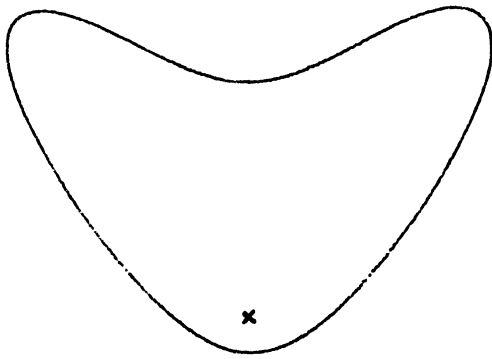
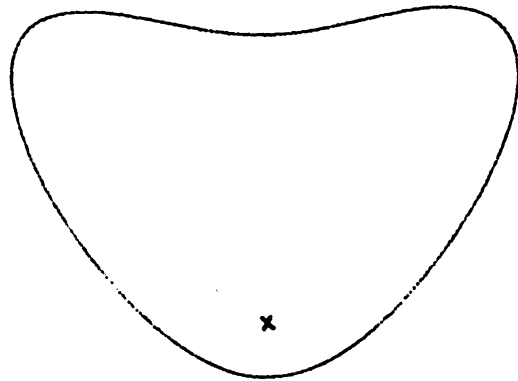
(a) $\beta_i/\beta_r = 0$ (b) $\beta_i/\beta_r = -0.1$ (c) $\beta_i/\beta_r = -0.2$ (d) $\beta_i/\beta_r = -0.3$

FIG. C-11: Effect of β_i on $|A(\theta)|$, $\beta_r/k = 0.8$, $kL = 12\pi$.

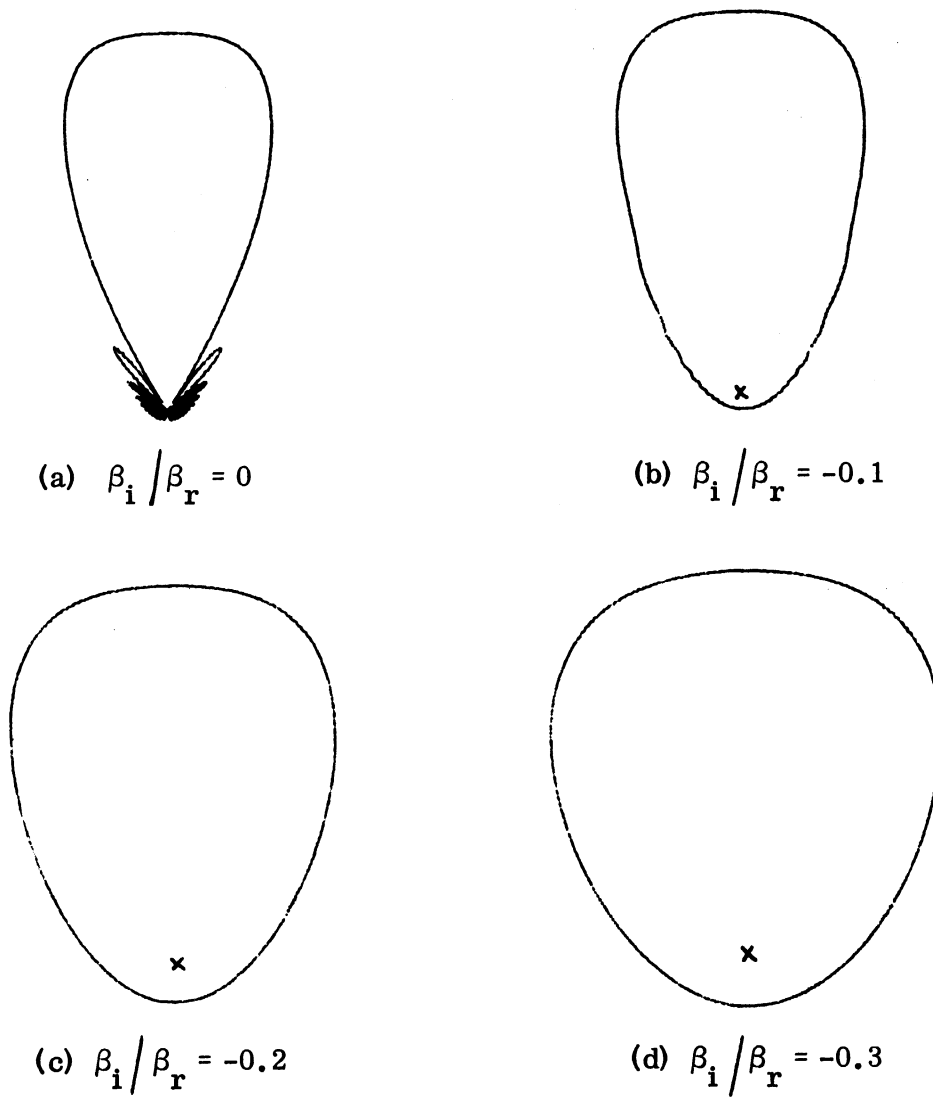
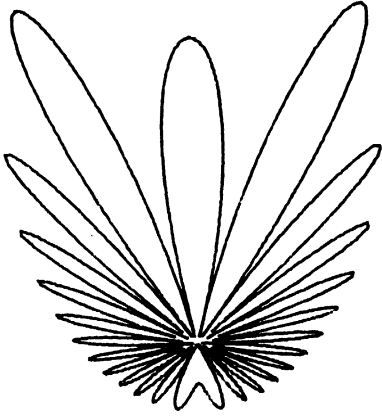
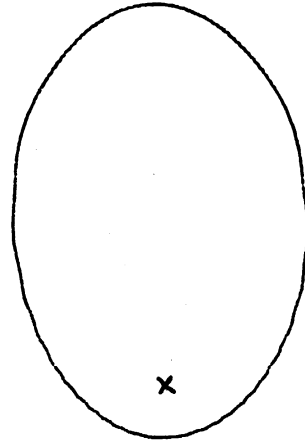


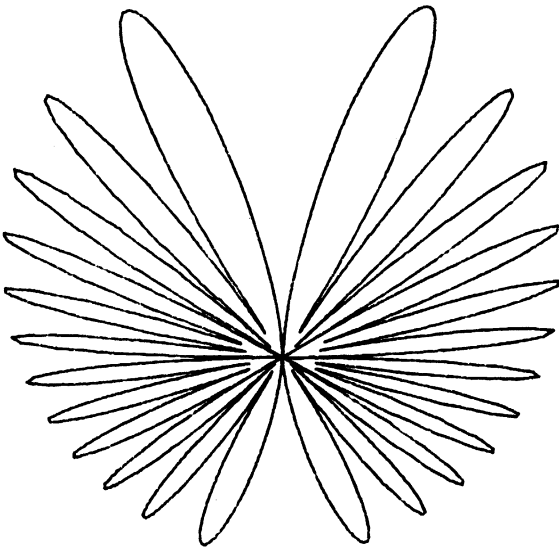
FIG. C-12: Effects of β_i on $|A(\theta)|$, $\beta_r/k = 1.0$, $kL = 12\pi$.



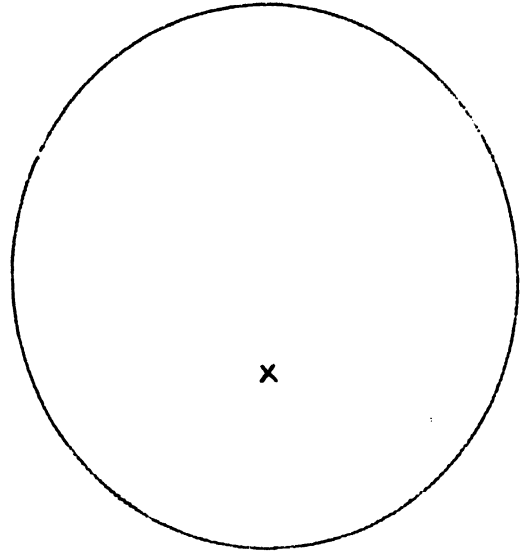
(a) $\beta_r/k = 1.3$ $\beta_i/\beta_r = 0$



(b) $\beta_r/k = 1.3$ $\beta_i/\beta_r = -0.1$



(c) $\beta_r/k = 3.0$ $\beta_i/\beta_r = 0$



(d) $\beta_r/k = 3.0$ $\beta_i/\beta_r = -0.1$

FIG. C-13: Effects of β_i on $|A(\theta)|$ $kL = 12\pi$.

DOCUMENT CONTROL DATA - R & D

(Security classification of title, body of abstract and indexing annotation must be entered when the overall report is classified)

1. ORIGINATING ACTIVITY <i>(Corporate author)</i> The University of Michigan Radiation Laboratory, Dept. of Electrical Engineering, 201 Catherine Street, Ann Arbor, Michigan 48108		2a. REPORT SECURITY CLASSIFICATION UNCLASSIFIED	
		2b. GROUP NA	
3. REPORT TITLE A BIFILAR HELICAL ANTENNA WITH AN OUTER LAYER OF FERRITE			
4. DESCRIPTIVE NOTES <i>(Type of report and inclusive dates)</i> Fourth Interim, Technical			
5. AUTHOR(S) <i>(First name, middle initial, last name)</i> Alan Geetran Cha			
6. REPORT DATE June 1970	7a. TOTAL NO. OF PAGES 105	7b. NO. OF REFS 14	
8a. CONTRACT OR GRANT NO. F33615-68-C-1381	9a. ORIGINATOR'S REPORT NUMBER(S) 01770-4-T		
b. PROJECT NO. 6278	9b. OTHER REPORT NO(S) <i>(Any other numbers that may be assigned this report)</i> AFAL-TR-70-189		
c. Task 627801			
10. DISTRIBUTION STATEMENT This document is subject to special export controls and each transmittal to foreign governments or foreign nationals may be made only with prior approval of AFAL (AVWE), Wright-Patterson AFB, Ohio 45433.			
11. SUPPLEMENTARY NOTES		12. SPONSORING MILITARY ACTIVITY Air Force Avionics Laboratory Air Force Systems Command Wright-Patterson AFB, Ohio 45433	
13. ABSTRACT In this text, a bifilar helical antenna with an outer layer of ferrite is studied. Both the characteristic equation and the far field patterns are investigated. The characteristic equation is found to have different branches of roots as in the case of the unloaded helix. The correct branch of roots is identified both on a theoretical basis and on an experimental basis. The calculated patterns based on this particular branch of roots are found to be in good agreement with the measured patterns. The antenna is found to be backfire over a wide band if properly designed. Tested models show sizable reduction in diameter results from the loading when compared with unloaded helical antennas. The analysis in this work also establishes important conditions on the backfire and endfire operations of the class of antennas that have a wave-like source distribution function along the axis.			

14. KEY WORDS	LINK A		LINK B		LINK C	
	ROLE	WT	ROLE	WT	ROLE	WT
Bifilar Antennas						
Helical Antennas						
Ferrite Antennas						
Reduced-Size Antennas						

UNIVERSITY OF MICHIGAN



3 9015 02652 8110